AD-A050 758 UNITED TECHNOLOGIES RESEARCH CENTER EAST HARTFORD CONN F/G 20/6
OPTICAL SYSTEM FOR DYNAMIC ANALYSIS OF ROTATING STRUCTURES.(U)
OCT 77 K A STETSON, J N ELKINS F33615-75-C-2013
UNCLASSIFIED UTRC/R77-992054 AFAPL-TR-77-51 NL

1 OF 2
AD A050758

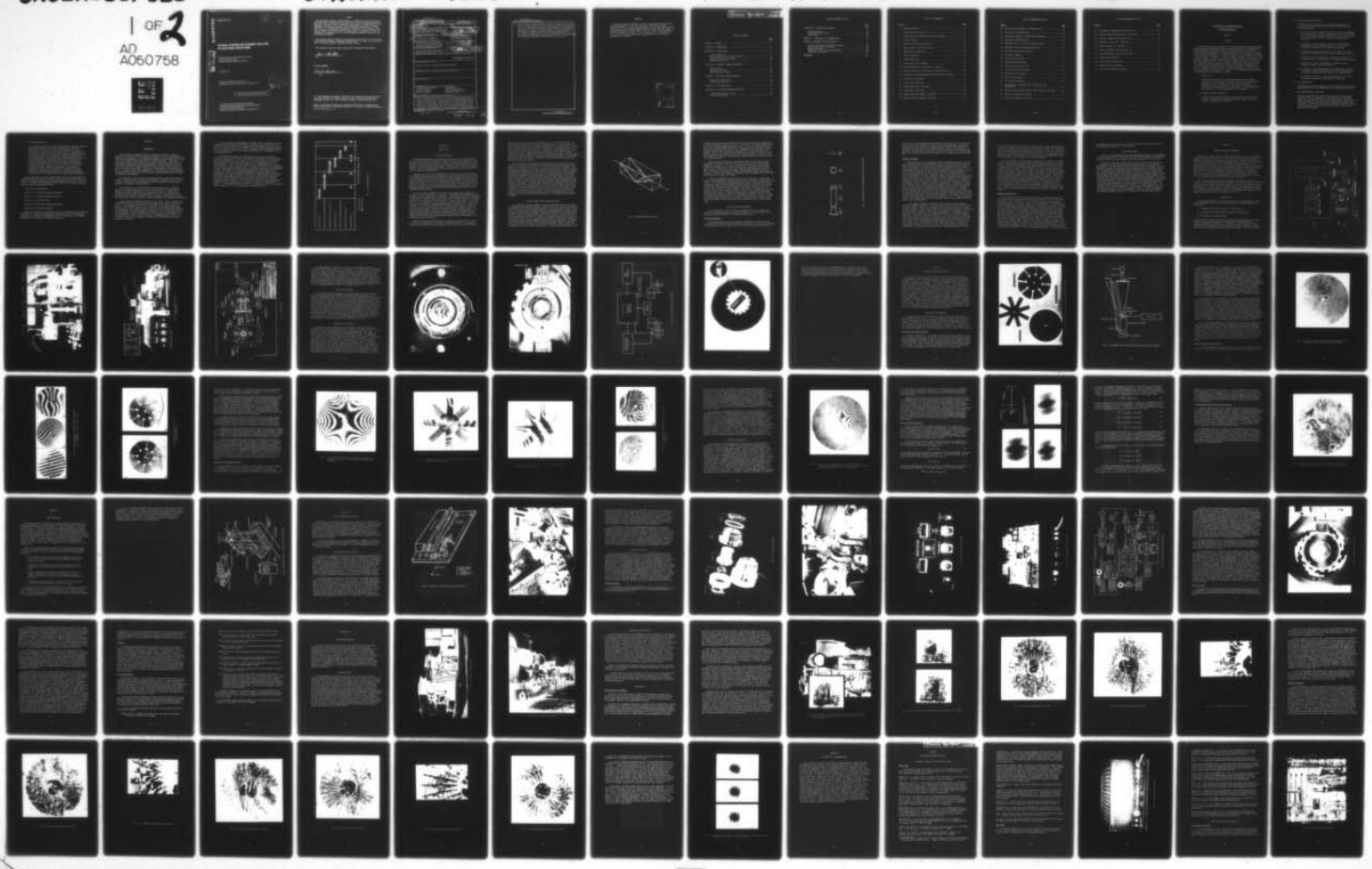

AFAPL-TR-77-51

(12) 7

OPTICAL SYSTEM FOR DYNAMIC ANALYSIS OF ROTATING STRUCTURES

UNITED TECHNOLOGIES RESEARCH CENTER
UNITED TECHNOLOGIES
EAST HARTFORD, CONNECTICUT 06108

OCTOBER 1977

TECHNICAL REPORT AFAPL-TR-77-51
Final Report for Period 20 January 1975 – 20 January 1977

AIR FORCE AERO PROPULSION LABORATORY
AIR FORCE WRIGHT AERONAUTICAL LABORATORIES
AIR FORCE SYSTEMS COMMAND
WRIGHT-PATTERSON AIR FORCE BASE, OHIO 45433

NOTICE

When Government drawings, specifications, or other data are used for any purpose other than in connection with a definitely related Government procurement operation, the United States Government thereby incurs no responsibility nor any obligation whatsoever; and the fact that the government may have formulated, furnished, or in any way supplied the said drawings, specifications, or other data, is not to be regarded by implication or otherwise as in any manner licensing the holder or any other person or corporation, or conveying any rights or permission to manufacture, use, or sell any patented invention that may in any way be related thereto.

This report has been reviewed by the Information Office (OI) and is releasable to the National Technical Information Service (NTIS). At NTIS, it will be available to the general public, including foreign nations.

This technical report has been reviewed and is approved for publication.

James C MacBain

FOR THE COMMANDER

Isaak J. Gershon

"If your address has changed, if you wish to be removed from our mailing list, or if the addressee is no longer employed by your organization please notify AFAPL/TBP *,W-PAFB, OH 45433 to help us maintain a current mailing list".*

Copies of this report should not be returned unless return is required by security considerations, contractual obligations, or notice on a specific document.

AIR FORCE/56780/26 January 1978 — 100

UNCLASSIFIED

SECURITY CLASSIFICATION OF THIS PAGE (When Data Entered)

REPORT DOCUMENTATION PAGE

READ INSTRUCTIONS BEFORE COMPLETING FORM

1. REPORT NUMBER: AFAPL-TR-77-51	2. GOVT ACCESSION NO.
3. RECIPIENT'S CATALOG NUMBER	
4. TITLE (and Subtitle): OPTICAL SYSTEM FOR DYNAMIC ANALYSIS OF ROTATING STRUCTURES.	5. TYPE OF REPORT & PERIOD COVERED: Final Technical Report • 20 Jan [redacted]75 - 20 Jan [redacted]77
6. PERFORMING ORG. REPORT NUMBER: UTRC/R77-992054	
7. AUTHOR(s): K. A. Stetson, J. N. Elkins	8. CONTRACT OR GRANT NUMBER(s): F33615-75-C-2013
9. PERFORMING ORGANIZATION NAME AND ADDRESS: United Technologies Research Center, a Division of United Technologies Corporation, East Hartford, Connecticut 06108	10. PROGRAM ELEMENT, PROJECT, TASK AREA & WORK UNIT NUMBERS: Project No. 3066-12-25
11. CONTROLLING OFFICE NAME AND ADDRESS: Air Force Aero Propulsion Laboratory (TBP), Wright-Patterson AFB, Ohio 45433	12. REPORT DATE: Oct [redacted]77 — 13. NUMBER OF PAGES: 109 — 114 p.
14. MONITORING AGENCY NAME & ADDRESS (if different from Controlling Office)	15. SECURITY CLASS. (of this report)
	15a. DECLASSIFICATION/DOWNGRADING SCHEDULE

16. DISTRIBUTION STATEMENT (of this Report)

Approved for public release; distribution unlimited.

17. DISTRIBUTION STATEMENT (of the abstract entered in Block 20, if different from Report)

18. SUPPLEMENTARY NOTES

19. KEY WORDS (Continue on reverse side if necessary and identify by block number)

Interferometric Holography	Image Derotator
Speckle Photography	Test Stand Application
Rotating Structures	Dynamic Structural Analysis
Vibration Analysis	Bladed Disk Studies

20. ABSTRACT (Continue on reverse side if necessary and identify by block number)

It has been demonstrated that interferometric holograms can be recorded, of objects rotating at high speeds, in a manner sufficiently practical to permit test stand application. This was shown with the successful pictorial acquisition of the vibration characteristics of a TS22 fan stage, operated at speeds up to ~8000 rpm, at an outdoor Pratt & Whitney Aircraft test facility located near Bradley Field. The theoretical and experimental work leading up to, and including, these tests was performed during a two-year study, which is reviewed herein. The work included: 1) a design study to

→ over

DD FORM 1 JAN 73 1473 EDITION OF 1 NOV 65 IS OBSOLETE

UNCLASSIFIED

SECURITY CLASSIFICATION OF THIS PAGE (When Data Entered)

approximately

409 252

20. select a practical image derotation scheme; 2) development of the hardware to implement the chosen method; 3) laboratory tests of the system to illustrate its application to the optical analysis of rotating structures; 4) consideration of the modifications and additions required for adaptation to an actual test stand environment; 5) design, fabrication, and assembly of hardware suitable for test stand installation; and 6) evaluation of the system at a Pratt & Whitney Aircraft test facility. The work was performed under Contract F33615-75-C-2013 for the Air Force Aero Propulsion Laboratory at Wright-Patterson Air Force Base.

FOREWORD

This final report was submitted by United Technologies Research Center, United Technologies, E. Hartford, Connecticut under Contract Number F33615-75-C-2013. The effort was sponsored by the Air Force Aero Propulsion Laboratory, Air Force Systems Command, Wright-Patterson AFB, Ohio under Project 3066, Task 12, and Work Unit 25 with Dr. James C. MacBain/AFAPL/TBP as project engineer in charge. Dr. K. A. Stetson, Mr. J. N. Elkins, and Mr. R. K. Erf of United Technologies Research Center were technically responsible for the work.

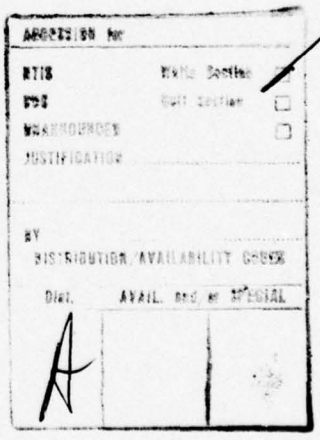

TABLE OF CONTENTS

TABLE OF CONTENTS (Cont'd)

LIST OF ILLUSTRATIONS

LIST OF ILLUSTRATIONS (Cont'd)

LIST OF ILLUSTRATIONS (Cont'd)

Optical System for Dynamic Analysis of Rotating Structures

SECTION I

SUMMARY

Presented herein are the results of a two-year technical program during which it was successfully demonstrated that the optical techniques of holographic interferometry, speckle photography, and moiré interferometry could be utilized to perform dynamic measurements on rotating structures in both laboratory and operational test stand environments. The work culminated with the successful recording of interferometric holograms of a TS22 fan stage (40 percent version of the JT10D) running at speeds up to 8000 rpm in Pratt & Whitney Aircraft's X-308 outdoor test facility. Supported under Contract F33615-75-C-2013, sponsored by the Air Force Aero Propulsion Laboratory, Air Force Systems Command, the program was divided into six phases which encompassed the design, development, and application of a laboratory image derotation system, followed by the study, fabrication, and test of an image derotation system for test stand application. Relevant to the six major phases of the contract, the results of the theoretical and experimental investigations may be summarized as follows:

I - Design Study:

Following an analysis of the interrelated alternatives, including such items as motor and prism selection together with synchronization procedures, in the operation of an image derotation system, a preferred design was established; a transmissive system, utilizing a folded Abbé inverting prism contained within a hollow shafted torque motor, which is, in turn, supported in an air bearing.

II - Laboratory Hardware Development:

An optical image derotation system was fabricated and tested; demonstrating a capability for holding stationary the image of an object rotating at speeds up to 10,000 rpm.

III - Laboratory System Application:

The image derotator was employed in laboratory investigations of various rotating structures with the following significant capabilities established.

1. The ability to depict contours of constant vibratory displacement by the generation of a moiré fringe pattern, formed by overlaying two interferometric holograms (recorded with bias fringes present) of a rotating disk in both a vibration and vibration-free condition.

2. The ability to record directly, via a single interferometric hologram with the bias fringing reduced to a minimum, the vibrational mode pattern of a rotating circular disk.

3. The ability to record bending and torsional modes of the flat blades on an eight-bladed disk rotating at speeds up to 2400 rpm.

4. The ability to show sensitivity to the phase of vibration of a rotating disk by recording triple- and quadruple-pulse holograms.

5. The ability to record interferometric holograms of disks rotating at speeds in excess of 9000 rpm.

6. The ability to record specklegrams of rotating disks, subjected to vibration, from which bending strain could be calculated by observing the diffraction halo fringes in the transform plane.

7. The ability to visualize, using speckle techniques, the vibrational mode patterns on a rotating disk in real-time.

IV - Test Stand Study:

Preliminary sketches and estimated costs were prepared for the design and fabrication of a test stand model of the image derotator system.

V - Test Stand Hardware Fabrication:

An entire image derotator system, with provision for mounting and alignment of both a continuous-wave and pulsed laser on the same pallet with the image derotator optics, film transport, and auxiliary optics necessary for beam steering and holography was designed and fabricated. In addition, the necessary electronic control and synchronization circuitry, including provision for remote operation, was designed and fabricated.

VI - Test Stand Evaluation:

On two separate occasions (December and February), the image derotator system was installed at the outdoor P&WA X-308 Test Stand at Bradley Field for evaluation with a TS22 compressor fan stage as the subject. Below freezing temperatures during the December test period and their effect on pulsed laser operation hampered testing, but data was secured at a fan speed of ~ 3000 rpm demonstrating proof-of-principle: interferometric holograms, depicting the vibration characteristics of rotating objects, can be recorded in an actual test stand environment using the image derotator system designed and developed during the initial phases of the contract. Rework of the laser system, and a break in the weather during February, permitted a dramatic demonstration of the system's potential; interferometric holograms were successfully recorded at various engine operating speeds (up to 8000 rpm) representing both synchronous and asynchronous blade dynamic response conditions.

The present report provides a comprehensive review of the investigations performed throughout the entire two-year contract period, although some of the details previously recorded in the interim technical reports (Ref. 1) have been omitted. The technical discussion has been divided into six areas in keeping with the study phases enumerated above.

Section III - Design Study

Section IV - Laboratory Hardware Development

Section V - Laboratory System Application

Section VI - Test Stand Study

Section VII - Test Stand Hardware Fabrication

Section VIII - Test Stand Evaluation

These are preceded by an Introduction (Section II) which briefly reviews the motivation for the current investigations and are followed by the References (Section IX). Included as an appendix at the end of the report is a detailed description of the Electronic Circuitry (Appendix I).

SECTION II

INTRODUCTION

The measurement of dynamic strains in rotating structures is a problem essential to the testing of turbine engine components. The most common method for making these measurements is by placing strain gages on the structure and recording their output signals through slip rings or by radio telemetry. This method occasionally suffers from problems in the output linkage, and perhaps more often from inadequate placement of the gages themselves. For static objects, optical methods have offered considerable benefit in that they allow rapid inspection of the full surface of the object, a feature that often leads to the quick identification of areas of high stress concentration. A wide variety of optical methods, including photoelasticity, moire interferometry, speckle photography and hologram interferometry are available.

In recognition of the utility of such an application, there were reports by researchers trying to apply hologram interferometry to rotating objects as early as 1970. Historically, three approaches have been considered for the optical analysis of vibration on rotating objects.

The first method is essentially a brute force approach; that is gating a laser into extremely short pulses, one per revolution, so that hologram interferometry could be accomplished on a rotating object (Ref. 2). The extreme difficulty associated with maintaining registration of the hologram and object, together with the low laser energy inherent to the short pulses required to stop the rotary motion, make this method an unlikely candidate for industrial applications.

A second method, developed by Tsuruta and Itoh (Refs. 3 and 4), makes use of a hologram fixed to the rotating object and a large mirror placed in front of the object. In this system, the fixing of the hologram to the object removes all relative motion between them, and it is, therefore, a self-compensating system. This approach has been purused by Sikora (Refs. 5 and 6) for the study of rotating propeller blades. The disadvantage of the system is that in many applications it is not practical to fasten a hologram to the rotating object, and further, it is often impossible to place a mirror the size of a rotating object in front of it (consider the inlet to a jet engine). Finally, such a system would not allow concomitant inspection.

The third alternative, developed by P. Waddell (Refs. 7 through 13) uses an image derotator (rotating erector prism) to optically compensate ("stop") the motion of the object giving it the appearance of a stationary object and thereby permitting use of the many, more or less, "standard" optical analysis techniques. It is this approach that forms the basis for the method to be utilized in the work described herein.

An important advantage of the rotating erector prism over stroboscopic methods for stopping the rotation of an object is its ability to provide continuous motion compensation of the object. This, in turn, means that the object may be subjected to continuous illumination for photoelasticity and moiré interferometry. Further, the motion compensation is independent of the object radius and limited only by the mechanics of rotating the prism, so that tolerances on pulse width and pulse repetition rate are greatly relaxed if pulse illumination is used. These factors are particularly important when the light is to be derived from a laser, as in speckle photography and hologram interferometry. Consequently, the present program was undertaken, considering that its successful development would permit extension of the various coherent optical metrology techniques, whose substantial worth has already been demonstrated in static structural analysis studies, to such problems as centrifugal strain measurement, simulated flutter investigation, and rotational effects on vibrational mode response. The technical work was divided into six phases, as noted in the summary, and was conducted over a 24-month period, as outlined in Fig. 1.

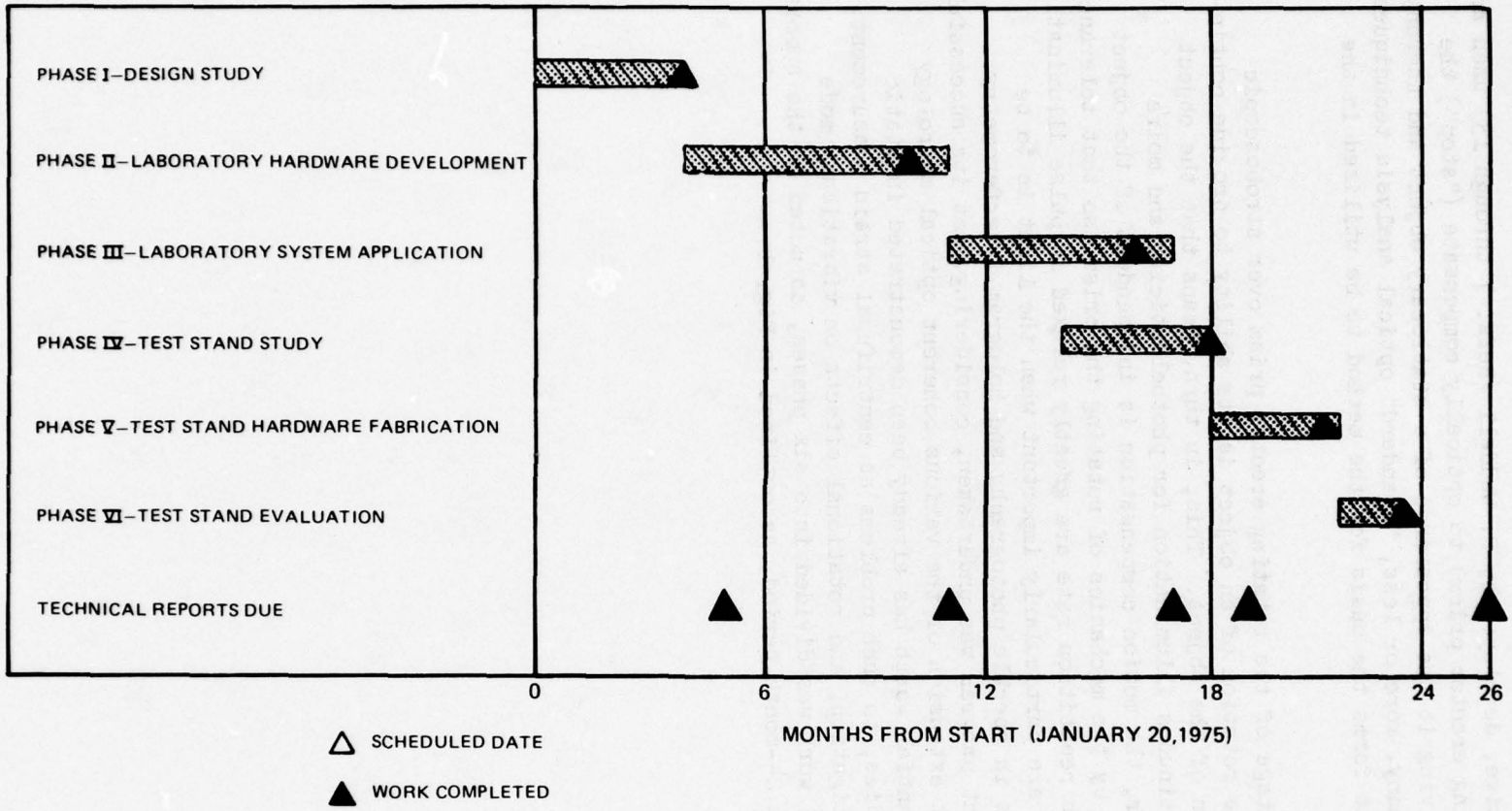

Fig. 1 Program Milestones

SECTION III

DESIGN STUDY

Design Alternatives

The important elements to be considered in the design of an image derotation system include the optics (transmissive or reflective), the motor and bearing, and the type of synchronization circuitry. Perhaps the overriding consideration is the performance of the optical element itself in terms of its field-of-view, numerical aperture, optical distortions, aberrations, and adaptability to precisely controlled rotation. The last consideration is greatly influenced by the choice of motor to be used in turning the image derotator.

Relative to the basic type (transmissive vs. reflective) of optical system, it must be remembered that reflective systems would require an additional beam splitter over transmissive systems in order to extract the final image from the system. This implies an unavoidable loss of 75 percent of the light otherwise available; equivalent to a reduction of two f-stops in photographic speed. Thus, if a transmissive system can be used, it is to be preferred over the reflective type because it transmits four times more light for the same numerical aperture. Utilization of such a system then depends upon the availability of hollow shaft motors compatible with a transmissive image derotator.

Just such items are available in the form of DC torque motors, designed to deliver high torque, especially at low speeds. Furthermore, it was determined that a variety of such torque motors, with adequate internal diameters and speed capability are available in component form such that they could be mounted directly on the shaft they are to turn, permitting the construction of a hollow shaft motor. Once a hollow shaft has been fabricated, and mounted within a bearing assembly which is fixed to a stationary outer frame, the armature may be mounted to the shaft and the stator to the frame. It was further decided that the bearing assembly could be greatly simplified by the use of air bearings, which are available in sufficient size (up to 2.0 inch internal diameter, and 4.0 inch length) to support the entire shaft. The runout of these bearings, as quoted by the manufacturer, is approximately three orders of magnitude less than that for class 8 ball bearings. Thus it could be assumed that all errors in the derotated image would be due to misalignment of the rotation axis, or to balancing.

Having determined the practicality of a transmissive approach, with a hollow shaft motor, the question as to the type of prism to be used has to be answered. A survey of such rotators has been compiled by Swift (Ref. 14), and of the various

designs considered, four could be conveniently used in a hollow shaft motor: the double-dove, the folded Abbè, the Räntsch, and the Pechan. The double-dove prism can be eliminated since it is generally restricted to use in collimated light because of its inclined entrance and exit faces. The Räntsch is undesirable because it is complicated to both fabricate and align. The Pechan has the disadvantage of having a cross section that is larger than the prism aperture, and further, it cannot tolerate too great an angular deviation of the rays passing through it without losing the essential total reflections. Therefore, the folded Abbè rotator (shown diagrammatically in Fig. 2) offering a uniform cross section, balanced design, and good angular tolerance was selected.

After selection of the motor-bearing configuration and the prism, all that remained for a complete specification of the design was the synchronization system. Because a DC motor had been chosen, a DC servo control system was required. Thus, speed sensing transducers were required on both the object and the derotation prism, and these were preferably in the form of markers that generated a number of equally spaced pulses per revolution of the object. The speed indicator for the prism was constructed to generate twice as many pulses as the object. Each of these pulse trains was converted to a square wave and the two waves were multiplied and integrated. When the two waves were in phase quadrature, the resulting signal was zero, and any slippage of phase yielded a positive or negative signal depending upon the direction of slippage. This signal was fed back to the hollow shaft motor to keep it phase locked with the rotating object. The choice of the number of pulses per revolution of the object depended upon the desired response of the system to object accelerations and upon the number of angular positions at which observations were required. For actual bladed disk studies, a logical choice would be to use the blades of the fan under study to generate pulses, and then matching these to the encoding disk on the prism assembly in such a way as to generate twice that number of pulses.

Optical Design of the Preferred System

The folded Abbè inverting prism has a physical path length that is 5.2 times the entrance or exit aperture diameter. (Because the prism is rotated, the aperture is circular and equal to the smallest dimension of the square end.) Since the light within the prism is traveling through glass, the actual path must be reduced by the reciprocal of the index of refraction to obtain the equivalent air path that should be used in computing numerical aperture and field of view. For an index of 1.50, the equivalent air path becomes 3.46 times the prism aperture, which is the physical length of the prism itself. In the design and operation of any optical system, it is desirable to have the same numerical aperture for every image point. This means that the lens aperture should subtend the same solid angle relative to each point in the image field. The failure to fulfill this condition is called vignetting. Considering the prism as a tunnel through which the optical system must look to form

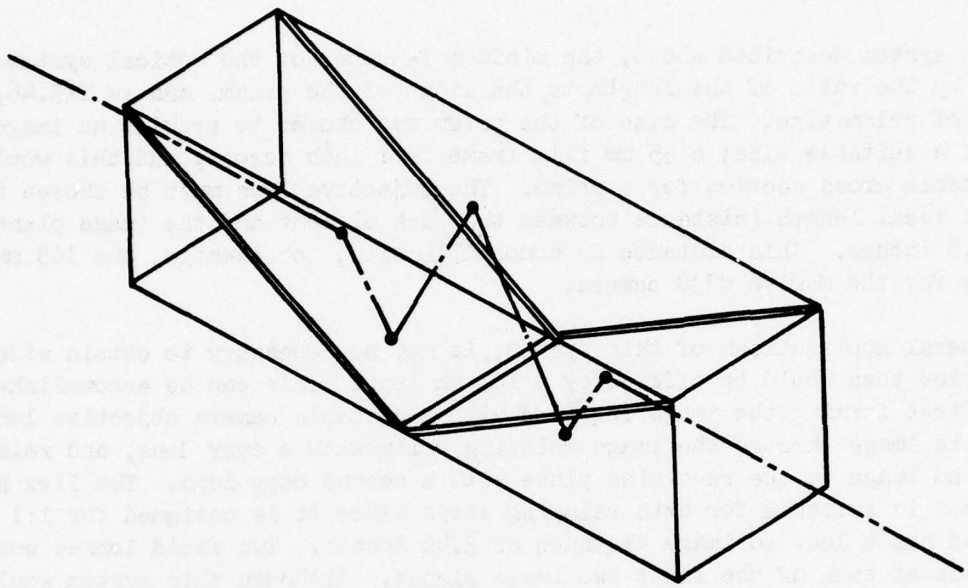

Fig. 2 Folded Abbé Inverting Prism

an image of the object, this condition is best met by placing the lens aperture at one end of the prism and forming the image at the other. To record the image (referring to the schematic diagram presented in Fig. 3), it is most convenient to use a copy lens to relay the image field with a 1:1 magnification to a suitable distance from the rotating prism. In order to avoid vignetting in the relay step, it is common to place a field lens at the image plane so as to image the aperture of the objective lens onto the aperture of the relay system (copy lens). The use of this relay system will permit the introduction of a reference beam at the recording plane for hologram recording.

In the system described above, the minimum f-number of the optical system is determined by the ratio of the length to the width of the prism, and is f/3.46, regardless of prism size. The size of the prism was chosen to provide an image diameter of a suitable size; a 35 mm film frame is 1 inch across, and this would make a suitable cross section for a prism. The objective lens must be chosen to have a back focal length (distance between the back element and the image plane) of at least 3.5 inches. This distance is compatible with, for example, the 105 mm focal length lens for the Mamiya C330 camera.

In general applications of this system, it may be necessary to obtain wider fields of view than would be offered by a 105 mm lens. This can be accomplished quite easily by first forming the image required with a suitable camera objective lens, relaying this image through the image rotating prism with a copy lens, and relaying the derotated image to the recording plane with a second copy lens. The Ilex No. 5007 CRT lens is suitable for both relaying steps since it is designed for 1:1 imaging, and has a lens to image distance of 3.46 inches. Two field lenses would be required, one at each of the first two image planes. Although this system would require two relay steps, it would allow virtually any objective lens to be used in the system from a wide-angle lens to a telephoto lens, or even a zoom lens. Conversion from a single relay system to the double relay system would be easily accomplished and would not alter the system from the derotation prism to the recording plane.

Optical Tolerance Requirements

The requirements in terms of optical performance that must be imposed upon this system vary depending upon whether the system is to be used for moiré interferometry, speckle photography, or hologram interferometry.

Moiré Interferometry

Moiré interferometry imposes the simplest requirements in that the optical system merely has to be able to resolve the moiré grid that is inscribed or projected onto the rotating object. Nothing can be done in this area to procure lenses of

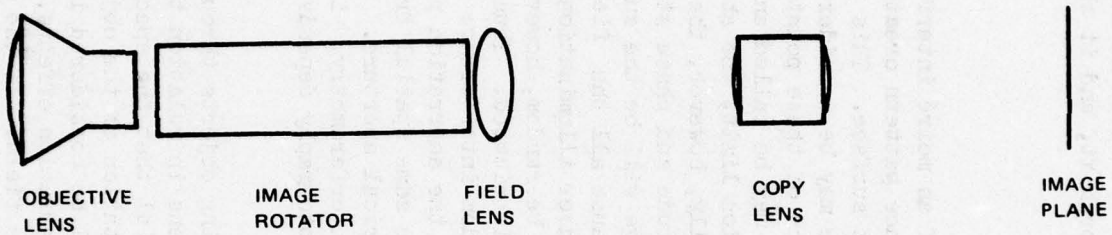

Fig. 3 Optical System for Image Derotation and Recording

proper design to form adequately resolved images through the prism. The prism will act as a long block of glass and as such will introduce aberrations; these may be compensated by proper design of the imaging lenses. Departures from flatness of the prism faces, however, will introduce aberrations that are not correctable, and therefore a tolerance can be expressed as the total distortion that the prism introduces into a plane wavefront passing through it, and it should be kept to less than $\lambda/4$.

Speckle Photography

Speckle photography can be thought of as moiré interferometry wherein the moiré grid is replaced by the random interference pattern created by forming an image of laser light scattered by a diffuse object surface. This pattern may be thought of in the following way. The object surface may be considered as an infinite set of infintesimal point sources of light. Each of these points will be imaged by the lens system into a distribution of light that may be called an aberration pattern. As the lens imagery approaches the diffraction limit, the aberration pattern will approach the familiar Airy disk. Generally, however, the aberration pattern is larger than the Airy disk and it contains amplitude and phase structure that is comparable in size to the Airy disk. The total image will be the summation of the fields corresponding to all the image points. Because all the fields from the object point are mutually coherent (a result of the laser illumination), the aberration patterns will interfere. Their interference will be random, however, because the phases of all the object points will be randomly distributed. Thus, even for a diffraction-limited lens, the image will contain random interference patterns, or speckles. With an aberrated lens, the structure in the aberration patterns will give structure in the speckle pattern that will have the same spatial frequency distribution as for a diffraction limited lens of equal numerical aperture. This leads to the main advantage of speckle photography over moiré interferometry: i.e., the spatial frequency content of the pattern used in speckle photography depends only on numerical aperture and not upon lens aberrations.

In the speckle photography of rotating objects through an image derotation system, the angular orientation of the lens in relation to both the object and prism constantly varies. Because it is essential that the speckle pattern in the image be kept the same for every angular orientation of the object, considerable constraints on polarization are implied. (These will be considered in a following section, restricting the present discussion to aberration effects.) The aberration pattern created by a lens varies across the image field. If the lens is made of elements that are all surfaces of revolution, the axes of which are colinear, then the aberration pattern will depend only upon radius and will have an orientation relative to the radius that is independent of angular orientation. Thus if the axis of the lens intersects the axis of rotation of the object, the speckle pattern will be rotationally invariant. Therefore, the lens to be employed must be checked for colinearity of its elements, and provision must be made for alignment of its axis

with the center of rotation of the object surface. With a simple cemented doublet or triplet, colinearity of the elements is quite easily obtained. With multielement lenses, such as camera objectives, more difficulty may be encountered. Irregularities in the prism surfaces and inhomogeneity of the glass of the prism may contribute variations to the aberration pattern of the prism that are not independent of angle. Again, these may be collected into a signal specification on the wavefront distortion of the prism, and a tolerance of $\lambda/4$ should be adequate.

Failure to maintain a specific speckle pattern which is constant with rotation of the object will adversely effect attempts to do speckle photography on rotating objects. Consider that most techniques of speckle photography involve making two exposures of an object at different stress levels within the object due to static or dynamic stress. If these two photographs do not possess speckle patterns that correlate with one another, it will be impossible to extract metrological information as to the change in shape of the object. Thus, changes in the speckle patterns in the derotated image with changes in angular orientation of the object will restrict the angular orientations of the object that may be compared. In short, the two exposures would have to be made at those angular orientations of the object at which the speckle patterns repeated themselves; for example, once every rotation of the prism, or every other rotation of the object. To minimize this effect, which could greatly reduce the utility of the system, the numerical aperture of the lens system can be reduced so that its performance approaches the diffraction limit. However, this in turn reduces the sensitivity of speckle photographic techniques to strain, and thus, care must be exercised to maintain a constant speckle pattern.

Hologram Interferometry

The visibility of the fringes that are observable in hologram interferometry will depend strongly upon the correlation of the amplitudes of the two fields being interfered. Lack of correlation in the two fields recorded by a double-exposure hologram will reduce the ability to observe fringes and make any useful measurement. Thus, in general, the requirements related to the correlation of the image fields are the same for holography and speckle photography. In addition, however, there should not be too great a phase profile across the image plane introduced by the prism; a problem which could occur, for example, if the exit face of the prism were wedged. This may be specified by the total departure from colinearity on an emerging wavefront with respect to an entering plane wave. With the three pieces of the folded Abbè prism, it is possible to compensate for a wedge effect by angular adjustments of the prism elements. If the image rotator is used in a relay step, then the field lens, used at the image formed by the first objective lens, must be centered on the rotational axis of that image. Failure to do so will also introduce a severe phase function across the image. The effect of an image phase function would be to generate a large number of meaningless fringes in the interferogram that will depend upon the two relative object angles at which the holograms were recorded. Aside from difficulties

in interpretation, these fringes, if too fine, could exceed the resolution of the system making it impossible to reduce the data.

Polarization Effects

The use of an image derotator for moiré interferometry requires no consideration of the polarization of the light used. Both speckle photography and hologram interferometry, however, are quite dependent upon the polarization of the light used.

Although retroreflective paint, used on the test objects to be studied, does not depolarize the light that strikes it to any great degree, it was found by experiment that the beam splitter and mirrors would introduce considerable change in polarization unless the light was polarized linearly vertical or linearly horizontal. Linearly vertical polarization was preferred because it gave a more nearly fifty percent division by the beam splitter. It was also found by experiment that the derotator prisms introduced very nearly a half-wave retardation between vertical and horizontal polarizations. Thus, with quarter-wave plates before and after the derotator, the entire unit could be made neutral regarding polarization. Consequently the illumination should be made vertically polarized; the quarter-wave plates set at $\pm 45^{\circ}$ to the vertical; and in this way the light in the object beam would remain vertically polarized regardless of the orientation of the derotator prisms. The rotation of the prisms would introduce a Doppler-shift phase modulation, but this is insignificant over the duration of the laser pulses. (It should be noted that the half-wave retardation achieved naturally by the prisms made it unnecessary to rotate the quarter-wave plates with the prisms as had been originally planned.)

SECTION IV

LABORATORY HARDWARE DEVELOPMENT

Following the design study, an optical image derotation system for the dynamic analysis of rotating structures, in the laboratory, was designed and fabricated. As described in Section III, the design of the system was based upon a transmissive image rotating prism located within a hollow shaft motor comprised of an air bearing and a dc torque motor. The three major components (prism, air bearing and dc torque motor) were purchased, while the mechanical assembly that makes up the hollow-shaft motor, and the fixtures that hold the optical elements in place were designed and fabricated at United Technologies Research Center (UTRC). The electronic circuitry to drive and synchronize the motor was also designed and fabricated at UTRC. The system was tested to object speeds of 10,000 rpm and a typical test result, illustrating a resolution capability of at least 15 cycles/mm in the image of a test object rotating at a speed of 5,000 rpm, is presented.

The overall laboratory optical system, shown in blueprint form in Fig. 4, is mounted on a large aluminum plate and is comprised of an objective lens, the derotator, a field lens, a copy lens, and a film transport. Pictures of the overall system are presented in Figs. 5 (side view) and 6 (axial view). A 35 mm camera back, to which the copy lens is directly attached, is used for photographic recording, as shown in Fig. 5; whereas a Jodon 35 mm film transport is used for hologram recording, with a separate copy lens, as shown in the blueprint of Fig. 4.

Image Derotator

The most complex portion of the optical system is the image derotator itself (shown in blueprint format in Fig. 7), containing three commercial components as noted above.

1. 3-element prism, Optical Systems and Technology, Inc.

2. dc torque motor (Model 2375-038), Magnetic Technology, Inc.

3. Air bearing, Apex Bearing Corp.

(In the laboratory system a brush type motor was utilized, whereas the test stand system, to be described subsequently, incorporated a brushless motor also supplied by Magnetic Technology, Inc. In addition, the air bearing for the test stand system was specially designed and fabricated by Dover Instruments, whereas the bearing unit incorporated in the laboratory system was a stock item from Apex.)

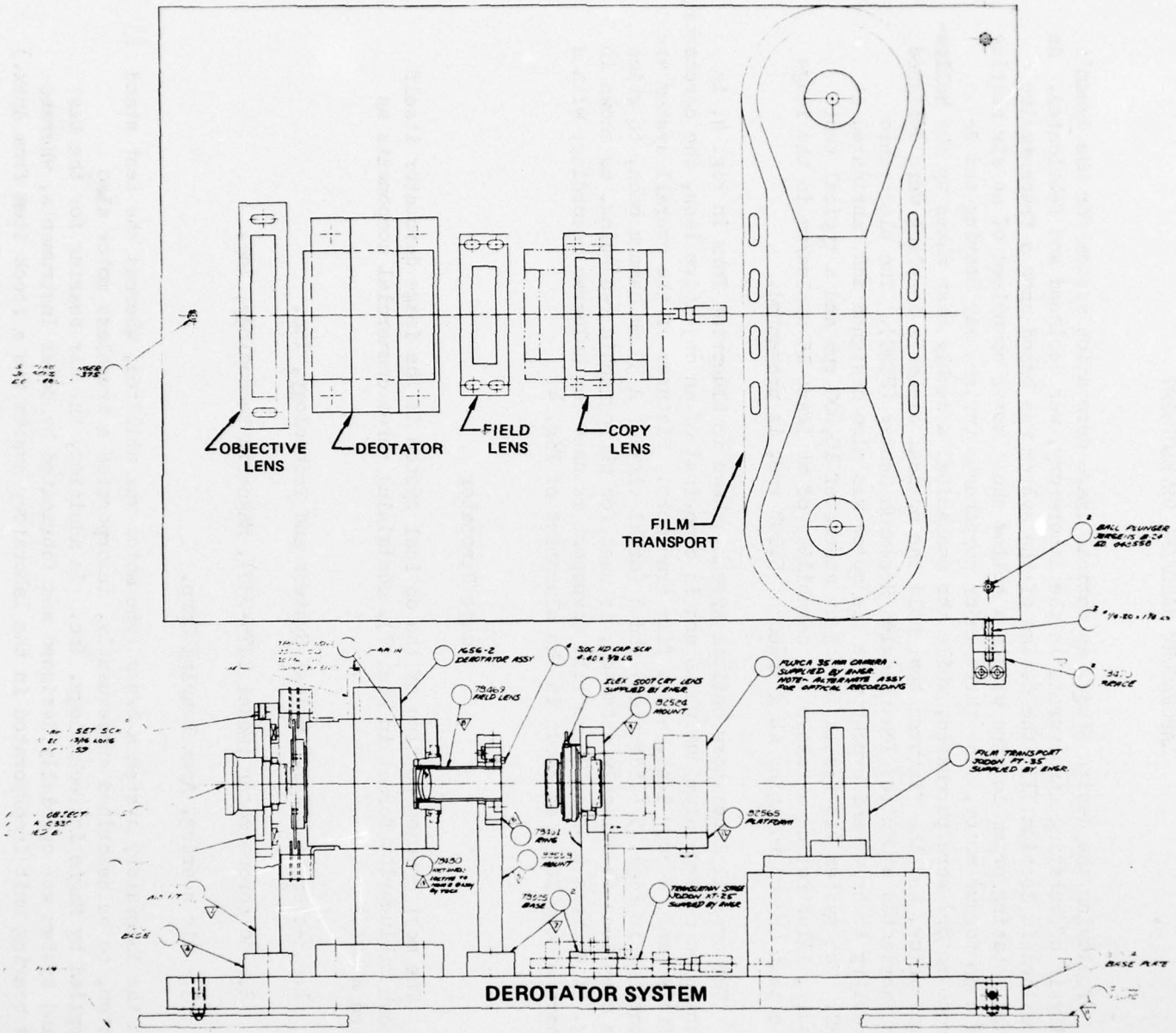
OBJECTIVE LENS
DEOTATOR
FIELD LENS
COPY LENS
FILM TRANSPORT
DEROTATOR SYSTEM

Fig. 4

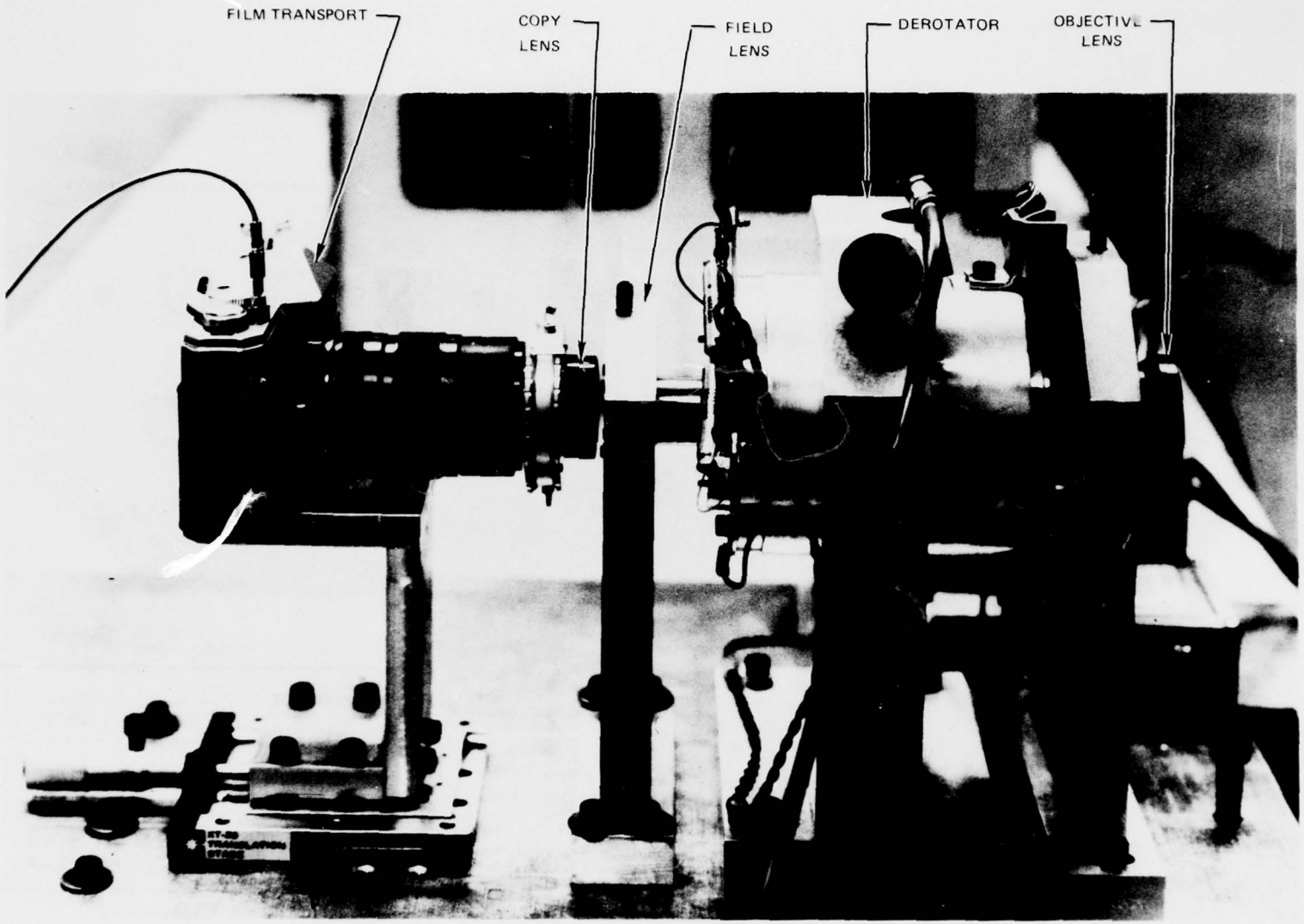

Fig. 5 Image Derotator System
(Side View)

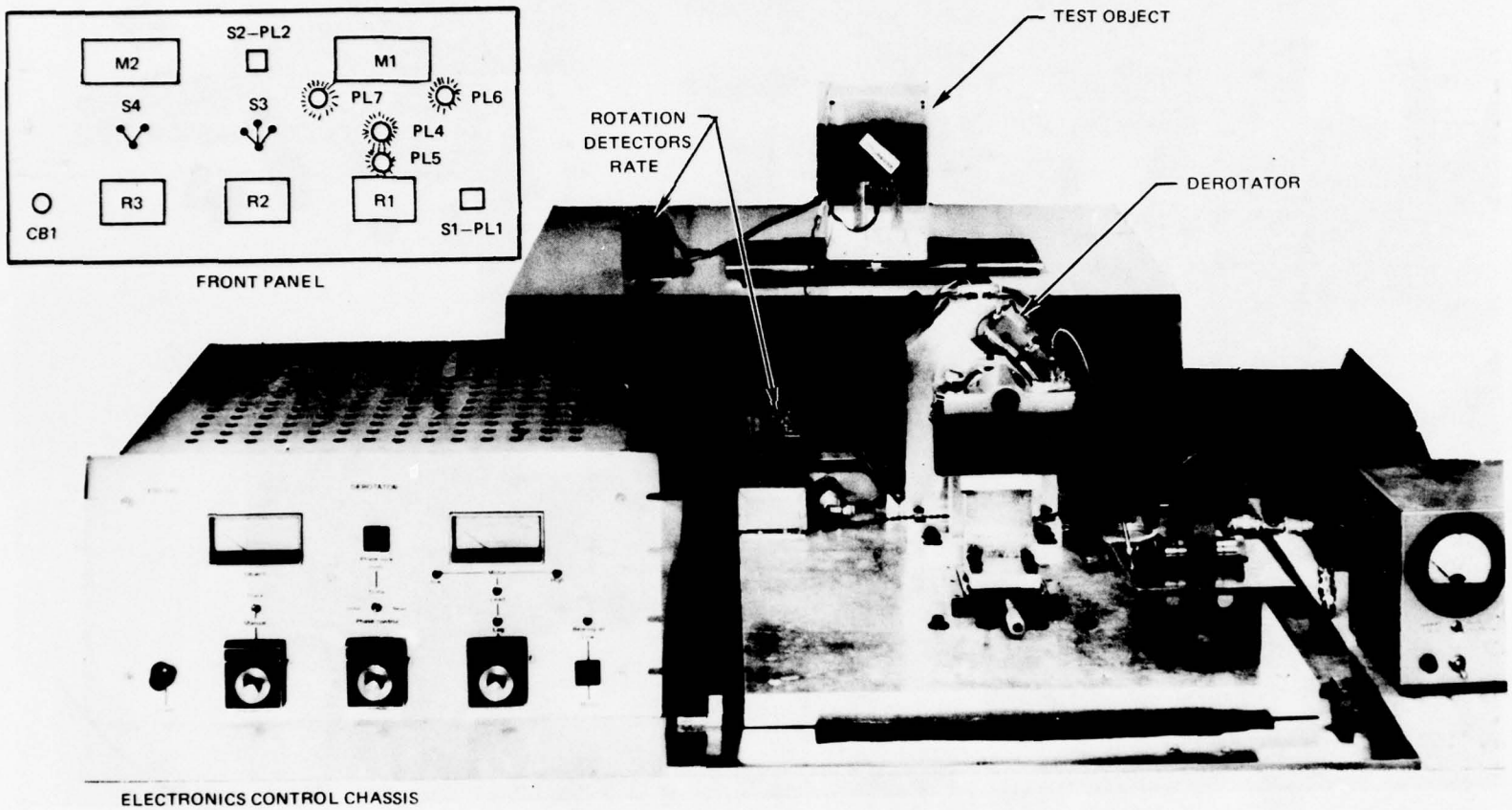

Fig. 6 Image Derotator System
(Axial View)

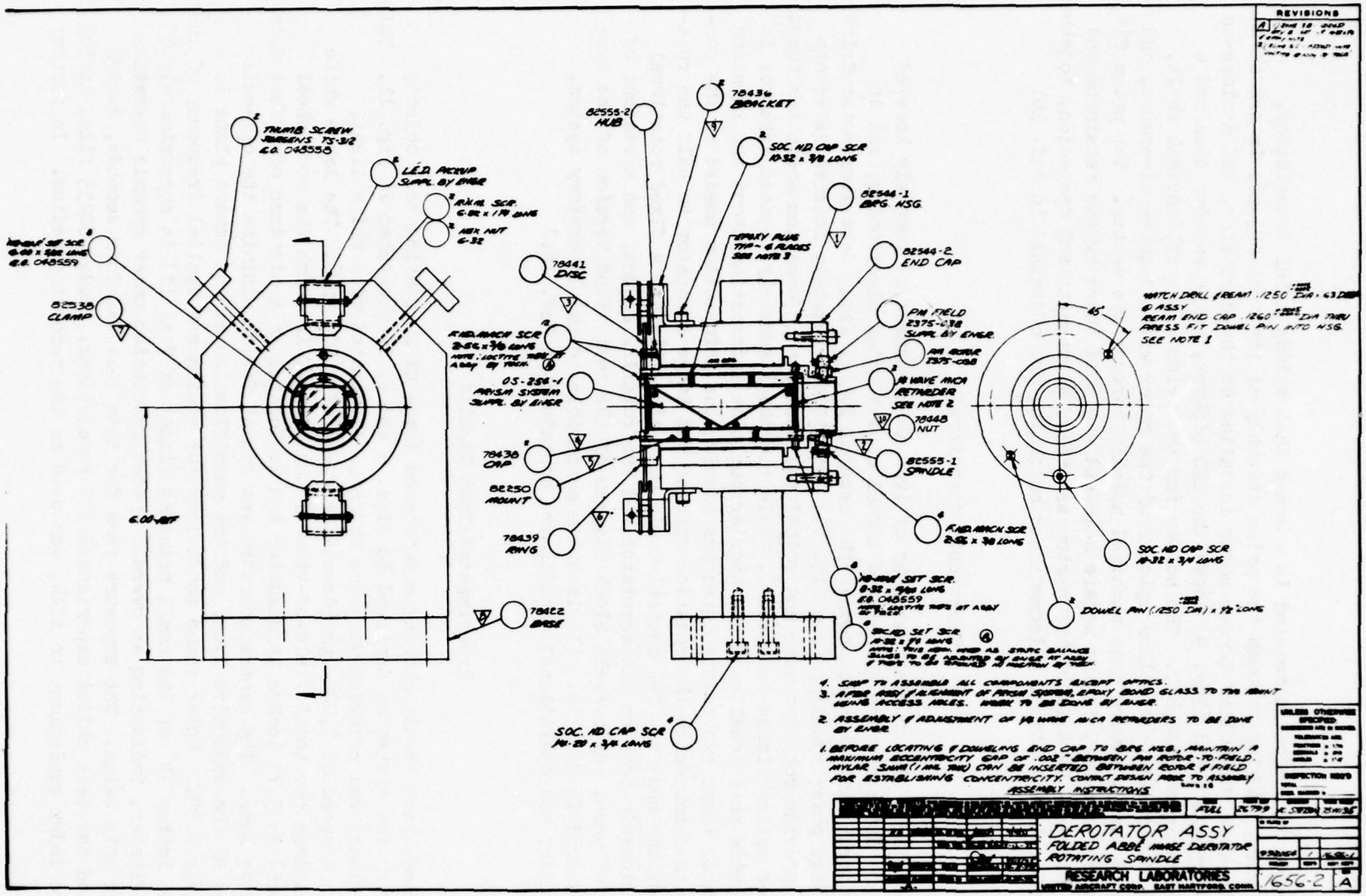

Fig. 7 Image Derotator

The image derctator is mounted in a stand that allows axial translation. A close-up view, looking through the prism assembly at the test object, is presented in Fig. 8 to show the hollow torque motor installed on the derotator, and a close-up view of the opposite end (Fig. 9) shows the LED pickups, angle encoder disk and a portion of the prism assembly. The holder for the prism was a cylindrical shaft, designed to fit inside the hollow spindle of the motor with adequate clearance, and which, itself, had a square hole machined axially through its center. The prism fit, with adequate clearance, in the square hole and was held there by the retaining and adjustment screws. Details of the system assembly, adjustment and operation, together with the prism installation, alignment and balancing are contained in Ref. 1b.

Electronic Circuitry

The derotator electronics consists of two cable connected, remotely located rotation rate detectors and associated signal conditioning electronics, and an operator control chassis which houses the control logic, image derotator motor driver and associated power supplies (see Fig. 6). One of the remotely located detectors is used to provide rotation rate and rotational position information about the torque motor driven optics (image derotator), while the other remotely located detector is used to provide rotational rate and angular position information about the rotating object. Thus, these two remote detectors provide the information needed by the control logic to synchronize the rotation rate of the image derotator to half the rotation rate of the object. The control logic must also maintain a fixed rotational phase relationship between the derotator and the rotating object, and a readout of the status of each. An overall block diagram of the test stand version of the system is presented in Fig. 10. (It is quite comparable to the laboratory system, whose circuitry and operational details are contained in Ref. 1b.)

Experimental Test Results

A typical test result showing a derotated image of a rotating test object, recorded with the system as depicted in Figs. 5 and 6, is presented in Fig. 11. This particular image was recorded with the object, illuminated with white light, rotating at a speed of 5,000 rpm (derotator speed of 2,500 rpm). The large white circle indicates the total field-of-view of the system, in which the code wheel (test object) is 3.75 inches in diameter and is located at a distance of 5 feet from the objective lens. The camera aperture was set at f/8 to minimize the off-axis aberrations of the objective lens, and the magnification at the camera plane is approximately 0.09X. Under these conditions the equivalent spatial frequency of the bars in the letter "E" of the small printing (inset of Fig. 11) is approximately 15 cycles/millimeter, indicating an overall system resolution under dynamic operation of at least this value. The exposure time for this test was four seconds, during which period the test object experienced 333 revolutions. Kodak S0253 film, having an exposure index equivalent to ASA4, was used as the recording medium. In further

Fig. 8 Hollow Torque Motor (Installed on Derotator) Cylinder Housing

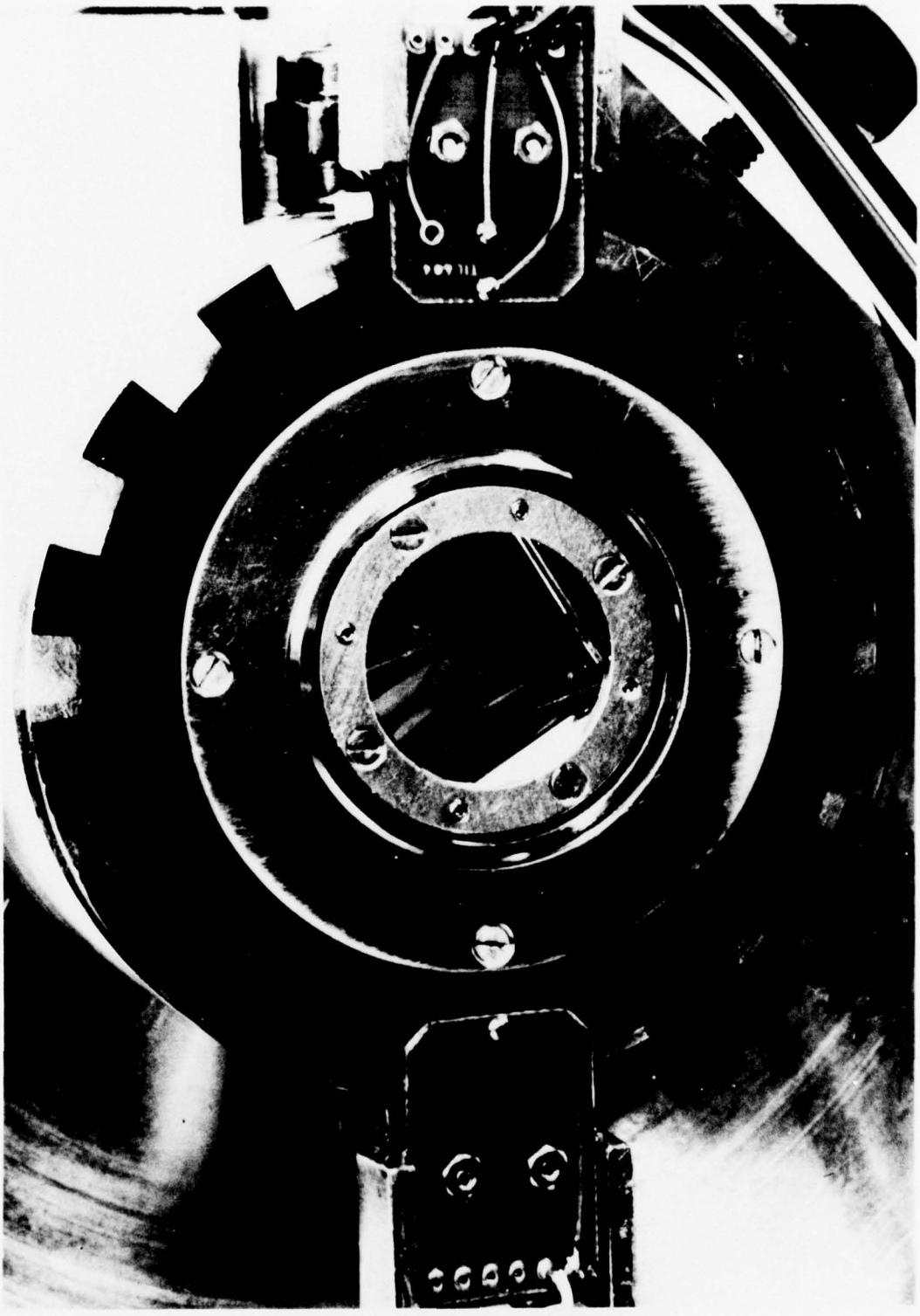

Fig. 9 Angle Encoder Disk (Installed on Derotator)

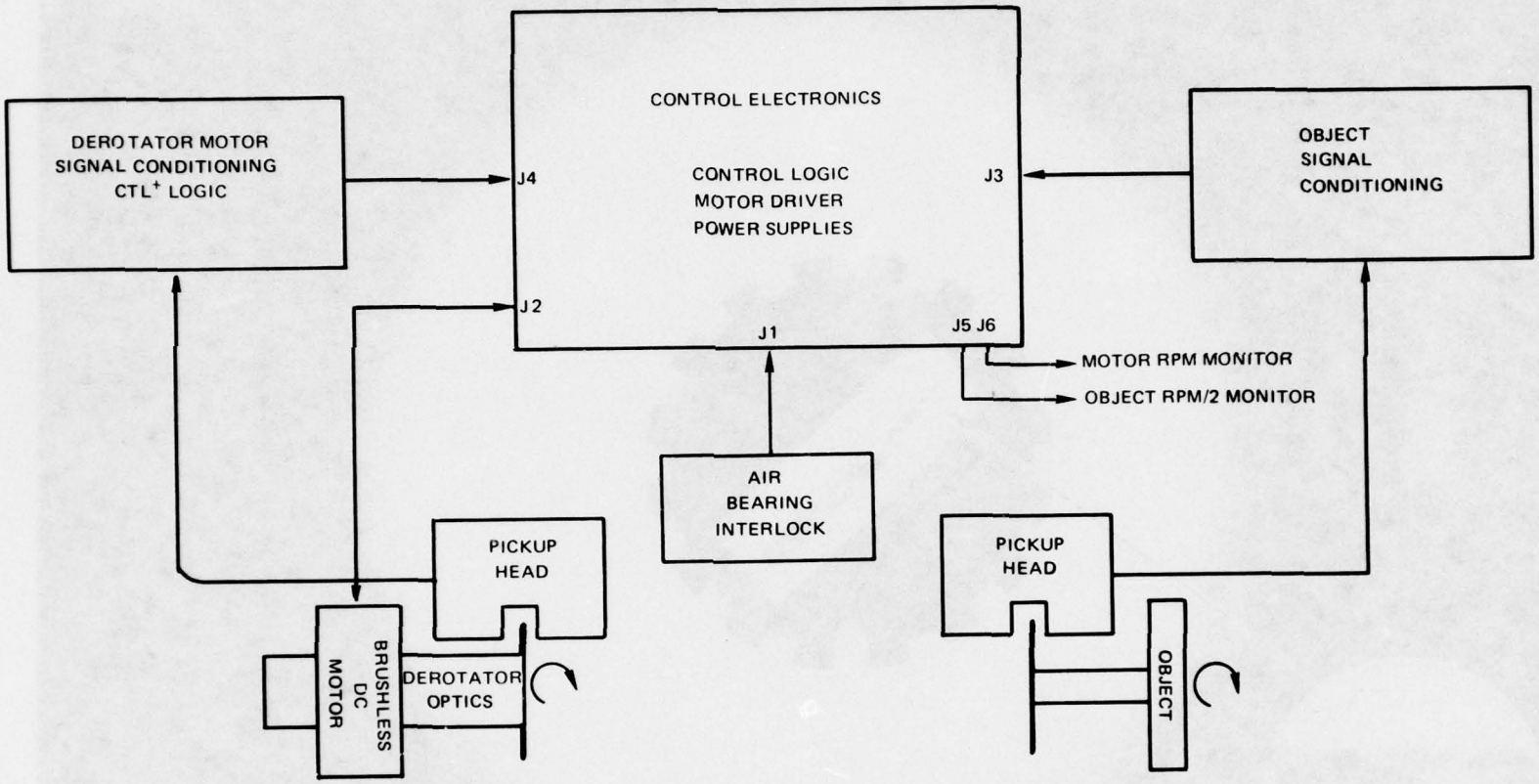

Fig. 10 Interconnection Block Diagram

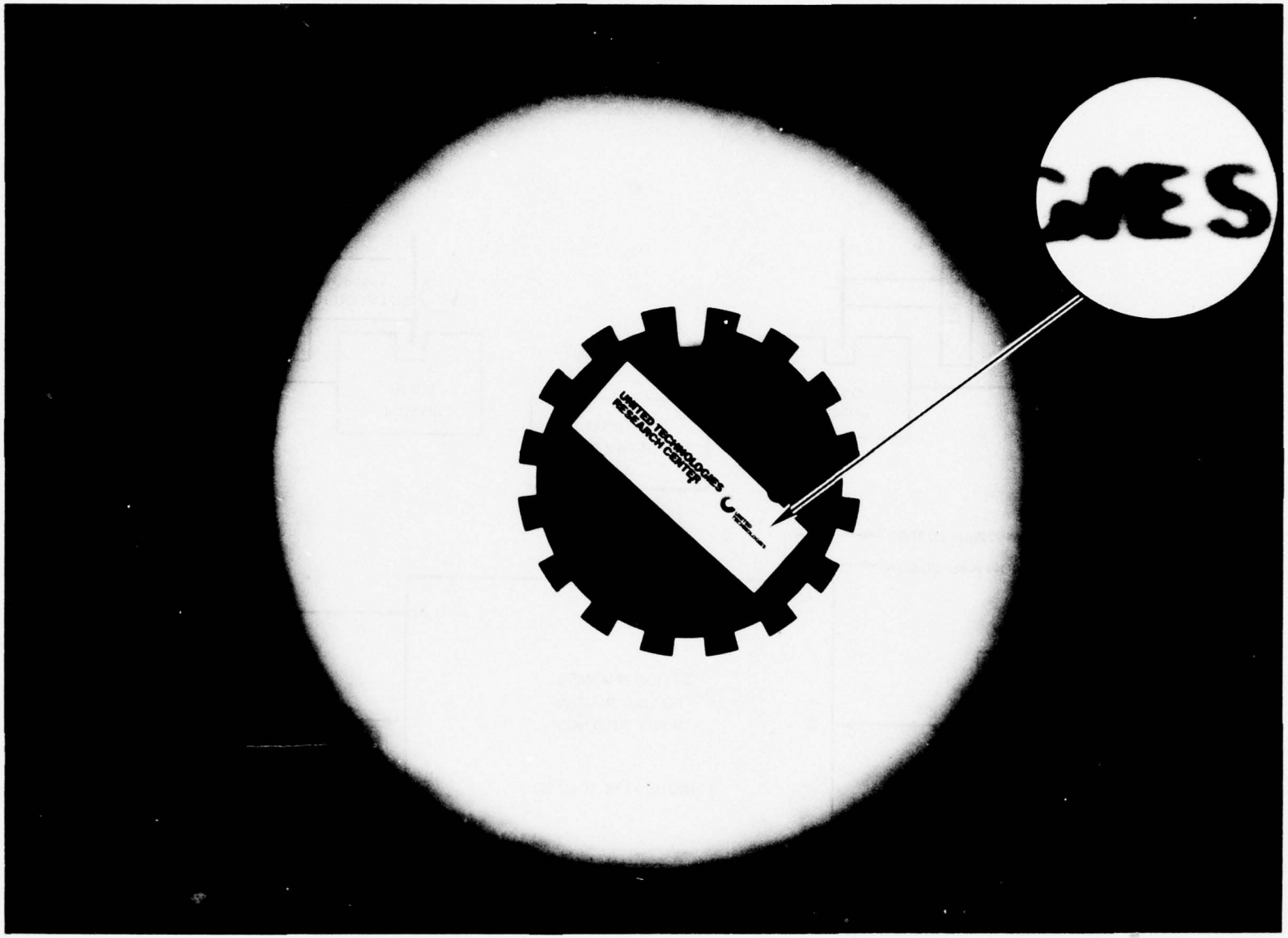

Fig. 11 Derotated Image Test Object Speed - 5000 RPM

tests, it was learned that there is no degradation of the image due to vibration, even at top speed (10,000 rpm on the object, 5,000 rpm on the derotator). Consequently, system evaluation tests were initiated to investigate its applicability to performing dynamic measurements on rotating structures using the optical techniques of moiré interferometry, hologram interferometry and speckle photography.

SECTION V

LABORATORY SYSTEM APPLICATION

Following the design study and system fabrication of the laboratory model, the image derotator was evaluated with regard to its applicability for performing dynamic measurements on rotating structures using moiré techniques, hologram interferometry, and speckle photography. A photograph of typical test objects used throughout these evaluation studies is presented in Fig. 12. Interferometric holograms, depicting the vibration mode patterns of flat bladed disks, canted blade disks and circular disks, using both moiré and direct data readout procedures, were recorded and reconstructed. While the majority of this laboratory testing phase was done in the 2000 to 3000 rpm speed range for convenience, successful interferometric holographic tests were conducted on circular disks at rotational rates in excess of 9000 rpm. In addition, multiple-pulse holographic techniques were used to ascertain the phase of the vibratory motion of rotating structures, and speckle photographs of rotating objects were recorded and optically processed to calculate bending strain. Further, the use of speckle methods for the real-time observation of the vibration mode patterns of rotating structures was also demonstrated. The results of this phase of the work are reviewed in the present section, with further details and additional examples previously reported in Ref. 1c.

Holographic Investigations

A schematic diagram of the optical system used to record interferometric holograms is presented in Fig. 13. As can be seen, the setup is quite conventional, using a beam splitter to provide the object and reference beams, along with the requisite turning mirrors for beam steering and path length matching, and a lens for diverging the object beam to fully illuminate the test object. It should be noted that the beam splitter is positioned directly in front of the objective lens of the derotator assuring that object illumination is from the axis of the derotator.

Bias Fringe and Moiré Techniques

Care must be exercised in the alignment of the derotator axis relative to that of the object's rotation axis. For direct vibration pattern recording (with double-pulse interferometric holography) these two rotation axes must be colinear, whereas slight misalignment will create a wedge of phase variation through which the object rotates, yielding a reconstruction with cosinusoidal fringes (bias fringes) modulating the image. The number of bias fringes obtained will be directly proportional to the degree of misalignment, laser pulse separation, and object speed.

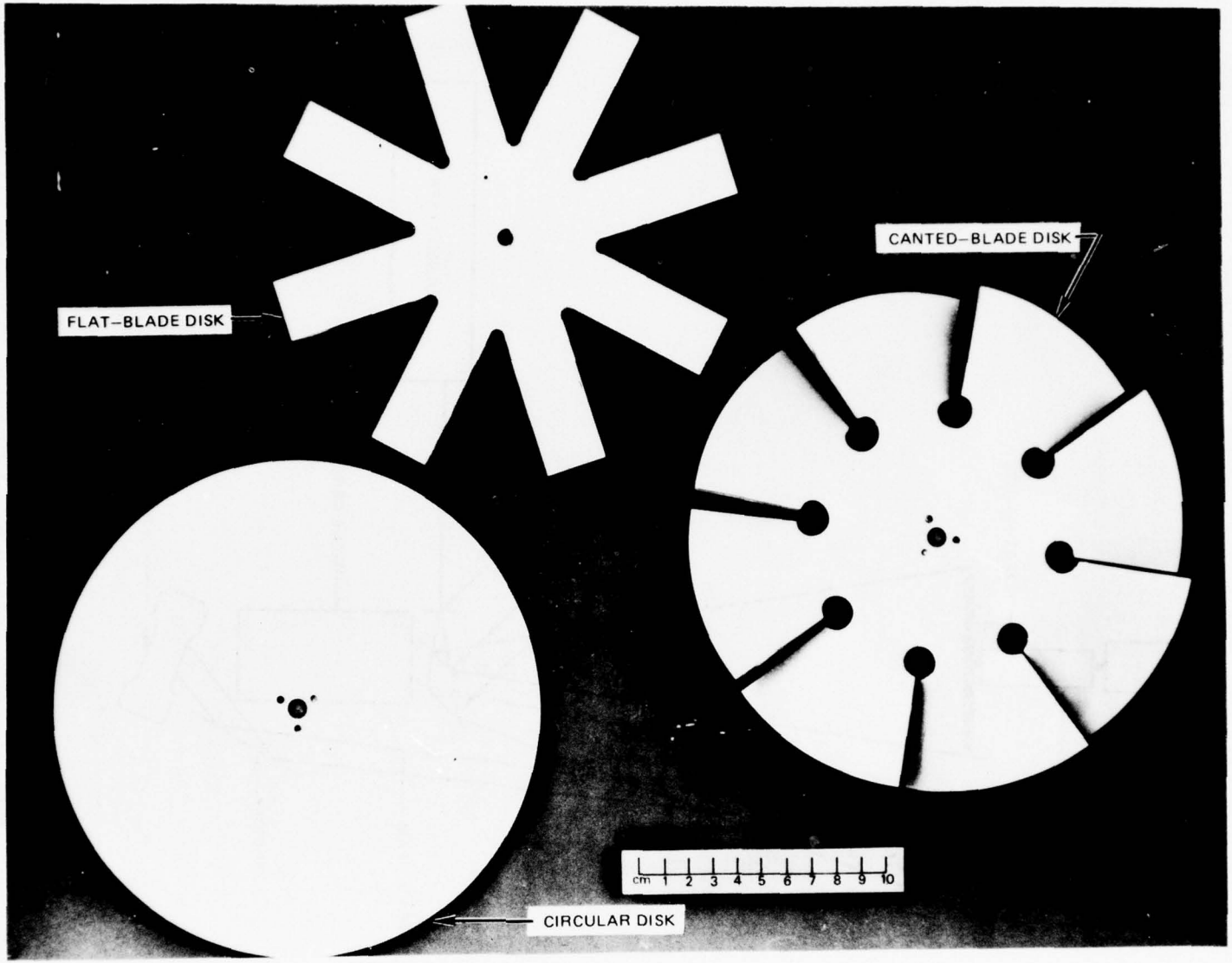

Fig. 12 Typical Test Objects for Rotating Structures Studies

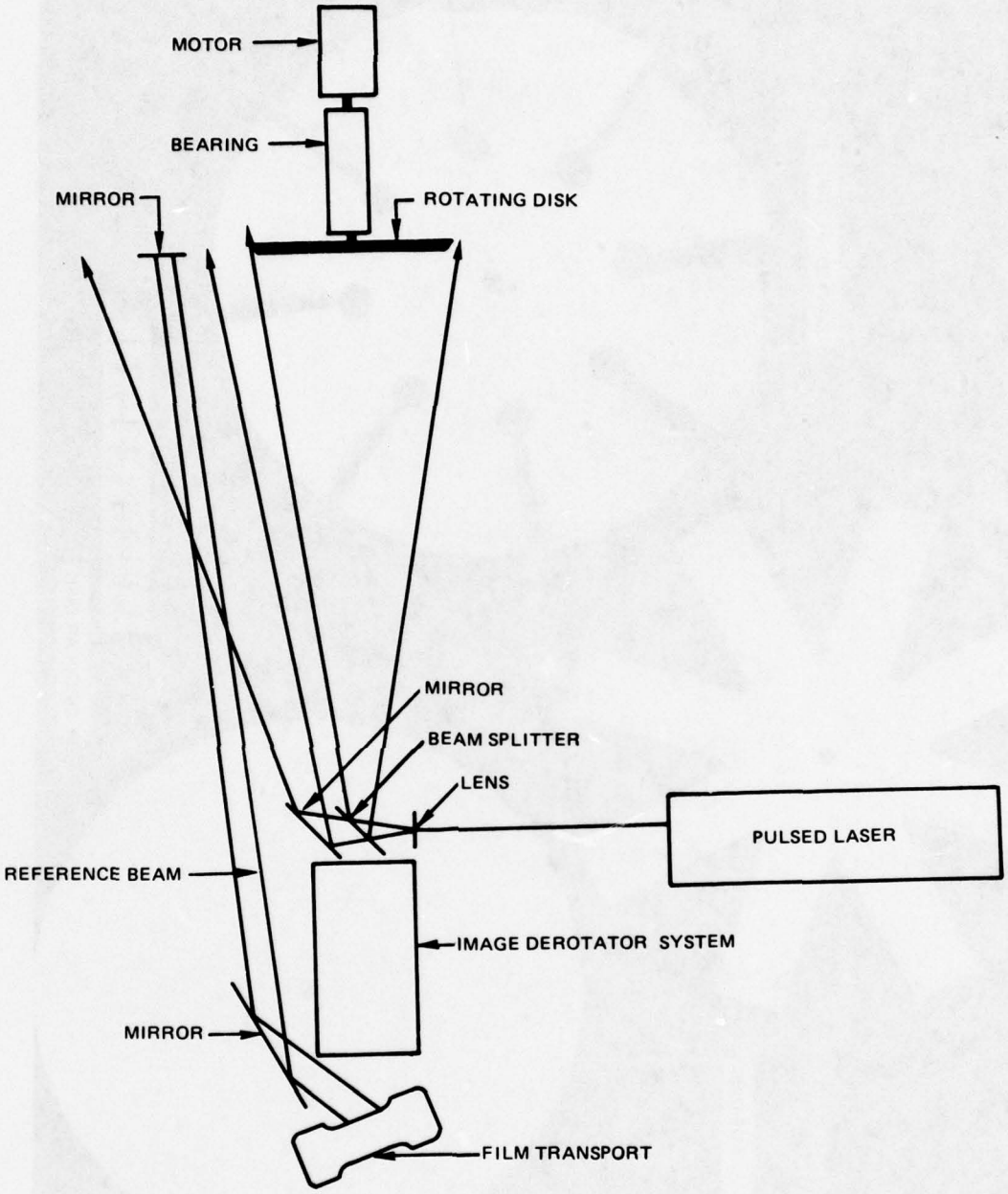

Fig. 13 Holographic Test Configuration Rotating Structures Analysis

These bias fringes can be of considerable value when they become modified by vibration of the object. Thus, interferometric holograms were recorded with vibration stimulated in an 8 inch diameter spinning disk by an electromagnetic transducer. A typical reconstruction from one of these holograms, recorded of the three-diameter mode at approximately 1000 Hz is presented in Fig. 14. By taking a similar interferometric hologram of a nonvibrating disk, and subtracting the linear fringes so obtained from the result in Fig. 14, the desired information about the vibration mode could be obtained. This subtraction could be done most precisely on a digital computer. However, a quick experimental approach, to provide a visual interpretation of the mode pattern, is possible by making transparent grids from two reconstructions similar to Fig. 14 and overlaying them such that the fringes curve in opposite directions. The resultant moiré pattern corresponds to the contours of constant vibratory displacement. The bias fringes, in and of themselves, however, have a value that should not be ignored in that they permit interpolation between what would be the interference fringes obtained without them, and therefore, they allow more data to be taken at lower vibration amplitudes.

In general, however, it is necessary to be able to control the number of bias fringes introduced. By rotating the object slowly and observing the image of the objective lens aperture, the laser speckles in this plane could be seen to rotate about a central point. The center of rotation of this pattern could be moved to the center of the objective lens aperture by tilting the axis of rotation of the object. The exact point to which the center of rotation of the field should be moved could be determined by stopping the object and slowly rotating the derotator. Ideally, with the object rotating and the derotator in synchronization, there would be no precession of the field in the image of the objective lens aperture. Figure 15 shows reconstructions of the same object as in Fig. 14, but with the system adjusted for fewer bias fringes; the two-diameter, one-circumferential mode at two different points in the vibration cycle is shown, together with a nonvibratory result.

One of the ultimate applications of the derotator system is the examination of bladed disks of jet engines. Therefore, tests were conducted using a disk with blades having some cant to them. Figure 16 shows the reconstructions from interferometric holograms recorded of an eight-bladed disk whose blades were twisted to an angle of 25°. The bias fringes should remain straight and equally spaced, even through the object itself is contoured. This bladed disk was not purposely stimulated into vibration, but it appeared to derive some stimulus from the air and/or from the driving motor. Figure 16A shows very definite slanting of the fringes across the blades, indicating their motion, whereas Fig. 16B shows very little motion.

Direct Interferometric Holography

By reducing the number of bias fringes to one or two, it is possible to record directly a double-pulse interferometric hologram whose fringes represent contours

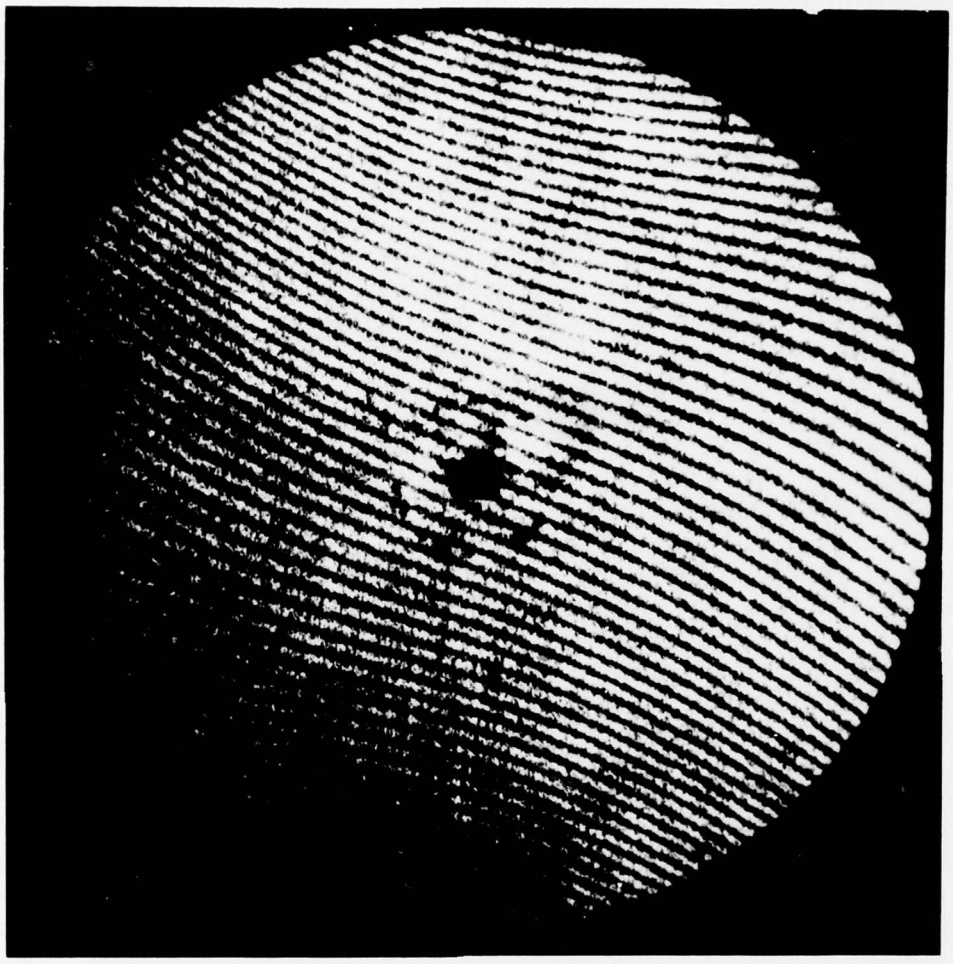

Fig. 14 8 In. Disk at 2000 RPM; a Double-Pulse Hologram of the 3-Diameter Mode at ∿ 1000 Hz (With Bias Fringes)

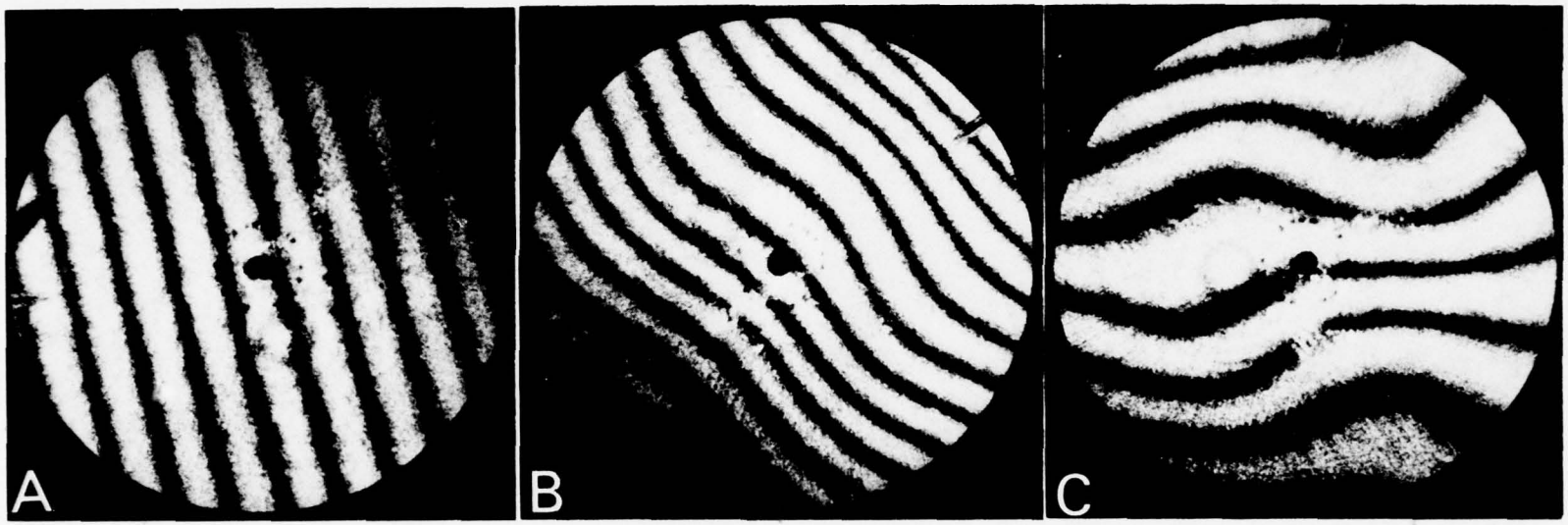

Fig. 15 8 In. Disk at 2000 RPM (Moderate Bias Fringing)
A - No Vibration
B & C - Vibration in 2-Dia., 1-Circ. Mode

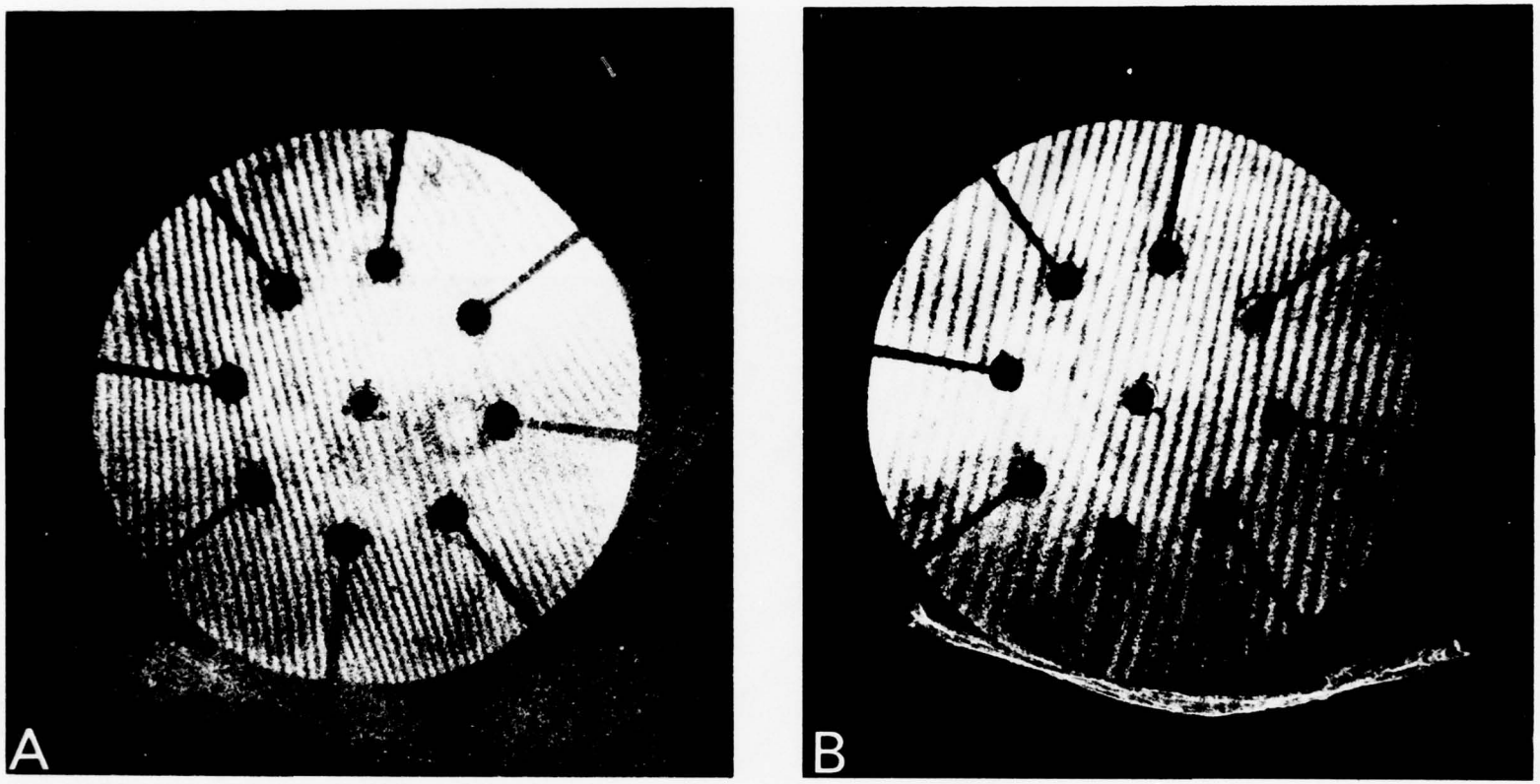

Fig. 16 Canted Blade Disk at 2000 RPM
A - With Blade Motion
B - Without Blade Motion

of constant vibratory displacement. An example to illustrate this technique, which depicts quite clearly the shape of the first three-diameter vibration mode of a circular disk rotating at 2000 rpm is presented in Fig. 17.

Further studies were conducted with the minimal bias fringing methods to obtain direct interferometric holograms of bladed disks. Since controlled excitation of a disk with canted blades posed some difficulties, a disk with eight flat blades lying in the plane of the disk was constructed. The central hub of the disk was .5 in. (12.5 mm) in thickness, and the blades were .22 in. (3 mm) in thickness. The overall diameter of the disk, including blades, was 8 in. (200 mm), and the aspect ratio of the blades was 7/3. The material was cold rolled steel so that resonant excitation could be obtained by placing a diametrically opposed pair of magnets near the tips of the blades and behind them. The magnets did not touch the blades, but they pulled upon them each time they passed.

At the proper speed of rotation (1800 rpm), the action of the blades passing the magnets caused a resonant excitation (600 Hz) of the first two-diameter mode. A reconstruction from one of the holograms recorded of this object under such a resonant excitation is shown in Fig. 18; note the pure bending of the four blades at 45° angles, and the relative inactivity of the vertical and horizontal blades.

By replacing the permanent magnets with an electromagnetic transducer, vibrations could be excited in the structure at any frequency. Thus, it was practical to excite the mode shown in Fig. 19 at 3100 Hz wherein the blade motion is essentially torsional. It is presumed that the blade asymmetries assert themselves more at this higher frequency and give a less symmetrical vibration mode than that depicted in Fig. 18.

The majority of the experiments were conducted at relatively low rotation speeds (2000 to 3000 rpm) in the interest of safety and convenience. To demonstrate the operation of the system at higher speeds, however, tests were run in the 5000-6000 rpm and 9000-10,000 rpm ranges. Two reconstructions from interferometric holograms recorded of a 6.5 in. (165 mm) disk spinning at 8900 rpm and 9200 rpm are presented in Figs. 20A and 20B, respectively. Excitation is derived from the air and/or from the drive motor. At 8900 rpm, the disk seems to be vibrating in a mode whose shape is similar to an umbrella. It is difficult to analyze the pattern at 9200 rpm without numerical analysis, but the results, as presented in Fig. 20, do establish that the system does indeed perform as anticipated at high rates of rotation.

Multiple-Pulse Holographic Studies

In many situations it will be important to know the phase of vibratory motion of the different parts of a rotating structure. It is important to note that in all the work discussed to this point, it has not been possible to tell whether the vibrations shown are of fixed orientation with respect to the disks, or whether they

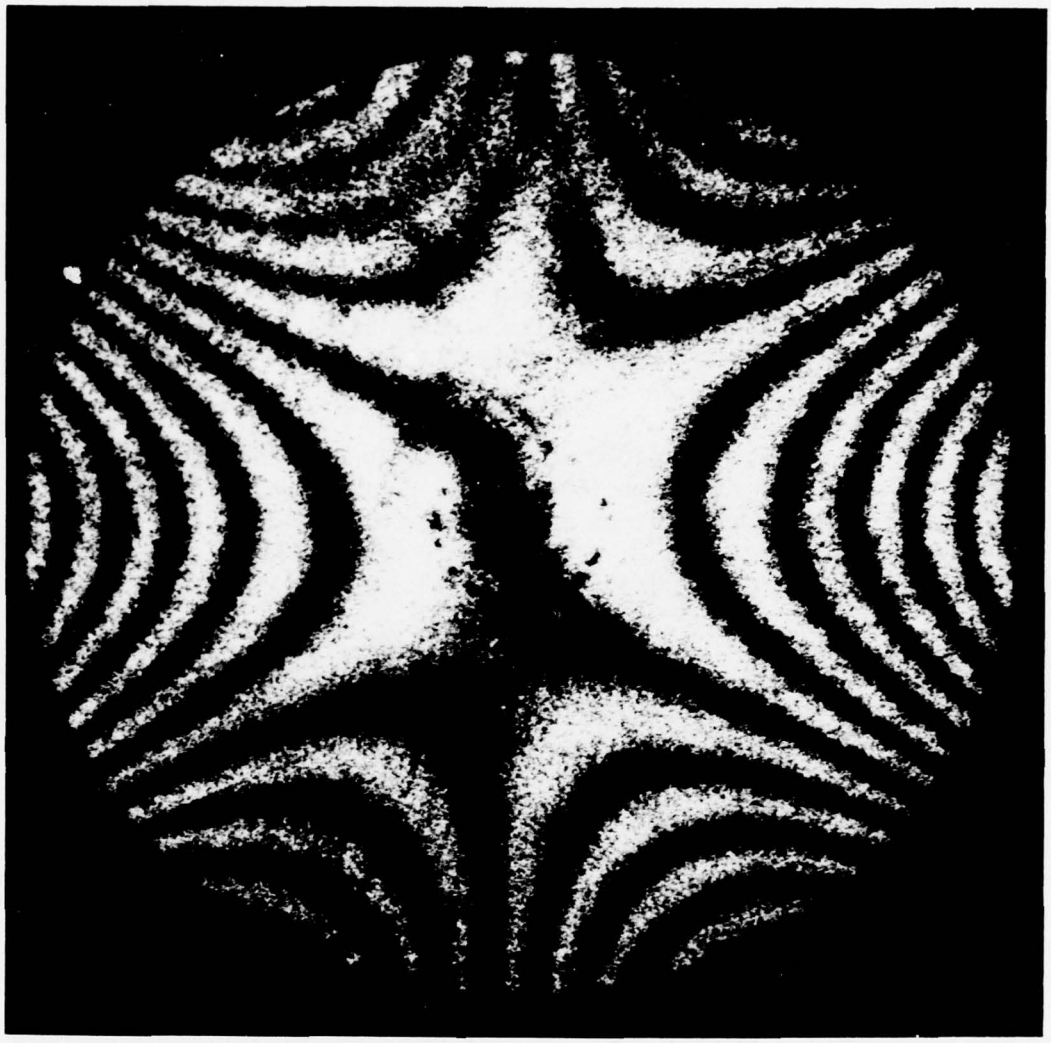

Fig. 17 8 In. Disk at 2000 RPM; a Double-Pulse Hologram of the 3-Diameter Mode at ∿ 1000 Hz (Adjusted for Minimal Bias Fringing)

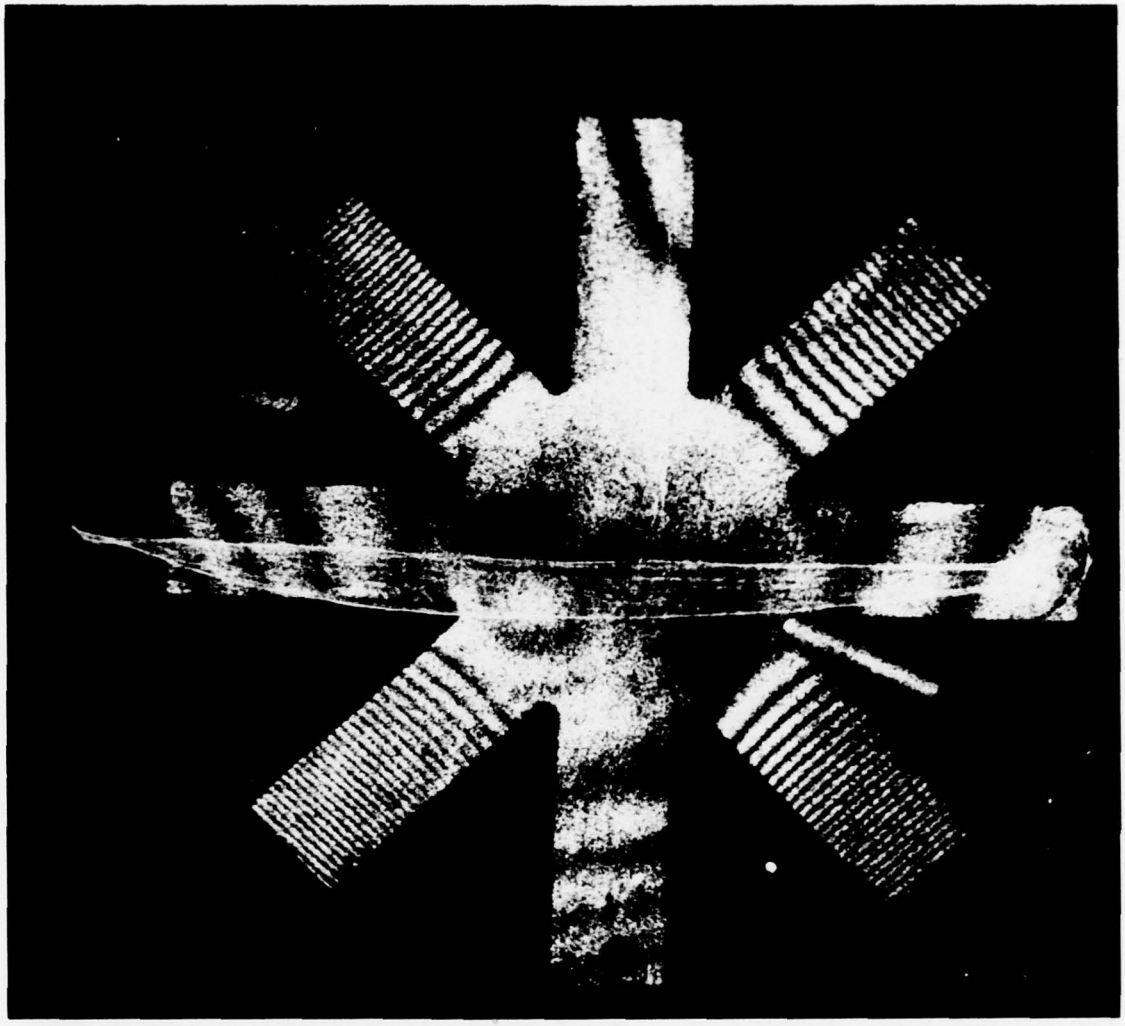

Fig. 18 Dynamic Vibration Analysis - 1800 RPM; a 2-Diameter Flap Mode at 600 Hz Resonant Vibration

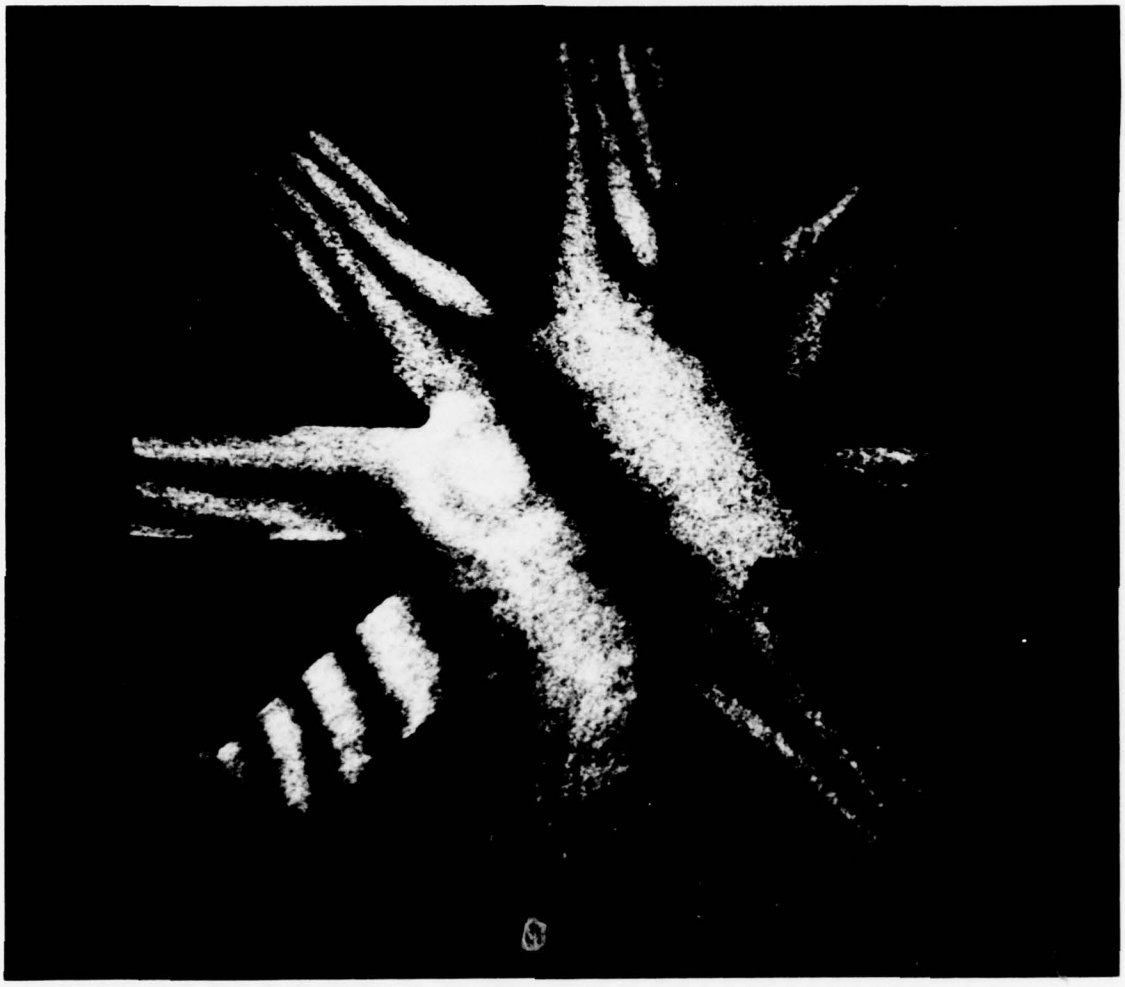

Fig. 19 Dynamic Vibration Analysis - 2400 RPM; 1st Torsional Mode at 3100 Hz Excited Vibration

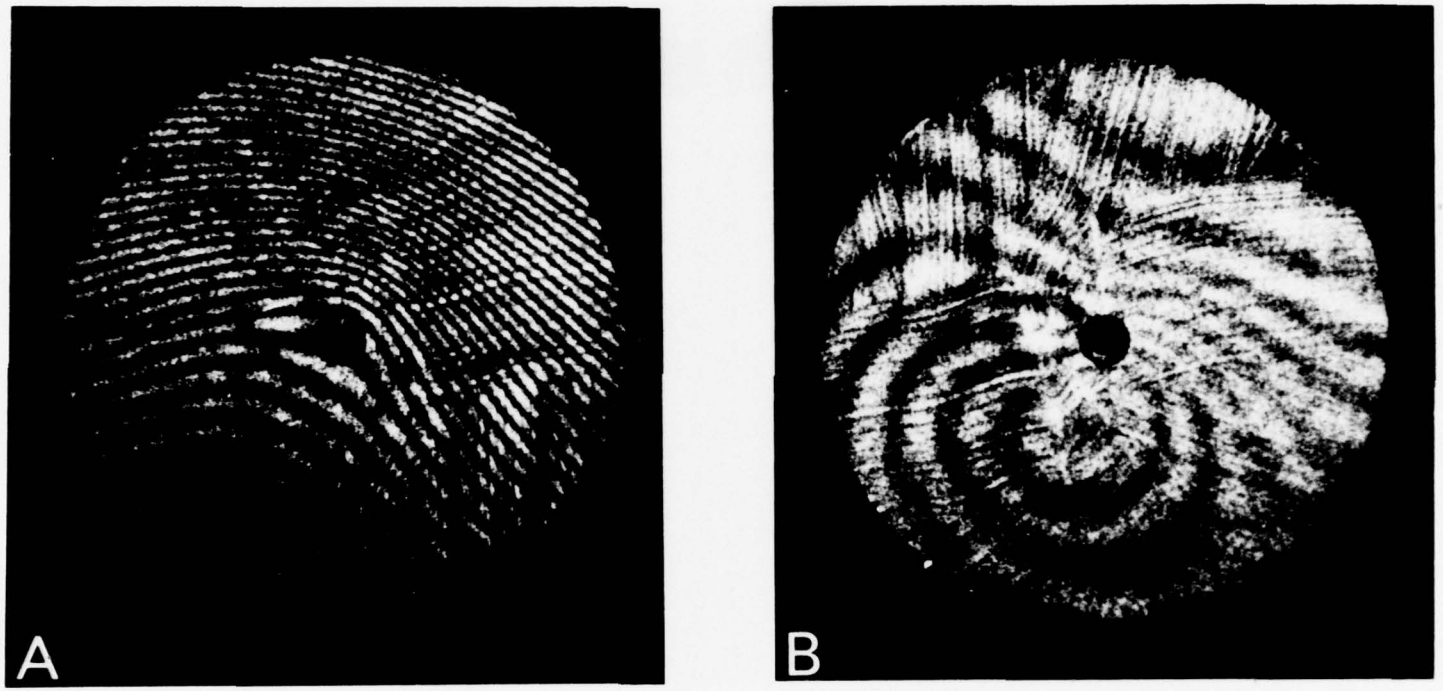

Fig. 20 Interferometric Holograms of 6-1/2 In. Disk
A - 8900 RPM
B - 9200 RPM

are traveling around them. If fixed, the contours shown would be contours of constant vibration amplitude, but if the vibration pattern is traveling, they would be contours of constant vibration slope. This makes quite a difference in any analysis to be performed with the resulting data. To determine the vibration phase, multiple-pulse holographic techniques were investigated. It can be said that, with three laser pulses, a considerable difference can be expected in the resultant fringe pattern, depending upon whether the object approaches and recedes from a vibration maximum, or passes at a constant velocity through a rest position during the three-pulse interval. A short analysis (Ref. 1c) of triple-exposure holograms of vibrating objects indicates that a straightforward interpretation of the resulting patterns is possible.

Thus, triple-pulse holograms were recorded of the eight-inch disk, rotating at 2000 rpm and vibrating in its three-diameter mode; a typical reconstruction is shown in Fig. 21. First, it can be seen in the variation from uninterrupted to interrupted fringes across the disk that the illumination beams formed by the three-pulses did not all have the same amplitude distribution across the disk. Second, the fact that the fringes do appear interrupted indicates that the disk was definitely not vibrating with all portions moving in or out of phase. Were this so, the fringe contours would be the same as in Fig. 17 and would be essentially unbroken, albeit the fringes would no longer be sinusoidal. It can be said that the moiré patterns appearing in the fringes of Fig. 21 represent the true contours of constant vibration amplitude at the instant of the central pulse. The fine interference fringes show the contours of constant vibration slope. From an inspection of the figure it can be concluded that this was, indeed, a wave traveling around the disk.

Speckle Investigations

In many applications of any experimental technique for vibration analysis of rotating structures, it may be expected that large vibration amplitudes may be encountered. This may be dealt with, to some extent, in double-pulse holography by reducing the time interval between pulses. There are practical limits to this, however; e.g., it may be difficult to reduce the pulse separation to less than 10 microseconds. On the other hand, speckle photography can be used to detect and measure vibrations at amplitudes that are quite large relative to holography, and a considerable number of techniques are available (Ref. 15). It was decided, therefore, to record speckle photographs of rotating objects using the image derotator and the double-pulse laser. Because it could be presumed that no transverse motion of the derotated image was likely to occur during the pulse interval of 100 microseconds, it was decided to record a single defocused speckle photograph according to the method described by F. P. Chiang and R. M. Jung (Ref. 16). This makes use of the fact that speckles move in front of an object lit by laser light in proportion to the tilting of the object surface. Separation of identical speckles in the resulting specklegram give an indication of the change in surface slope between the exposures

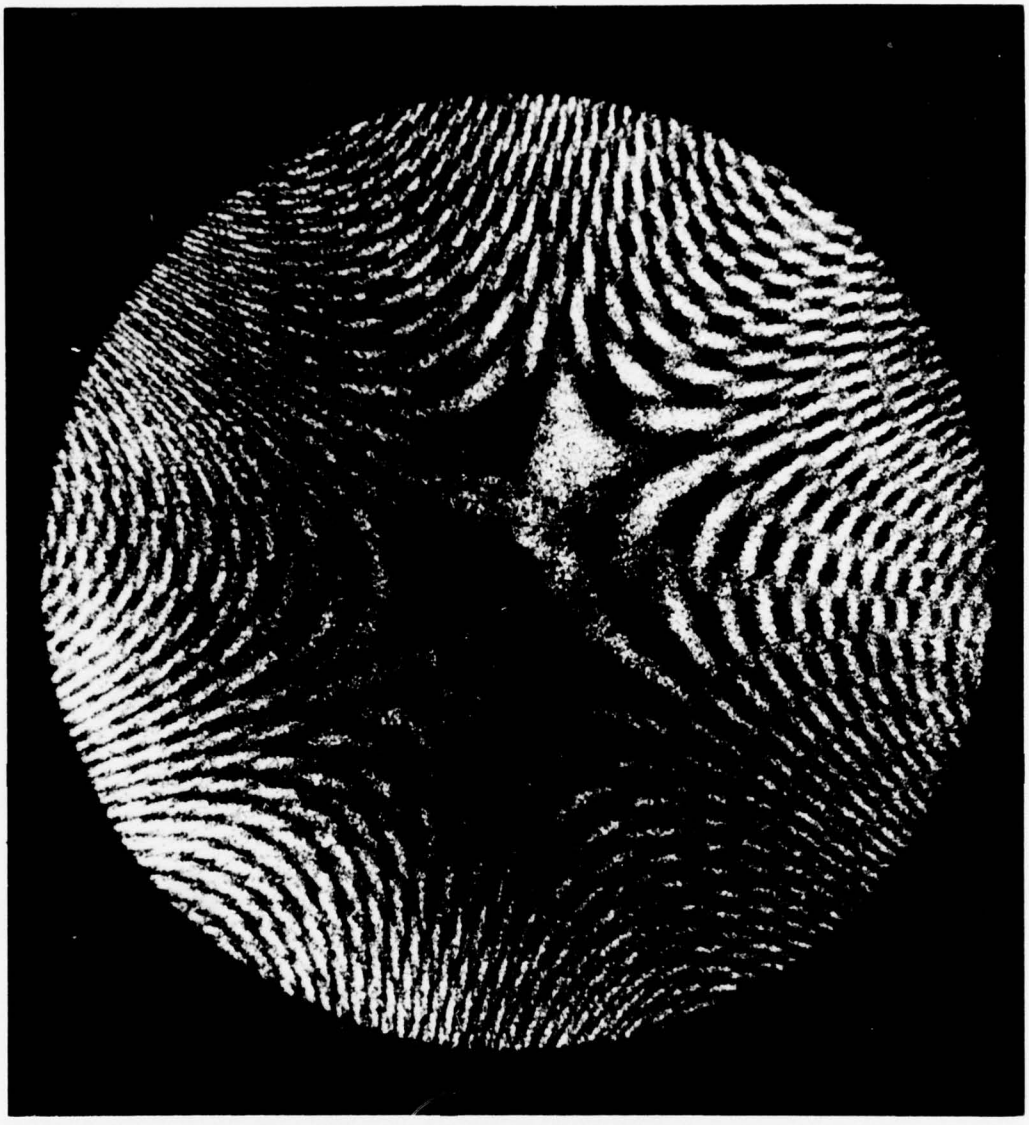

Fig. 21 8 In. Disk in 3-Diameter Mode (2000 RPM); Triple-Pulse Hologram; Moiré Fringes-Lines of Constant Vibration Amplitude; Interferometric Fringes-Lines of Constant Slope

of the specklegram. The speckle separations can be measured easily by performing an optical Fourier transform on a small region of the specklegram, and measuring the fringe spacing that occurs in the halo of scattered light around the zeroth diffraction order.

Specklegrams were recorded of the eight-inch disk, spinning at about 3000 rpm and vibrating in the first three-diameter mode, with the camera focused 8 in. (200 mm) in front of the disk. Two sets were recorded as double exposures, one set with vibration and one without vibration; and two sets were recorded as triple exposures, one set with vibration and one without vibration. The pulse intervals were 100 microseconds. The specklegrams recorded without vibration indicated that, as expected, there was little if any motion to the speckles between exposures. Halo fringes were observed, however, within the transform plane of the specklegrams recorded with vibration. Cosinusoidal fringes were seen from the double-exposure specklegrams, and three-beam fringe patterns were seen from the triple-exposure specklegrams. Figure 22 shows three sets of halo fringes taken from one of the double-exposure specklegrams.

Bending Strain Calculations

The data available from the defocused specklegrams is in a form that is particularly suitable for the analysis of bending strain. The speckle displacements, which are determined from the fringes in the diffraction halos, are directly proportional to surface tilt of the flat disk which was photographed. By measuring the tilts at three locations on the disk, spanning an incremental change in the x-coordinate and an incremental change in the y-coordinate, finite difference theory may be used to determine the bending strain and shear.

The procedure is as follows. Linear functions of x and y are first fitted to the fringes in the halos; i.e., functions of the form Ax+By. The coefficients of the fit determine a halo fringe vector, $\underset{=}{F}_h$, where

$$\underset{=}{F}_h = \hat{i}A + \hat{j}B. \tag{1}$$

The magnitude of this vector equals the reciprocal of the fringe spacing. The image speckle displacement, $\underset{=}{H}_i$, equals the wavelength, λ_c, times the halo fringe vector, times the distance from the specklegram to the halo, R_h,

$$\underset{=}{H}_i = \lambda_c R_h \underset{=}{F}_h. \tag{2}$$

The speckle displacements in front of the object are proportional to the gradient of the out-of-plane displacement of the object surface, L_z, by the relationship:

$$\text{Grad}(L_z) = iL_z^x + jL_z^y = \underset{=}{H}_{ob}/2D_{ob} \tag{3}$$

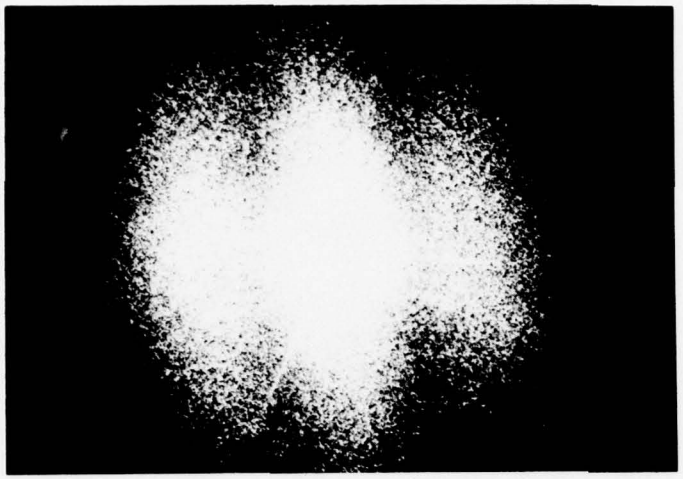

HALO FROM Y

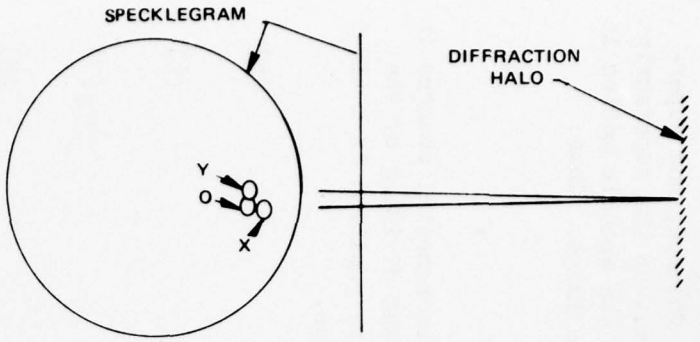

LASER BEAM INTERROGATION OF SPECKLEGRAM
TO OBTAIN DIFFRACTION HALOS
FROM 3 POINTS

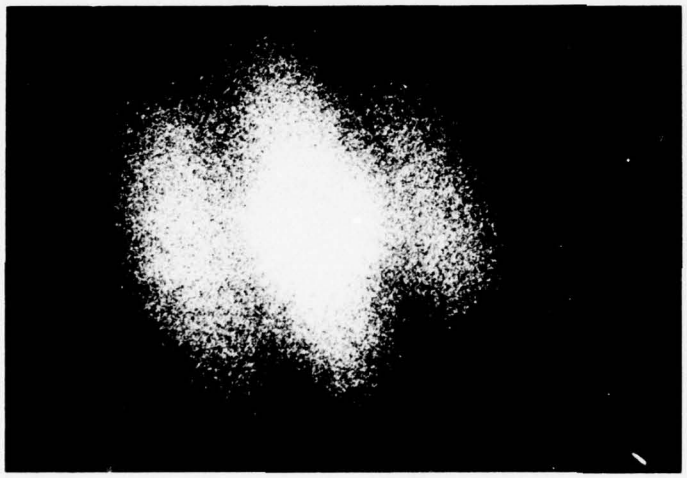

HALO FROM O

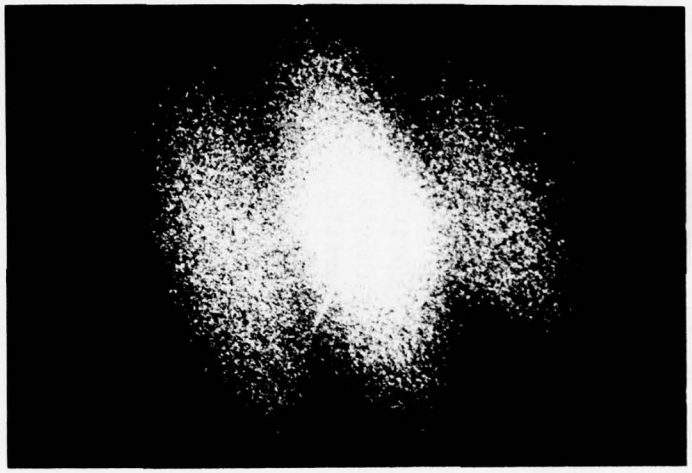

HALO FROM X

Fig. 22 Experimental Prologue to Bending Strain Calculation

where $\underset{\sim}{H}_{ob}$ is the speckle displacement in front of the object, D_{ob} is the distance in front of the object to the plane upon which the camera is focused, and superscripts are used to denote partial differentiation with respect to the superscript variable. The speckle motion in the object space is m times the speckle motion in the image space, where m is the demagnification factor of the image. Thus:

$$\text{Grad}(L_z) = \underset{\sim}{F}_h \lambda_c R_h m/2D_{ob}. \tag{4}$$

The four second partial derivatives are found by taking the incremental changes in the first partials as a function of position on the object, and dividing by the incremental changes in position. On the object, the change in position is m times that on the specklegram, which cancels the m in Eq. (4). Thus,

$$L_z^{xx} = (\lambda_c R_h/2D_{ob})\ (A_x - A_o)/\Delta x_i \tag{5}$$

$$L_z^{yy} = (\lambda_c R_h/2D_{ob})\ (B_y - B_o)/\Delta y_i \tag{6}$$

$$L_z^{xy} = (\lambda_c R_h/2D_{ob})\ (A_y - A_o)/\Delta y_i \tag{7}$$

$$L_z^{yx} = (\lambda_c R_h/2D_{ob})\ (B_x - B_o)/\Delta x_i\ . \tag{8}$$

The crossed partial derivatives, Eqs. (7) and (8), should give the same value in the absence of any misalignment of the sort that would give bias fringes. If, in practice, they are not equal, the correct value is easily obtained by taking their average. This is because the bias fringes are analogous to a rotation of the object in its own plane, which would give crossed partials of equal magnitude but opposite sign.

The specklegram halos shown in Fig. 22 were analyzed by the procedure outlined above and the results are:

$$L_z^{xx} = 2.372 \times 10^{-6}\ (\text{mm}^{-1})$$

$$L_z^{yy} = 0.7399 \times 10^{-6}\ (\text{mm}^{-1})$$

$$L_z^{xy} = -3.489 \times 10^{-6}\ (\text{mm}^{-1}).$$

The principle coordinates were found to lie at an angle of 39° to the ones used, and the principle second derivatives were found to be 6.0765×10^{-6} and $-.7445 \times 10^{-6}$ (mm^{-1}). It is important to note that the principle second derivatives are of opposite sign, indicating anticlastic bending, which should be expected for

modes with no circumferential node lines. It may be assumed that the principle bending would be in the tangential direction, and from this the number of fringes may be estimated under the assumption that the data was taken at an antinode. Such a calculation indicates that there would have been 21 fringes from the center to the antinode at the edge had a hologram been recorded. This is quite in keeping with the known level of excitation for this recording relative to that used in the hologram recordings.

Concomitant Observation of Rotating Structures

A number of methods were tried to observe vibration through the derotator concomitantly; however, any method that required preserving long-term interferometric stability or continuous illumination failed. Finally, a successful method was found that merely required illuminating the object stroboscopically, and observing the object out of focus. The method simply requires viewing, directly, the type of pattern that had been recorded previously as a defocused specklegram. If the vibration is large enough, the streaking of the speckles can be seen directly, giving an indication of the presence and shape of the vibration. The stroboscopic illumination was required in order to acquire a speckle field that would not focus, but could be observed at all planes along the optical axis.

The synchronous gating of the laser beam was accomplished by drilling a hole in the object disk under study, and passing the laser beam through it. Ultimately, the code wheel of the derotator could be used to provide the gating of the laser by means of two diametrically opposed holes. Figure 23 shows a photograph as taken of one of these patterns which was observable through the derotator. (It should be noted that the speckle streaking is much more evident in practice than it is in the photograph; a not uncommon occurrence in the photographic recording of real-time speckle and holographic experiments.)

Fig. 23 Photograph of Speckle Pattern; Observable in Real Time, a 4-Diameter Vibration Mode of a 6-1/2 In. Disk at 3000 RPM

SECTION VI

TEST STAND STUDY

Having established the feasibility of applying hologram interferometry and speckle photography to the dynamic analysis of rotating structures, a brief study was undertaken to examine the requirements for a test stand model of the image derotator system. Of primary concern were the additional adjustments considered to be necessary to provide the versatility in installation and alignment required to facilitate field operation. In particular, more versatility was desired in the axial alignment procedure associated with the rotating prism assembly, and additional adjustment capability for the optical beam illuminating the rotating structure under test was necessary to facilitate making the axes of the rotating object and derotator colinear. The latter requirement necessitated the incorporation of angular tilt and rotation, as well as horizontal and vertical translation, in the outgoing beam.

Relative to the axial alignment procedure for the rotating erector prism, the heart of the image derotation system, several changes were deemed necessary for test stand operation. The more important items in this area included the following:

1. The inclusion of pads at the corners of the hypotense faces of the two 30° -60° -90° prisms to assure better alignment when assembled within their holder.

2. Fabrication of the prisms to assure that the optical axis of the system would be centered when they are mounted within a 1.000 inch holder.

3. Use of a square (rather than round) prism holder to fit within a slightly rectangular hole in the air bearing spindle, thereby centering the holder in one direction while permitting adjustment in the other.

4. Incorporation of access holes for cocking the 30° -60° -90° prisms within their holder after assembly into the air bearing.

In addition, the air bearing was redesigned to avoid resonances which existed in the laboratory model, and it was decided to replace the brush type dc motor with a brushless dc motor to provide more stable operation. Finally, provision was to be made for installing the 1/4 wave retarders outside the derotator, adjacent to the objective and copy lenses.

In order to facilitate alignment of the object and derotator axes of rotation, provision was to be made for axially centering all the optical mounts and, more importantly, it was decided to incorporate a large double-folding mirror assembly into the optical train to provide both coarse and fine adjustment of angular rotation, angular tilt, vertical translation, and horizontal translation. A schematic diagram of this last unit is included as Fig. 24, indicating the reasonably compact character of the method selected.

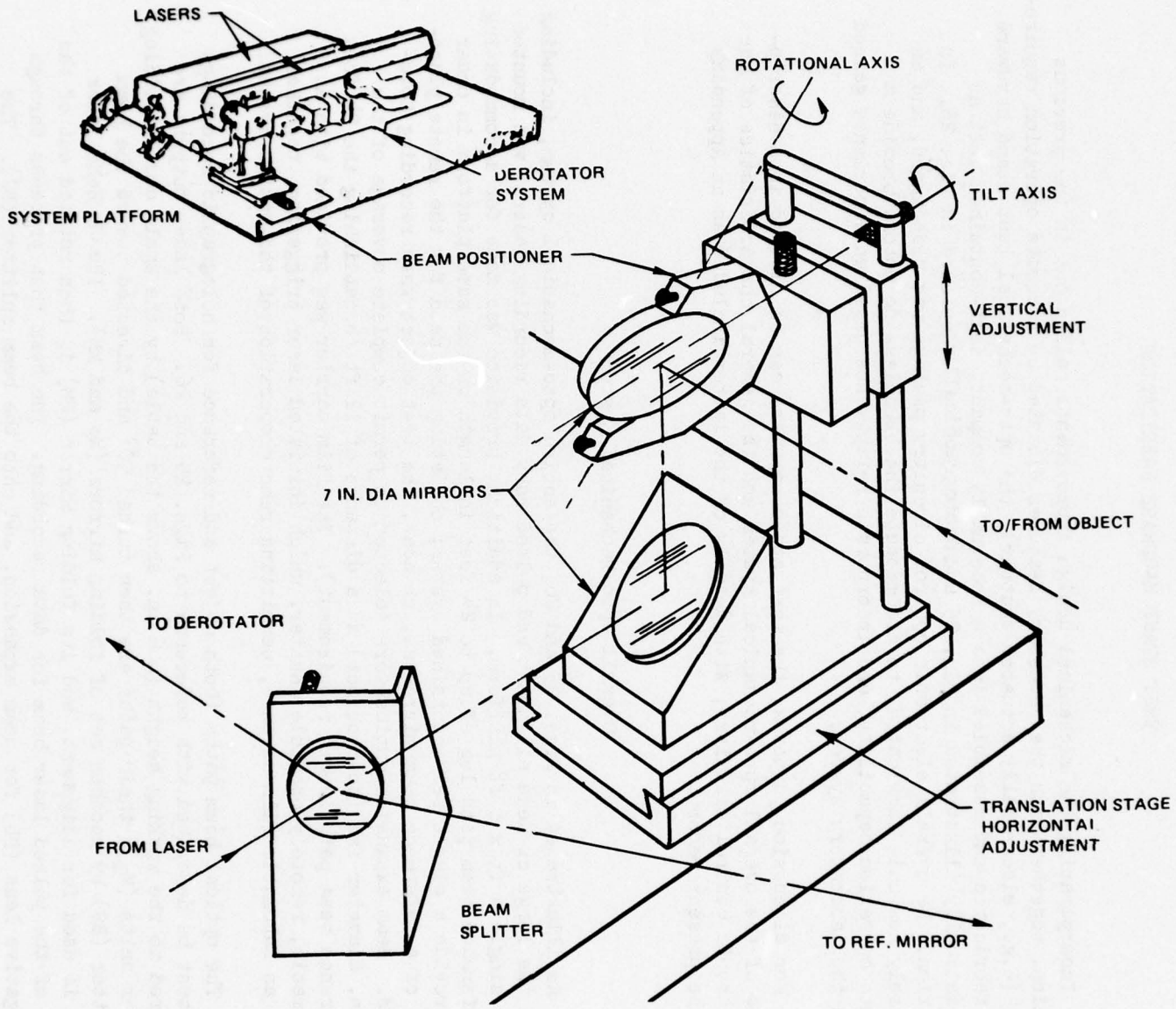

Fig. 24 Conceptual Layout - Test Stand Derotator System

SECTION VII

TEST STAND HARDWARE FABRICATION

Incorporating the mechanical design improvements called out in the previous section, together with the necessary features dictated by a remote operation requirement (e.g., electrically actuated shutter), the opto-mechanical test stand hardware was fabricated and assembled into a reasonably compact, self-contained unit as schematically illustrated in Fig. 25 and photographically depicted in Fig. 26. In addition, the overall electronic control circuitry package was redesigned, and an entirely new unit fabricated, to accommodate the brushless dc motor, provide a remote operation capability, and incorporate refinements based on experience gained with the laboratory system.

For discussion purposes, the test stand hardware can be divided into descriptions of the overall opto-mechanical system and the general characteristics of the electronic control circuitry, with details of the latter included as an Appendix to the present report.

Overall Opto-Mechanical System

As illustrated in Figs. 25 and 26, the entire opto-mechanical system, including both the large cw HeNe alignment and pulsed ruby data recording lasers, was mounted on a single 4 ft x 6 ft platform. In addition, provision was made for accommodating a reference beam path leg of up to 24 feet in length on the same platform in order to provide a single self-contained system; obviating the need for the remote placement of a reference beam mirror at, or near, the test object when recording holograms. Beam expansion optics were selected to permit complete coverage of the 32 in. diameter fan (test object) at a distance of 12 ft (establishing the 24 foot reference beam path length requirement). The film carrier was provided with an automatic, remotely operable shutter, which initiated laser triggering, together with an automatic film advance, permitting remote operation of the entire system.

The optical beam paths (both object and reference for holographic recording) can best be described with reference to Figs. 25 and 26. Both laser outputs are lowered to the working height ($\sim$ 6 in. above the table) by the small double-folding mirror units (M_1); their paths are then turned 90° and directed toward the beam splitter (BS) by another set of folding mirrors (M_2 and MM). The cw HeNe laser unit is used for alignment, and its folding mirror (MM) is then rotated out of the path of the pulsed laser beam for data recording. The beam then proceeds through a negative lens (DL) for beam expansion, and onto the beam splitter (BS). The transmitted light becomes the object beam, reflecting through the large double-folding mirror assembly (M_3) which directs it to the object. The reflected return

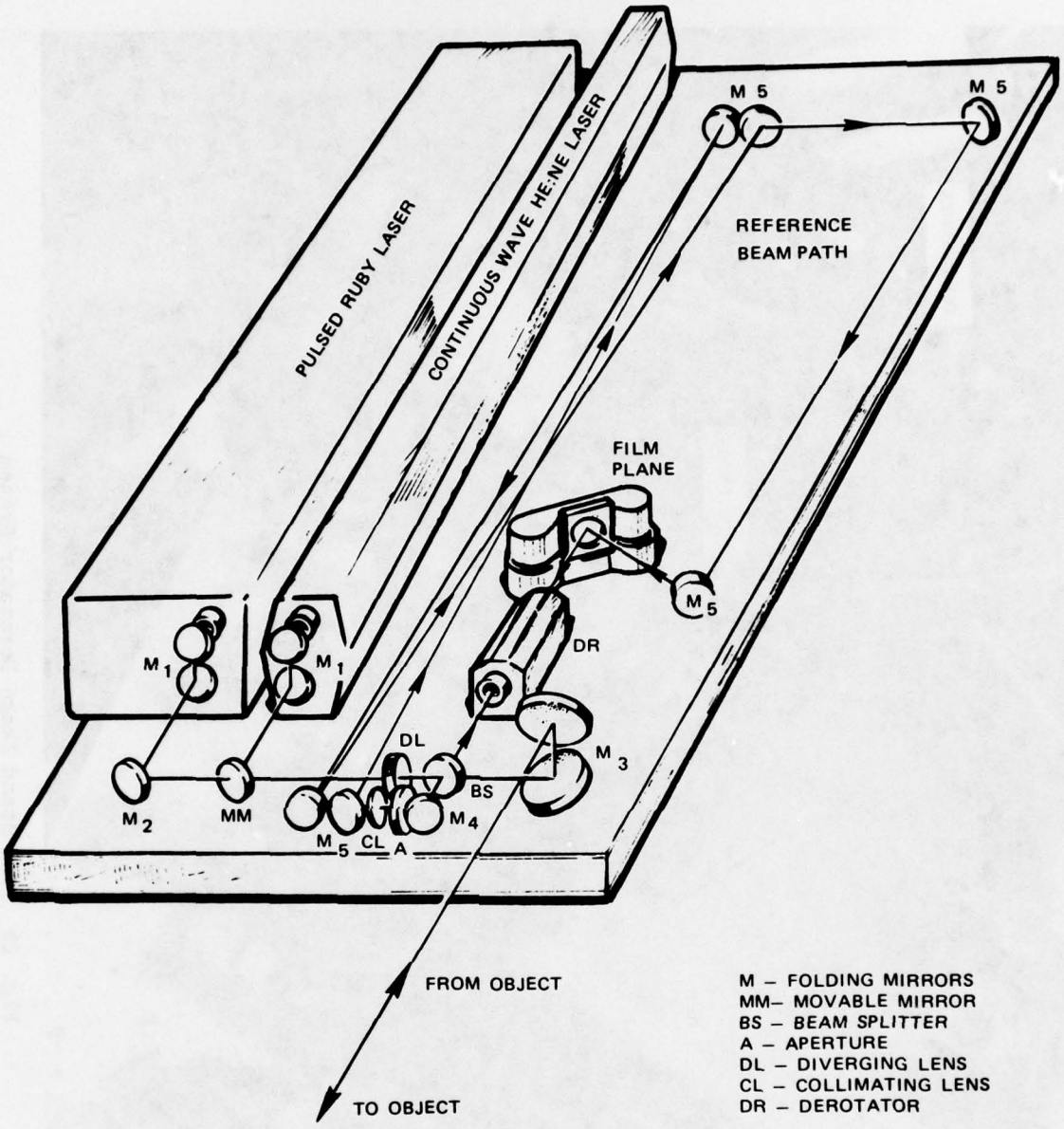

Fig. 25 Schematic of Overall Opto-Mechanical System

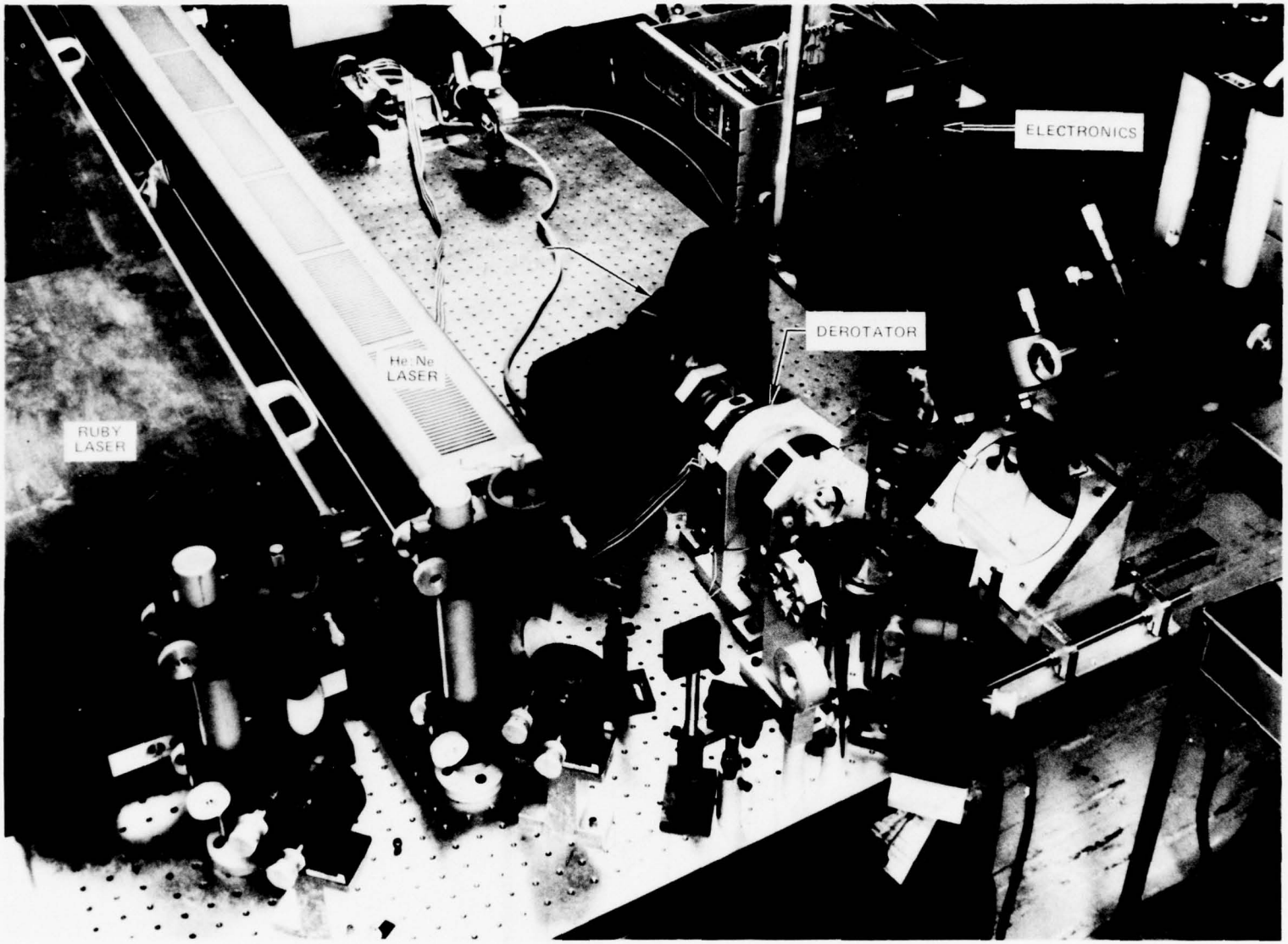

Fig. 26 Test Stand Image Derotator System

illumination from the object retraces the same path back to the beam splitter (BS) where it is directed into the image derotation unit (DR) and on to the film plane. The original beam of reflected light from the beam splitter (BS) serves as the reference beam, and is folded by mirror M_4, directed through an aperture (A) and collimating lens (CL), and folded an additional 6 times by mirrors M_5 to develop the 24 foot path length before striking the film plane. (For speckle interferometry work the reference beam leg is blocked off, and the film plane is rotated into a position normal to the light beam transmitted through the derotator.)

As noted earlier, a new air bearing assembly was specially designed and fabricated, by Dover Instrument Corp., for the test stand system to avoid some resonances which existed in the laboratory model; and the rotational drive was provided by a brushless dc motor for greater stability. The new unit is shown in both exploded and assembled views in Fig. 27. The motor stator is seen on the far left of the exploded view, separated from the rotor by a cylindrical mount. Also seen in the figure is the spindle, with its slightly rectangular hole to accommodate the prism unit, the air bearing itself, a retaining ring and thrust plate. A view of the air bearing assembly as it was mounted in the overall system, immediately in front of the film holder and automatic transport unit is presented in Fig. 28.

Electronic Circuitry

The test stand derotator electronics consist of an operator control chassis, a pickup head and remote signal conditioning electronics for the rotating object, a brushless dc motor which drives the derotation optics, a pickup head and remote logic and signal conditioning electronics for the derotator assembly, and a pressure monitor interlock for the derotator assembly air bearing. The operator control chassis houses the control logic, controls, readouts, derotator motor driver, and power supplies. A front panel and interior view of the control chassis are presented as Figs. 29 and 30, respectively. As with the laboratory model electronics, briefly described in Section IV, one of the remotely located detectors is used to provide rotation rate and rotational position information about the image derotator, while the other remotely located detector provides similar information about the rotating object, thereby providing the information needed by the control logic to synchronize the rotation rate of the image derotator to half the rotation rate of the object. Further, the control logic must maintain a fixed rotational phase relationship between the derotator and the rotating object, and a readout of the status of each.

System Description

A block diagram of electronic synchronization circuitry is presented in Fig. 31, and the overall interconnection diagram for the various electronic subassemblies was presented previously as Fig. 10.

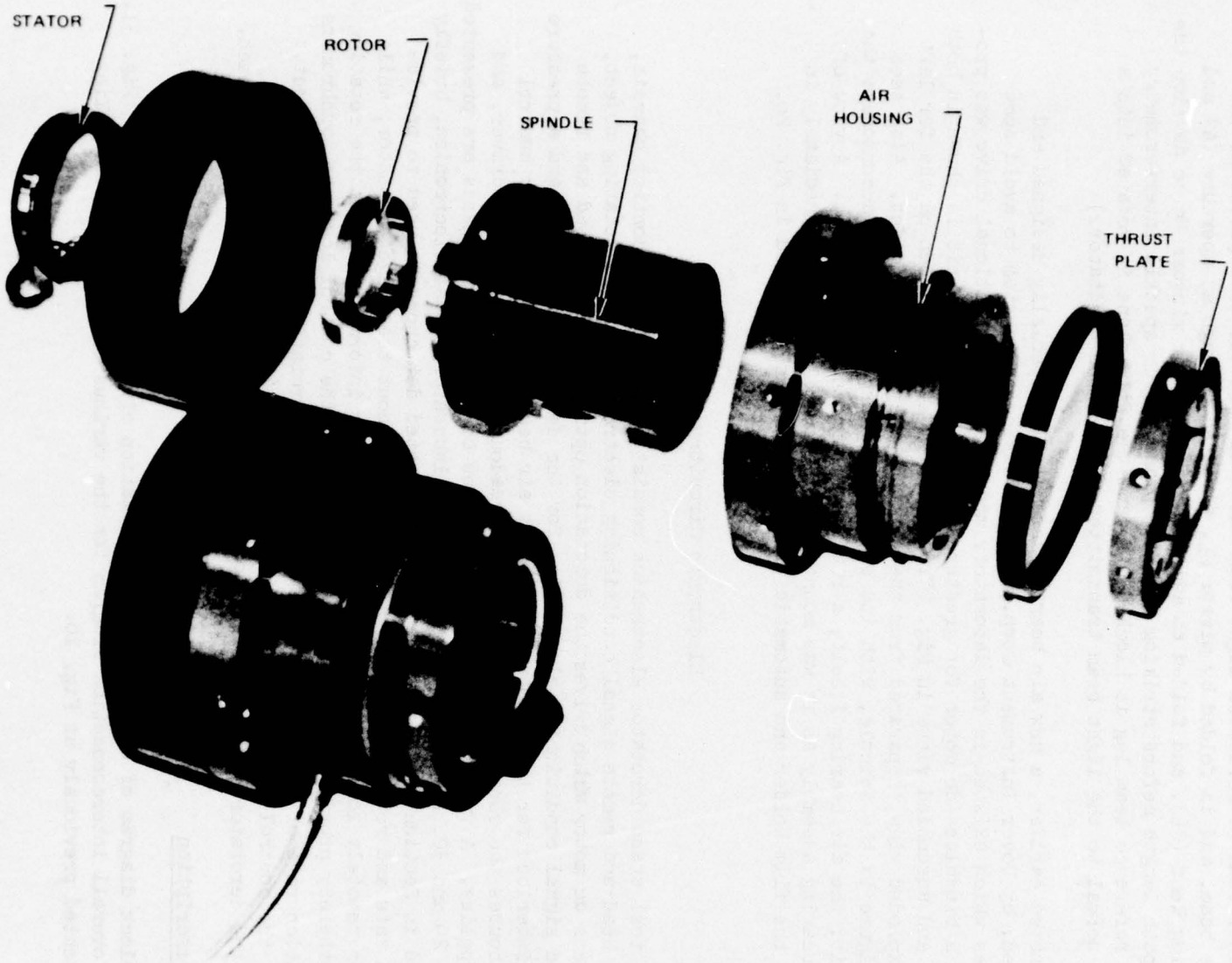

Fig. 27 Air Bearing Assembly

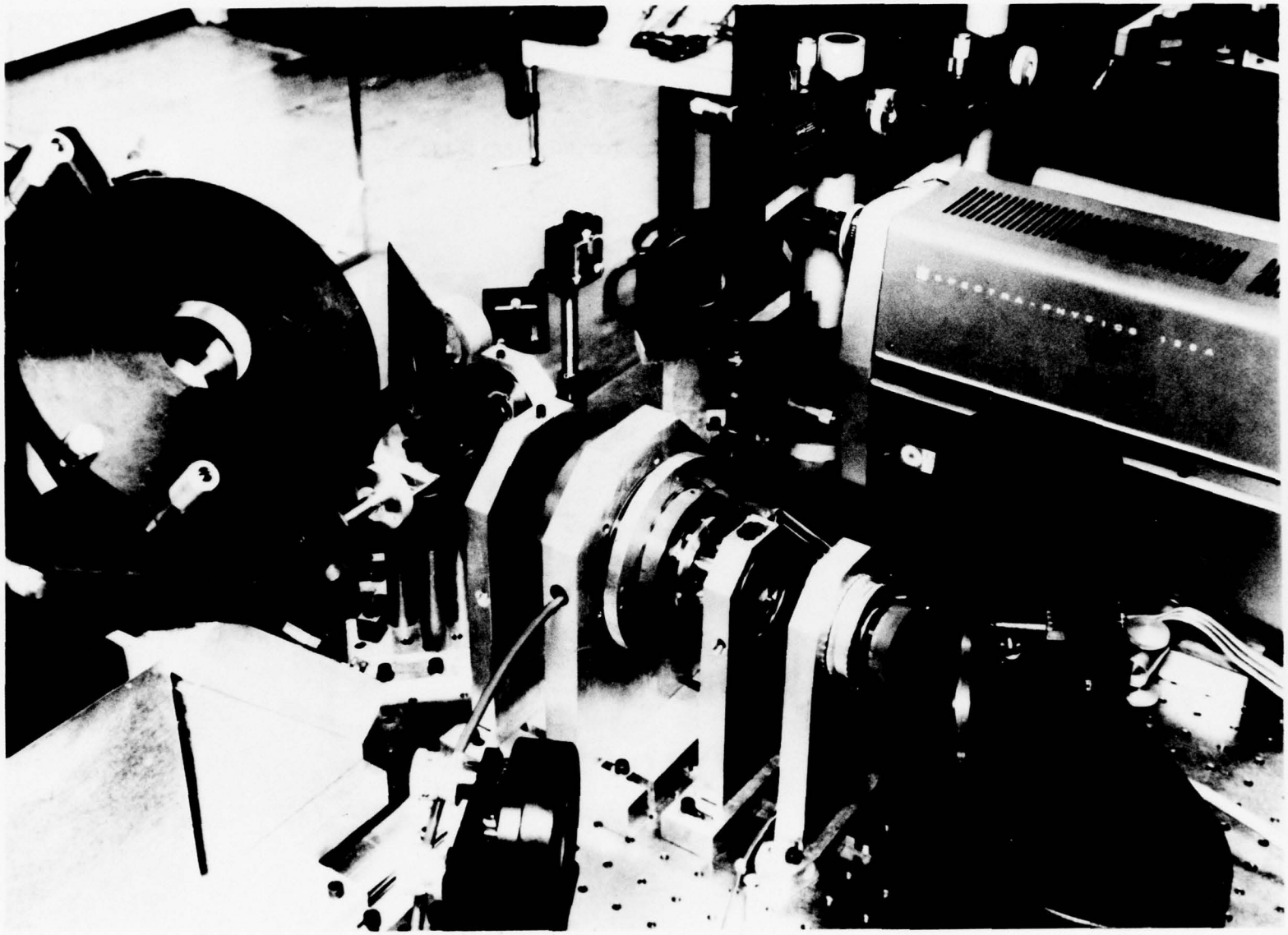

Fig. 28 Derotator and Film Plane

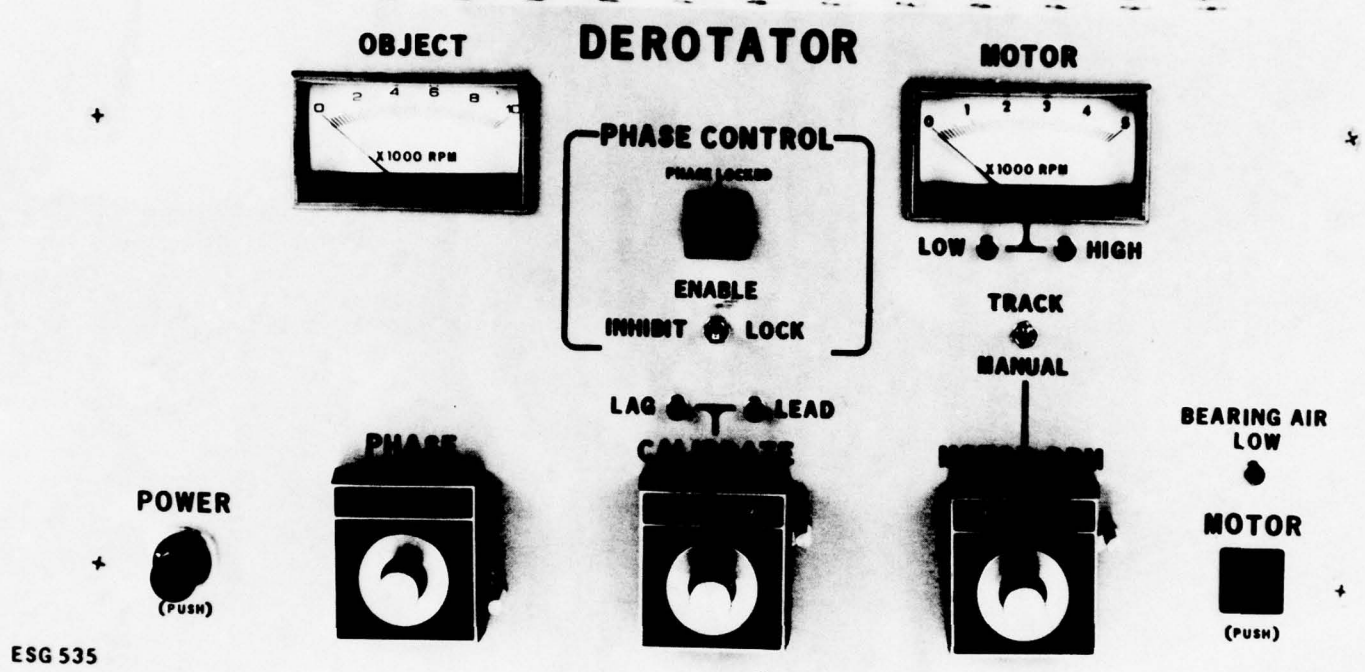

Fig. 29 Control Chassis Front Panel

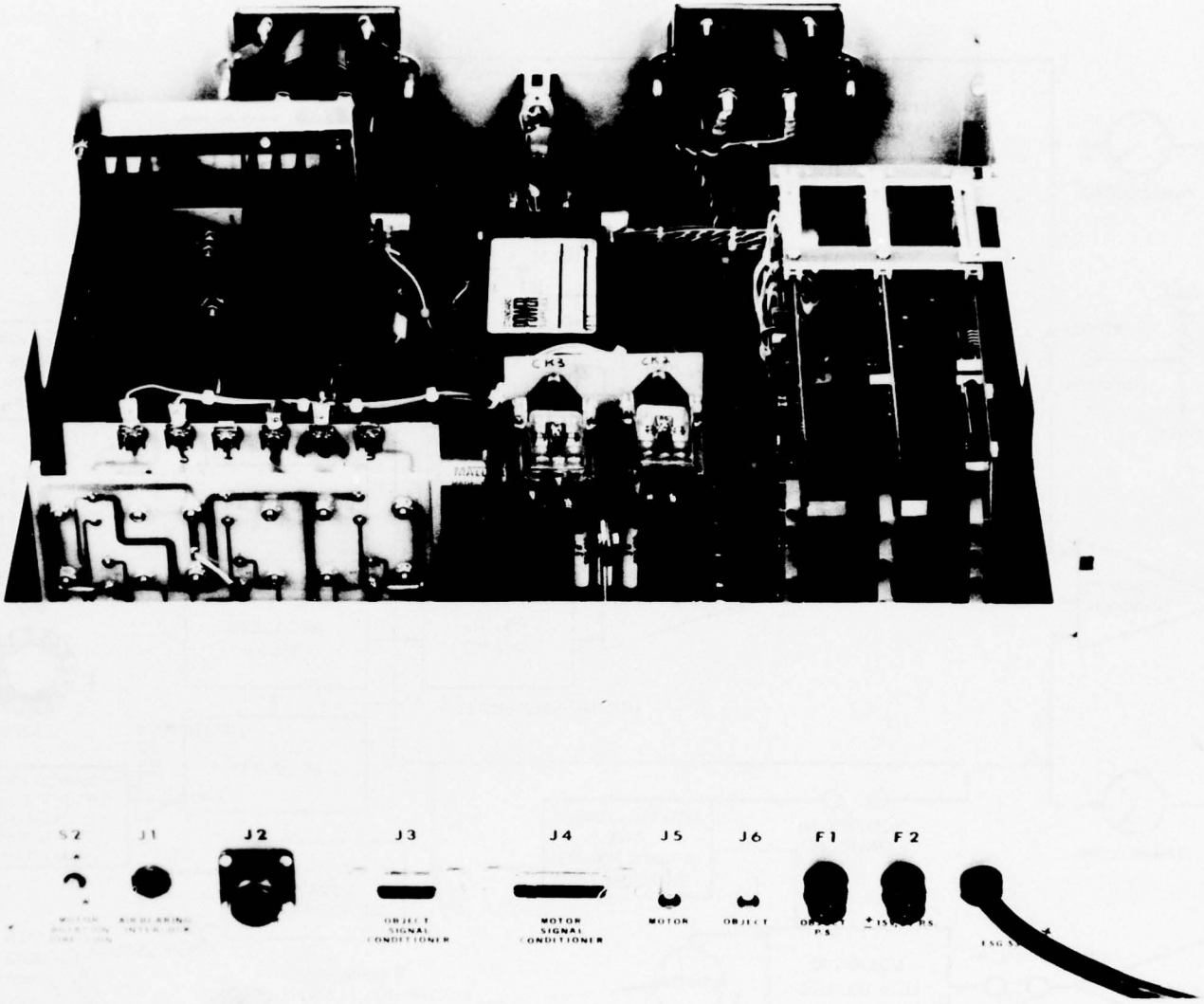

Fig. 30 Control Chassis Interior View

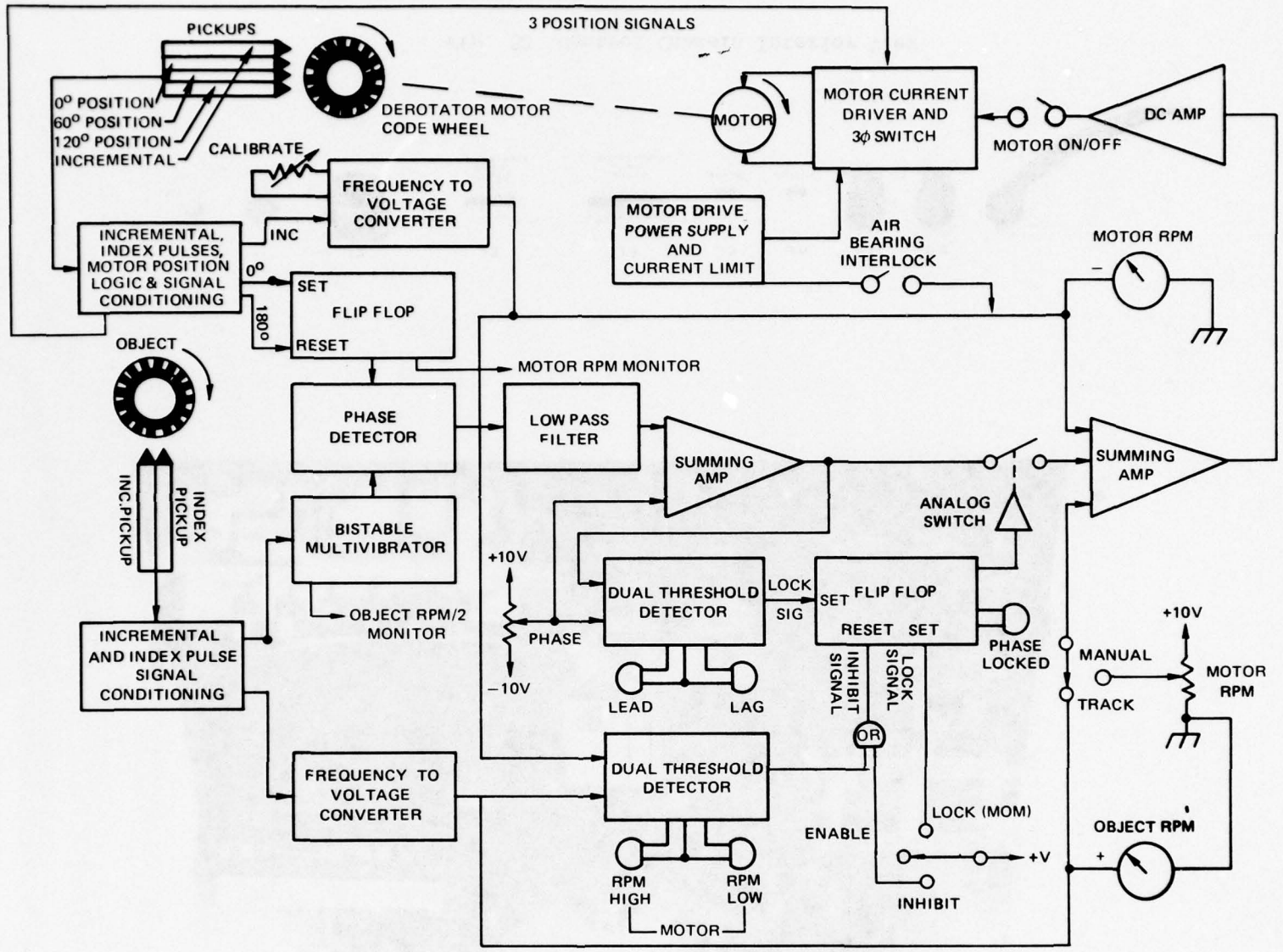

Fig. 31 Electronic System Block Diagram

The function of the electronics depicted in the block diagram of Fig. 31 is to perform the tasks noted above: sychronize the derotator and test object, the image of which is to be held stationary; and maintain a constant phase relationship between them. To accomplish this, a code wheel is attached to the derotator motor shaft and another code wheel is attached to the rotating test object. The derotator motor code wheel and pickup head are depicted in Fig. 32. The outer three channels of this code wheel provide the five cycle per revolution three phase position information required to provide commutation information for the brushless dc motor logic and driver. The inner channel provides 16 cycle per revolution of incremental rotation rate information used to generate an analog signal proportional to rotation rate of the motor and to generate the index position signals. The pickup head, consisting of four light-emitting diodes and four phototransistor detectors, straddles the code wheel. The test object code wheel has only two channels; the outer channel provides 16 cycles per revolution of incremental rotation rate information, and the inner channel provides one index position signal per revolution. The test object pickup head consists of only two emitter-detector pairs.

The signals from each code wheel are remotely processed by their respective logic and signal conditioning boxes. The electronics in these remote boxes maintain proper bias to the pickup heads, detect the pickup head signals, and condition the signals for transmission over the long cables (up to 150 feet) between the remote boxes and the control chassis.

For both the object and the derotator, the incremental signal is applied to a frequency to voltage converter (F to V). The F to V's convert rotation rate to a DC analog signal. These signals drive the RPM meters, and are used by the rotation rate tracking control loop. For the derotator channel, the 0° and 180° index pulses are applied to the set and reset inputs, respectively, of a flip-flop type multivibrator; thus, the output of the flip-flop completes a cycle for each full revolution of the derotator. The single index pulse from the object is applied to the input of a bistable multivibrator; thus, the output of the bistable completes a cycle for every two revolutions of the test object. With this circuit configuration, the frequency output from the two multivibrators are equal when the derotator motor is rotating at half the rate of the object. These two signals are applied to an electronic multiplier type phase detector whose output varies as the cosine of the phase angle between the input signals. The output of the phase detector is filtered to provide a DC analog signal which is proportional to the rotational phase relationship between the derotator and a test object. This signal is used to automatically maintain this phase relationship at a constant, preset value by a phase lock control loop.

Modes of Control

The rotation rate of the derotator may be controlled in any one of the three following ways: 1) by manually setting a front panel control potentiometer; 2) by automatically tracking the rotation rate of the object; and 3) by tracking plus phase control.

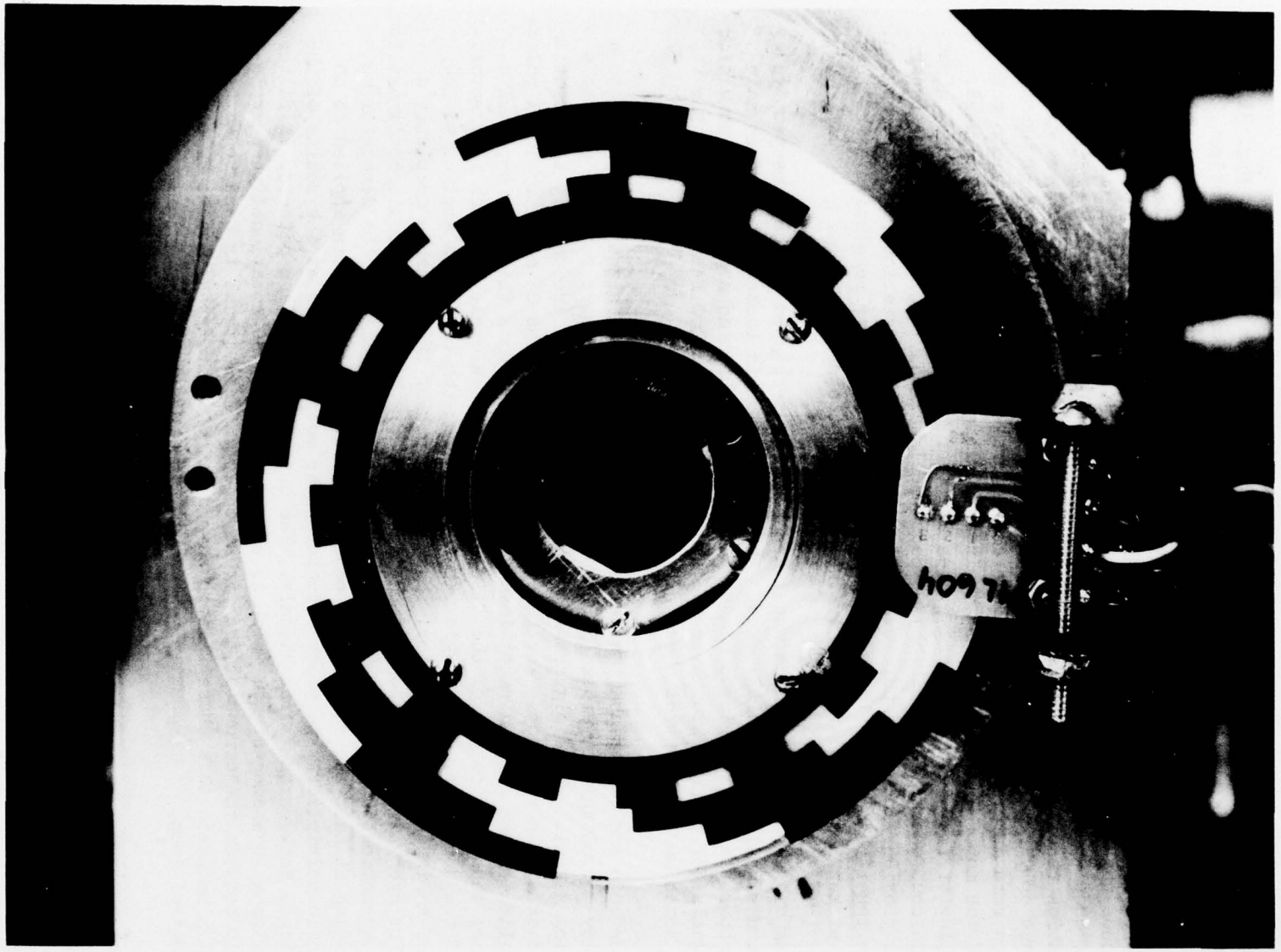

Fig. 32 Derotator Motor Code Wheel

In the manual control mode, the phase control switch should be in the inhibit position. This inhibits the automatic phase control loop. With the control switch in the manual position, a positive DC voltage from the manual control potentiometer is applied to one input of a summing amplifier. At the other input to the summing amplifier, the negative output of the motor frequency to voltage converter is applied. The output of the summing amplifier is amplified and used to control the output level of the motor driver electronics. When the derotator RPM, and hence, the F to V output is of proper value, the inputs to the summing amplifier are equal and of opposite polarity, and the necessary balanced control loop conditions have been met. The control loop will maintain this set speed. The manual control mode is used to test the derotator without the need for a rotating test object.

The track mode of controlling the rotation rate is used when a test object image is to be derotated. With the control switch in the track position, the object F to V output is compared to the derotator F to V output at the summing amplifier input. The control loop forces the two to be equal by maintaining the derotator rotational speed at half the test object rotational speed. The front panel calibrate control potentiometer fine tunes the two F to V's to have an equal transfer function. The lead and lag lights give a visual indication of the object-motor rotational phase relationship. The calibrate control is set to minimize the lead to lag rate of frequency. When one light stays on, the object and derotator are rotating at the same RPM.

The tracking plus phase control mode is used when a test object image is to be derotated and a constant preset rotational phase relationship is to be maintained. The phase lock control loop can be closed either manually (by use of the momentary LOCK position of the control switch) or automatically (by use of the ENABLE position of the control switch). If the control switch is in the INHIBIT position, the phase lock control loop is inoperative. When the phase lock control flip-flop is in the SET state, the analog switch is closed and the phase signal is applied to the control loop summing amplifier. The control loop response is to phase position the derotator motor with respect to the test object such that the phase signal at the output of the inner summing amplifier (Fig. 31) is zero. The phase position of the derotator motor (image angle) may be changed by rotating the PHASE control potentiometer. The PHASE offset voltage is summed with the filtered phase detector signal, and the control loop response is to modify the phase position of the derotator motor such that the output of the inner summing amplifier is zero. The PHASE control will rotate the image angle approximately $\pm 75^{\circ}$. The LEAD-LAG dual threshold detector will automatically lock the phase control loop when the control switches are in the ENABLE and TRACK positions. When the derotator motor accelerates to within the capture range of the phase control loop, the lead-lag signal amplitude at the output of the inner summing amplifier will be of sufficient amplitude to trip either the lead or lag threshold of the detector. The detector output will SET the flip-flop and lock the phase control loop. The RPM HIGH-RPM LOW dual threshold detector prevents lock of the phase control loop (either manually or

automatically) if the rotation rate difference between the test object and derotator is greater than the loop capture range. The detector output prevents phase control loop-lock by applying a SET inhibiting RESET signal thru the OR gate to the loop control flip-flop. The RPM HIGH and RPM LOW indicators indicate the status of this detector.

Derotator

An air pressure operated interlock is located at the derotator air bearing inlet port and prevents power from being applied to the derotator motor unless adequate air pressure is applied to the air bearing. If air pressure fails during operation of the derotator, maximum dynamic breaking is applied to the motor in order to minimize damage to the air bearing. The derotation optics are driven by a hollow shaft, brushless, dc servo motor. Such brushless motors have the following advantages: they may be operated at high speed and at full torque; the stator is in the wound member and may be mounted on a substantial heat sink; there are no brushes to wear out, or brush wear particles; there is less EMI than in brush type motors; and, they have extremely long life. The motor is driven by a three phase current source switching driver, and the prism fits within the hollow shaft of this motor. The combination of a hollow shaft torque motor, with no gearing involved, and a current source driver, gives a quick responding mechanical driver for the derotation optics.

Test Stand Interface

To facilitate operation of the derotation system at the P&WA X-308 Test Stand, a separate control chassis containing interface, control, and sequencing electronics was designed and fabricated specifically for that series of tests. This chassis was cable connected to the derotator control chassis at the OBJECT SIGNAL CONDITIONER (J3) rear apron connector. This connection provided control power to the separate chassis, and provided 16 cycle per revolution incremental and one pulse per revolution test object signals required by the derotator control and logic electronics. Thus, during the X-308 test series, the normal object code wheel, pickup head, and signal conditioning electronics were not used.

Existing test stand instrumentation provided 32 cycle per revolution, and one pulse per revolution, test object signals. The incremental signal was signal conditioned, divided by two and applied to the derotator control chassis through a line driver; while the index signal was simply signal conditioned and applied to the derotator control chassis through a line driver.

A list of the remaining connectors and controls on the separate chassis and their function follows:

CAMERA connector: camera shutter open/closed input signal, film advance signal and film advance output signal.

LASER connector: output signals to charge, discharge, and fire the laser.

SCOPE TRIGGER connector: output signal used to trigger an oscilloscope on the leading edge of the laser fire signal.

RECORDER FIRE SIGNAL connector: output signal used to drive the timing channel on the test stand data recorder.

INCREMENTAL connector: output for oscilloscope monitoring of the incremental rotational signal quality.

LASER FIRE control: momentary pushbutton switch used to manually fire the laser.

LASER CHARGE control: alternate action lighted pushbutton switch used to maintain the laser in the capacitor bank charge mode.

LASER DISCHARGE control: alternate action lighted pushbutton switch used to dump the charge on the laser capacitor banks.

FILM ADVANCE control: momentary pushbutton switch used to advance the film in the transport by one frame.

AUTO SEQUENCE control: alternate action lighted pushbutton switch used to enable an automatic sequencing circuit. The following sequence is initiated by sensing closure of the "X" flash signal from the shutter: immediate firing of laser ("X" flash closure indicates shutter is in full open position), immediate triggering of laser monitoring scope trace, immediate time mark signal to test stand data recorder, delay for shutter to close, and output of a film advance pulse. The shutter is actuated by a remote shutter control attachment.

Included as an Appendix to the present report is a detailed description of the electronics including: a) controls, indicators, connectors and fuses; b) main control chassis; and c) remote electronics, calibration procedures, and brushless motor control logic.

Also available, under a separate binding, for those personnel requiring such information, is a compete set of circuit drawings.

SECTION VIII

TEST STAND EVALUATION

The entire system, as depicted in Fig. 26, together with the associated electronics was transported to the X-308, P&WA outdoor test stand near Bradley Field for two separate test periods (December of 76 and February of 77). A frame had been built to hold the derotator platform at the proper height (approximately 10' off the ground) so that its optical axis could be aligned with the rotation axis of the TS22 fan: the test object, which is a 40 percent version of the 1st stage JT10D engine. Mechanical, optical, and electronic installation and checkout proceeded smoothly, and was essentially completed within three days during the first test period, and two days during the second test period. Photographs to illustrate the derotator installation at the test stand are presented in Fig. 33 (looking toward the TS22) and Fig. 34 (looking towards the derotator).

System Alignment

Optical alignment was made difficult by the fact that the fan could not easily be turned over at low speed, a requirement to set the center of the derotator entrance aperture (as seen through the two large mirrors) on the center of rotation of the fan. The fan was turned by hand, therefore, while coarse alignment of the two large mirrors was accomplished. Next the fan was turned at about 400 rpm with the starter motor to permit fine adjustment of the optics. This was done, as briefly described in Section V of the present report and in more detail in Ref. 1c, by observing the rotation of the laser speckles in the aperture of the copy lens. (At fan idle speed, approximately 3000 rpm, the motion of the speckles could not be observed by eye necessitating the use of the starter motor to kick it over.) Finally, the fan had to be alternatively started and brought to idle, where the alignment of the axis of the derotator could be centered on the center of rotation of the fan, and then brought back to rest. As the fan coasted down to rest, the speckles could be observed in the center of the copy lens, permitting fine tuning of the adjustment as noted above. Alternating between these two adjustments was required because they were coupled to a small degree.

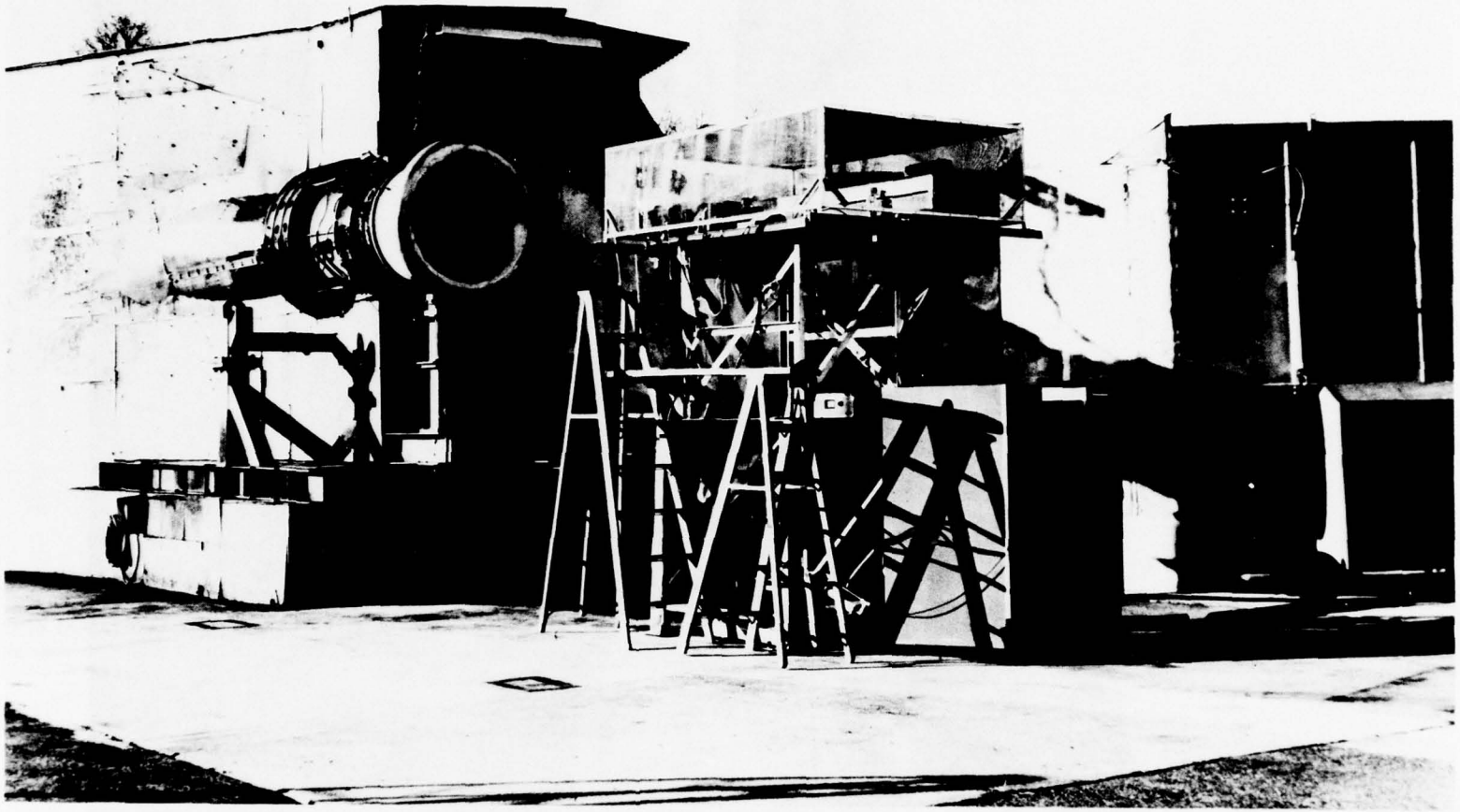

Fig. 33 Test Stand Installation

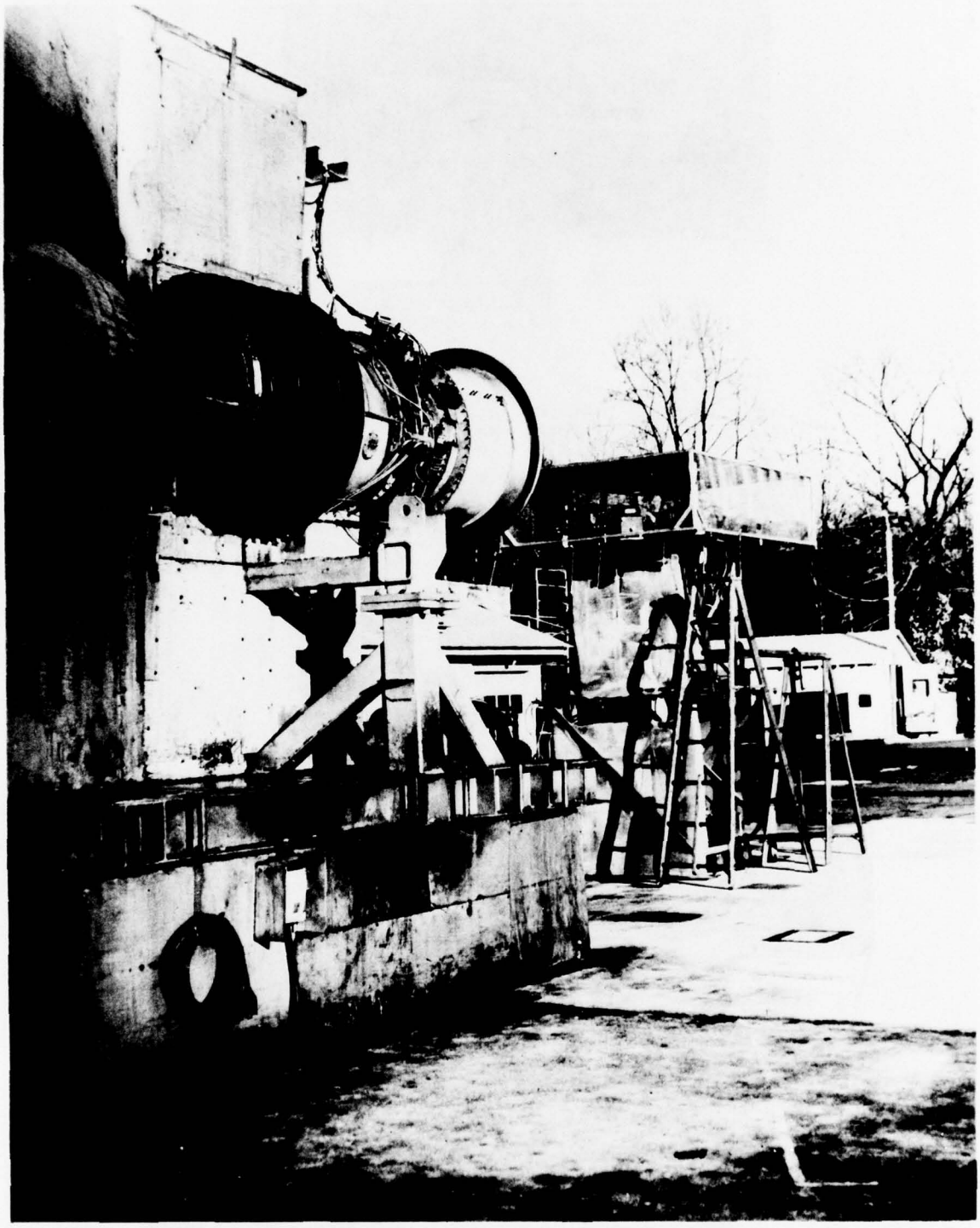

Fig. 34 Test Stand Installation

Operational Difficulties

During the first test period in December, the actual operation of the system was beset by numerous difficulties associated with the cold weather. The component most adversely affected was the pulsed laser system, whereas the test rig itself suffered failure of a speed control valve during very cold weather (-5° C and lower) which made it impossible to run above idle. In addition, the opto-mechanical mirror positioners became very hard to move due to increased viscosity of the lubricating grease. Considerable difficulty was also encountered in providing adequate signal processing to the speed signal (32 pulses per revolution) from the test fan to operate the derotator control electronics. This was dealt with by sensitive adjustment of the electronics during the actual test runs. The only serious failure in the optics was a deterioration ("orange peeling") in the over-coating of one of the large mirrors that caused a great deal of scatter. Difficulty was also met in getting the retroreflective paint to adhere to the fan well enough to take the high rotation speeds. This was essentially solved by curing the paint on the fan with a large portable heater for several hours.

Based on the experience accumulated during the first test period, and taking advantage of a brief warming trend (above freezing temperatures), the second test period ran much smoother.

It should also be noted that throughout both the first 3 1/2 week test period and the second 4 day test period, the brushless dc motor driven, air bearing supported, image derotation prism system, and its electronic control circuitry, together with the remotely actuated shutter, sequence triggering and film advance, performed beautifully.

Test Results

Interferometric Holography

During the first test period, two sets of interferometric holograms were recorded; one with the fan at idle ($\sim$2700 rpm), and one with the fan at five different engine operating speeds (representing both synchronous and asynchronous blade dynamic response) up to approximately 8000 rpm.

The first set, although recorded with a slightly offset reference beam (because of slippage in the last mirror) obscuring a small portion of the fan since image plane holography is being utilized, was successfully reconstructed and the results dramatically demonstrated proof-of-principle: Interferometric holograms, depicting the vibration characteristics of rotating objects, can be recorded in an actual test stand environment using the image derotator system designed and developed

during the initial phases of the contract. Three typical results are shown in Figs. 35 and 36. (The black line across the image is the shadow of a wire strung across the illumination beam so that the orientation of the rig reference frame could be determined.) The pulse separation time was 20 microseconds, and the lack of fringes on the central hub of the fan prove that the system can be sufficiently well aligned to eliminate bias fringes in the hologram reconstructions. As can be seen in the figures, there is considerable motion of the fan blades (bending outside the shroud, twisting inside the shroud) at this engine idle condition.

The second set of holograms from the first test period were recorded at the following conditions: flutter at 7570 rpm, no flutter at 7570 rpm; 5E resonance at 7920 rpm; 3E resonance at 4340 rpm; and full-scale flutter at 7570 rpm. These hologram reconstructions suffered from the fact that the coating on one of the 6 inch diameter turning mirrors had deteriorated and developed an "orange peel" texture. This caused a great deal of return scatter, which made it very hard to align the system, and projected a random pattern on the illumination of the fan, against which it was very hard to observe fringes.

During the second test period in February interferometric holograms were successfully recorded at various engine operating speeds representing both synchronous and asynchronous blade dynamic response conditions, in addition to the engine idle condition. Optical data were recorded at speeds of approximately 7500 rpm (with and without flutter), 4500 rpm (a 3E resonance) and 5000 rpm. The last test condition was selected on the basis of the test stand instrumentation, which indicated a reasonable vibration level; subsequent analysis at P&WA suggested this may have been a 12E resonance, but this has not been substantiated. Typical results are presented in Figs. 37 through 44. As in the previous figures, the black line across the image is for establishing a reference orientation. The small black rectangle into the fan just adjacent to this line and the five missing blade tips are caused by a mirror shadowing.

Representative vibration patterns, recorded of the third engine order resonance at approximately 4500 rpm, are reproduced in Figs. 37 through 39. Figures 37 and 38 include the entire fan, and Fig. 39 is a close-up of a smaller area of the latter to illustrate the fringe resolution attainable. The general characteristics in both are quite similar; that is, blade flap from the shroud out to the tip, and blade twist inside the shroud. The only real difference is in the fringe density, or degree of motion between the two exposures used to record each interferometric hologram. Since a 15 microsecond pulse interval was used in both cases, the figures suggest that possibly one (Fig. 37) was recorded with the blades at a higher amplitude position (lower velocity) in their vibratory cycle than the other (Fig. 38). The airflow for this particular 3E synchronous blade dynamic response was approximately 90 pounds/second with a pressure ratio of 1.0.

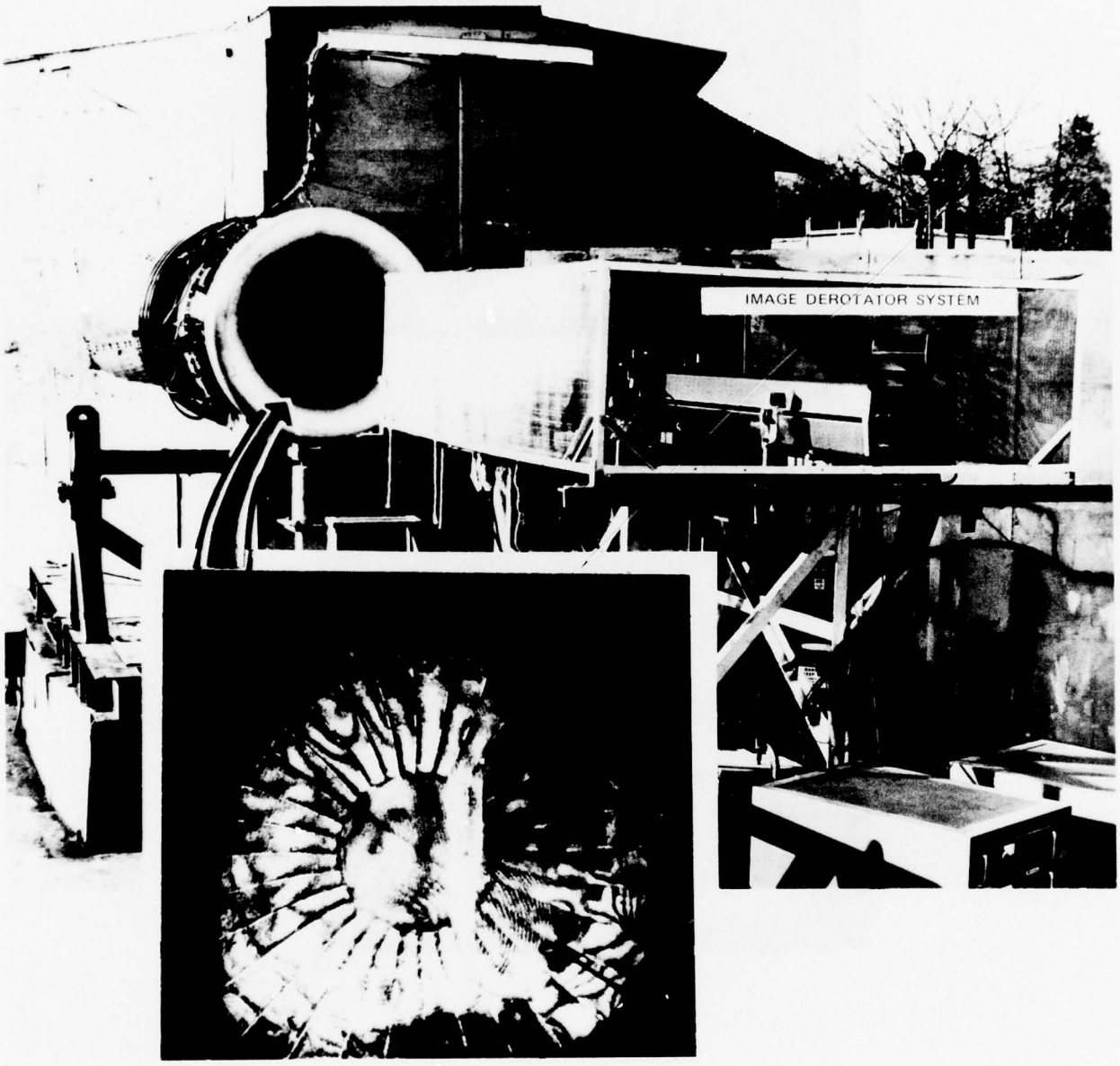

Fig. 35 Interferometric Holographic Tests at P&WA Test Stand - Bradley Field
Rotational Speed: ∿ 2700 RPM; X-308 Test Stand - December 9, 1976;
Ambient Temperature: -5 °C

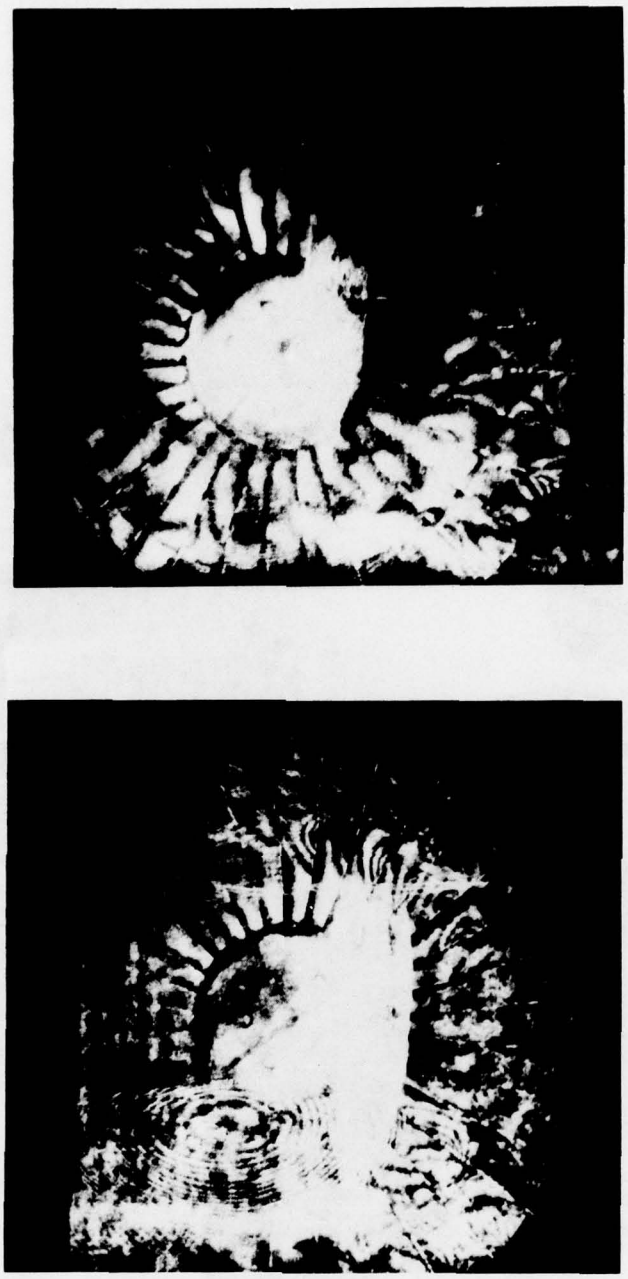

Fig. 36 TS22 Fan Vibration Characteristics; Idle Conditions: 2700 RPM

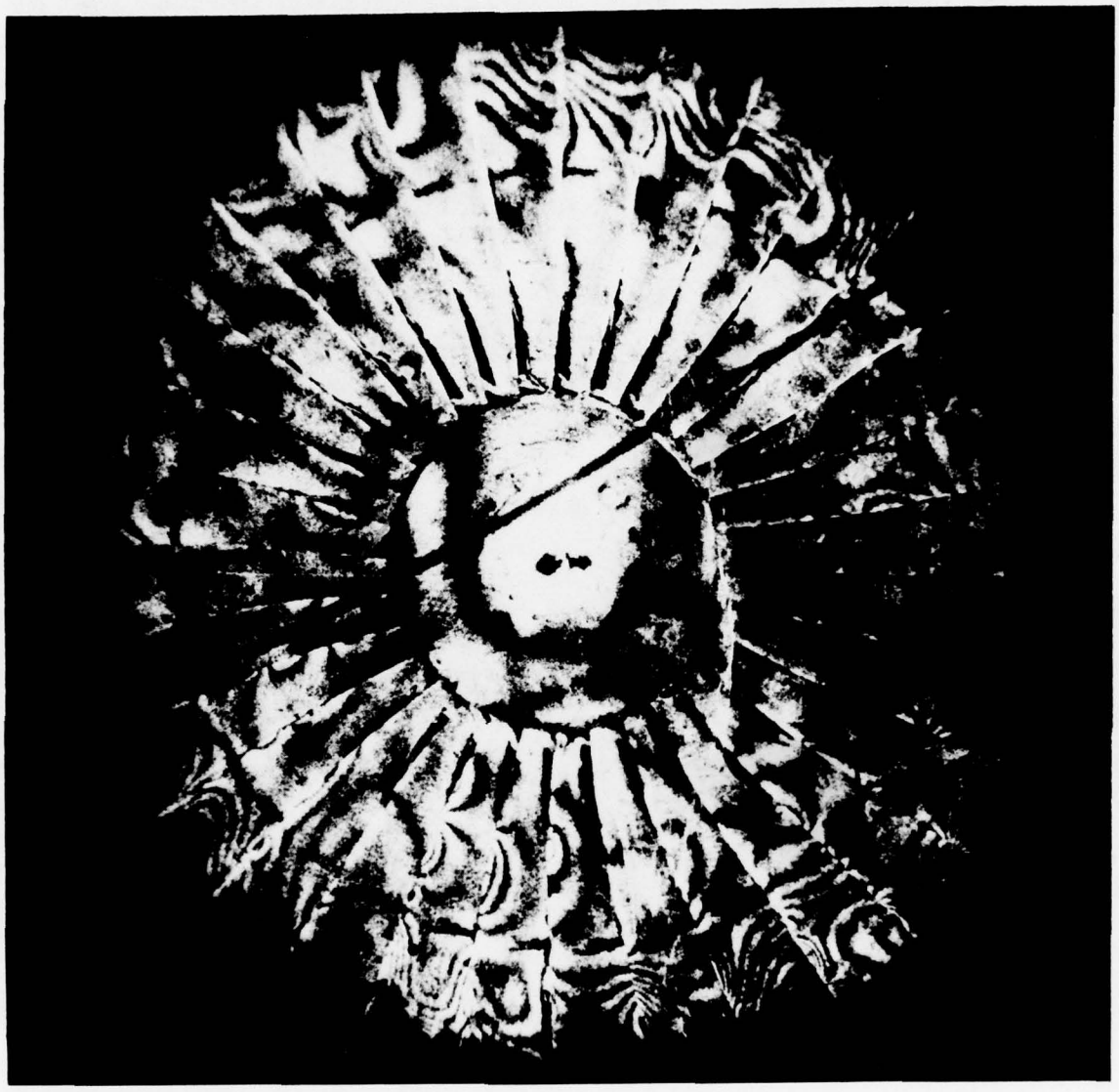

Fig. 37 TS22 Fan 3E Resonance at 4460 RPM

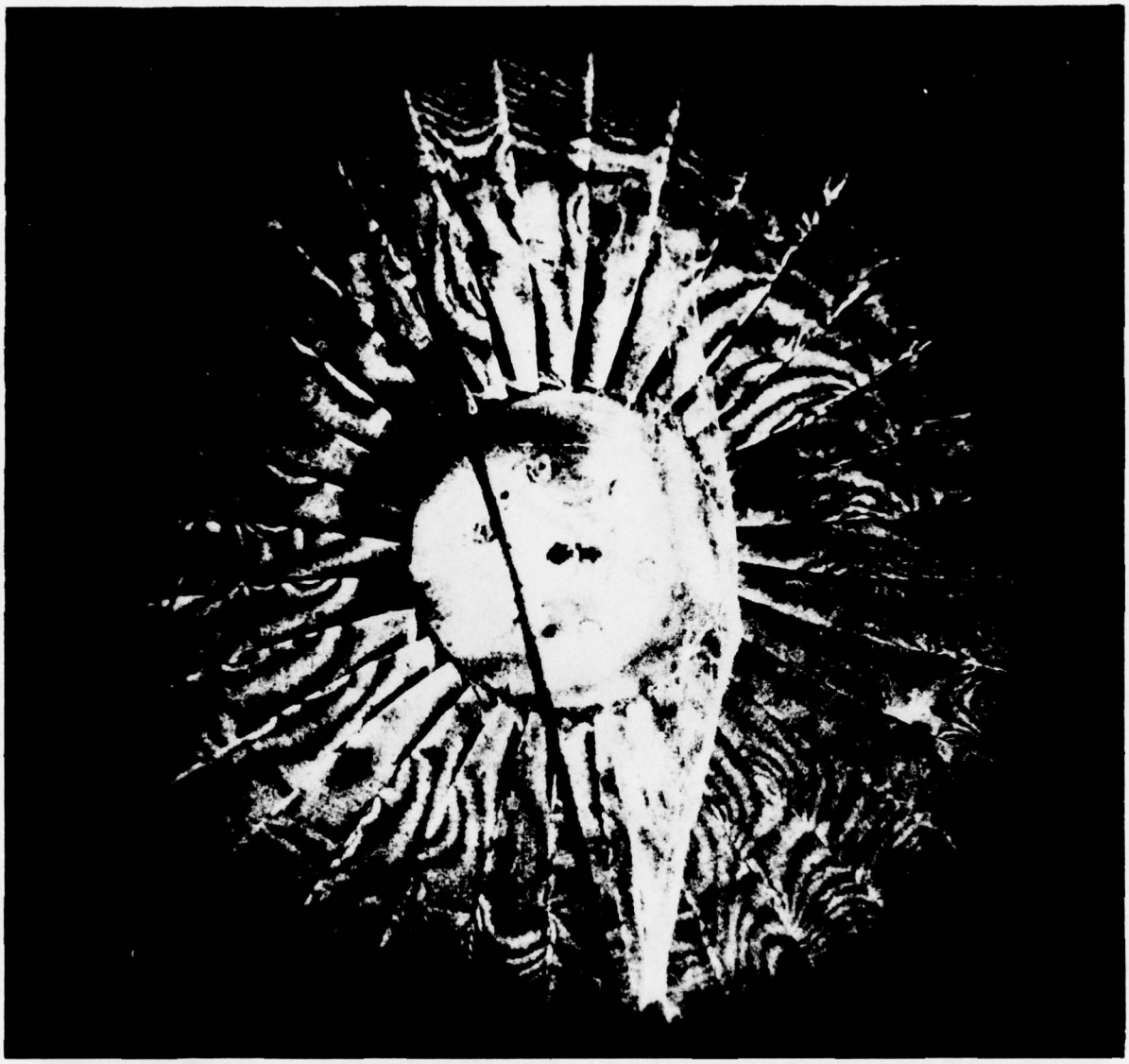

Fig. 38 TS22 Fan 3E Resonance at 4460 RPM

Fig. 39 3E Resonance - Magnified View from Fig. 38

Figure 40 (with a close-up in Fig. 41) is a result obtained at approximately 5000 rpm, with the fringes suggesting a twisting characteristic; in some instances all the way out to the tips of the blades. Airflow was calculated to be 101 pounds/second with a pressure ratio of 1.0.

Figures 42 through 44 were recorded at approximately 7500 rpm with different back pressures applied to minimize, or establish, a flutter response in the fan. The first (Fig. 42), representing a nonflutter condition, suggests the same general characteristics as the previous examples; that is, a twisting inside the shroud and a flapping outside the shroud, but both in a considerably more complex vibration pattern. The airflow for this condition was calculated to be approximately 128 pounds/second with a pressure ratio of 1.272, and the back pressure valve set at 70 percent. To induce a flutter condition (Fig. 43), the back pressure valve was reduced to 53 percent, reducing the airflow to approximately 117 pounds/second while maintaining essentially the same pressure ratio (1.277). Again, there is a very strong twisting of blades inside the shroud, but a somewhat more complex motion of the tips at a considerably increased amplitude as evidenced by the much greater fringe density. As in some of the previous examples, in order to more graphically demonstrate the capability of the system to depict the blade motion in the high deformation regions (high fringe density) of the fan, a portion has been enlarged, and is presented in Fig. 44.

In most of the hologram reconstructions, a bright back reflection is noticeable; this is most probably due to the reference beam being reflected first from the film and then back from the copy lens of the derotator system (see Fig. 4). Its brightness, compared to the reconstruction of the fan, indicates that the reference beam is too strong relative to the object beam.

Speckle Photography

Speckle photography, requiring considerably more laser intensity, was only performed during the first test period when all three laser amplifier stages were available; the third amplifier was not used during the second test series since it appeared to affect the operational repeatability of the laser system. Speckle photographs were recorded of the TS22 fan at idle, and at the following conditions: 3E resonance at 4400 rpm, 5E resonance at 8113 rpm, flutter at 7673 rpm, and no flutter at 7673 rpm. A sample speckle photograph taken under flutter conditions at 7673 rpm is presented in Fig. 45. To record the specklegrams, the film transport was rotated until its film plane was normal to the optical axis of the derotator. The image plane was then adjusted to coincide with a focal plane located one meter in front of the fan blades. Due to the high demagnification of the image (lateral demagnification = 36 and axial demagnification = 1300), this meant a shift of only 0.77 mm backward in the image space from the plane of focus for the fan blades. This adjustment was performed by placing a tape across the rig, one meter in front of the fan, and focusing the camera on the tape. The focusing was done by observing

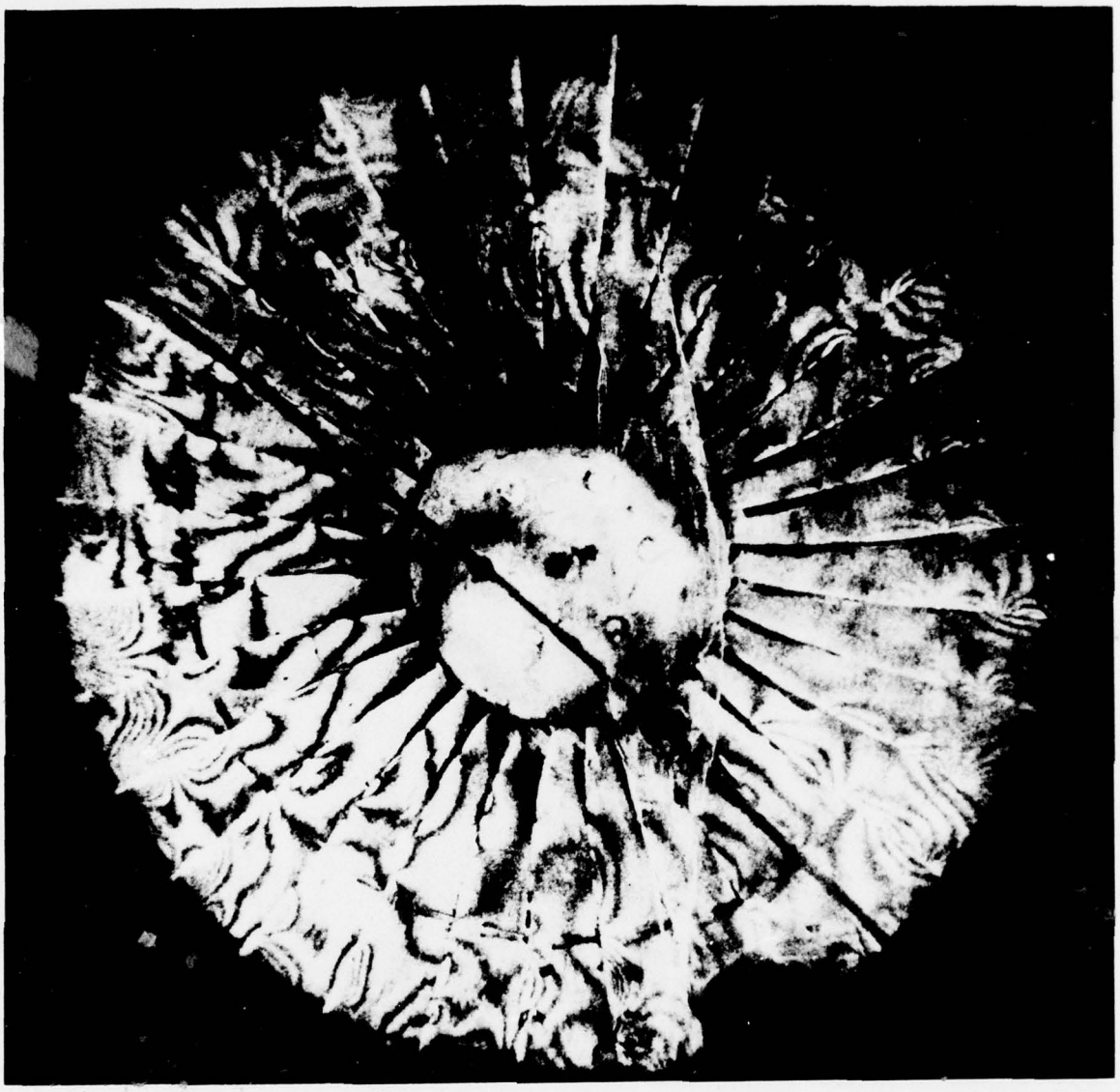

Fig. 40 TS22 Vibration Characteristic at 5000 RPM

Fig. 41 5000 RPM - Magnified View From Fig. 40

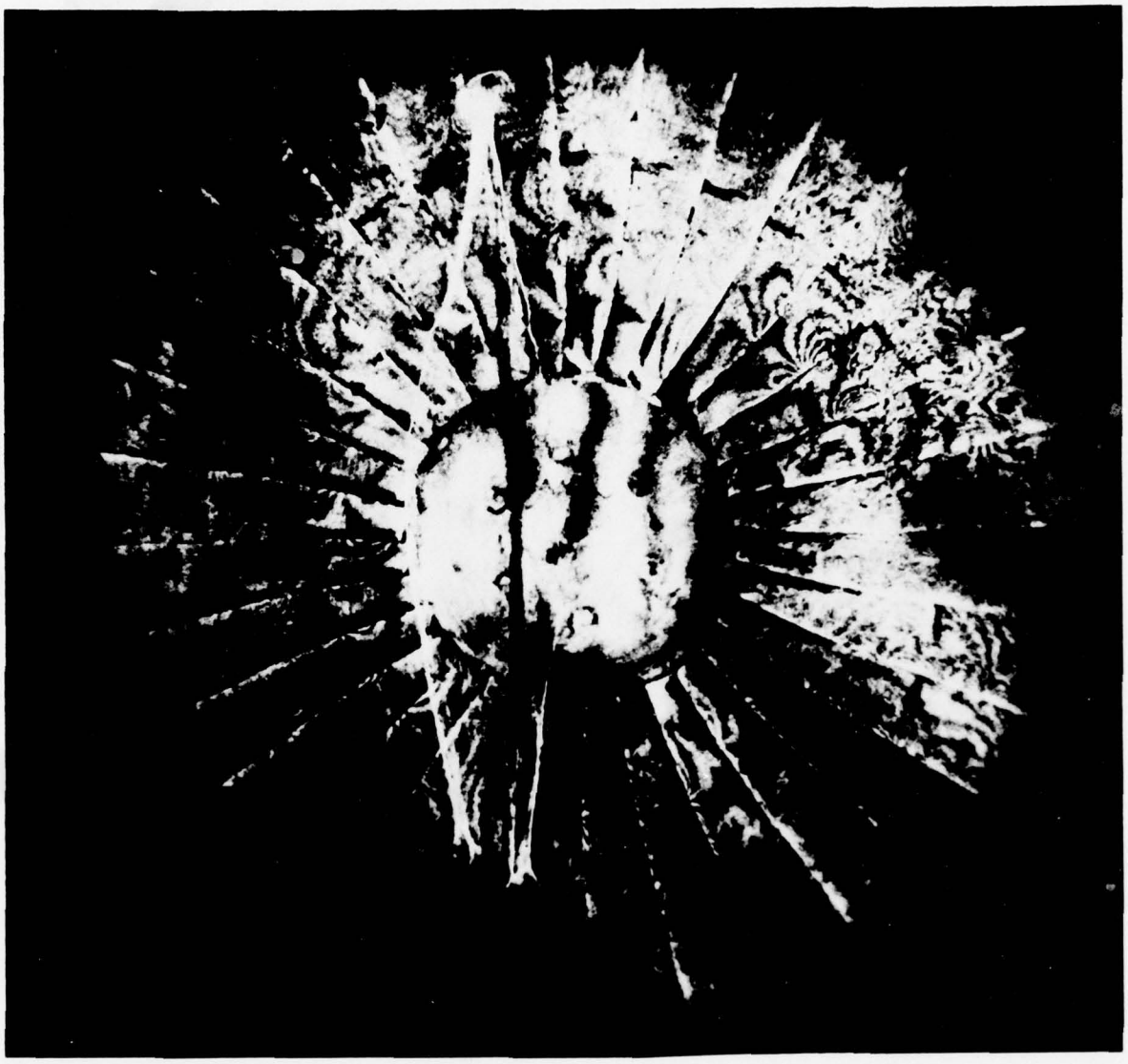

Fig. 42 TS22 Fan at ∿ 7500 RPM - No Flutter

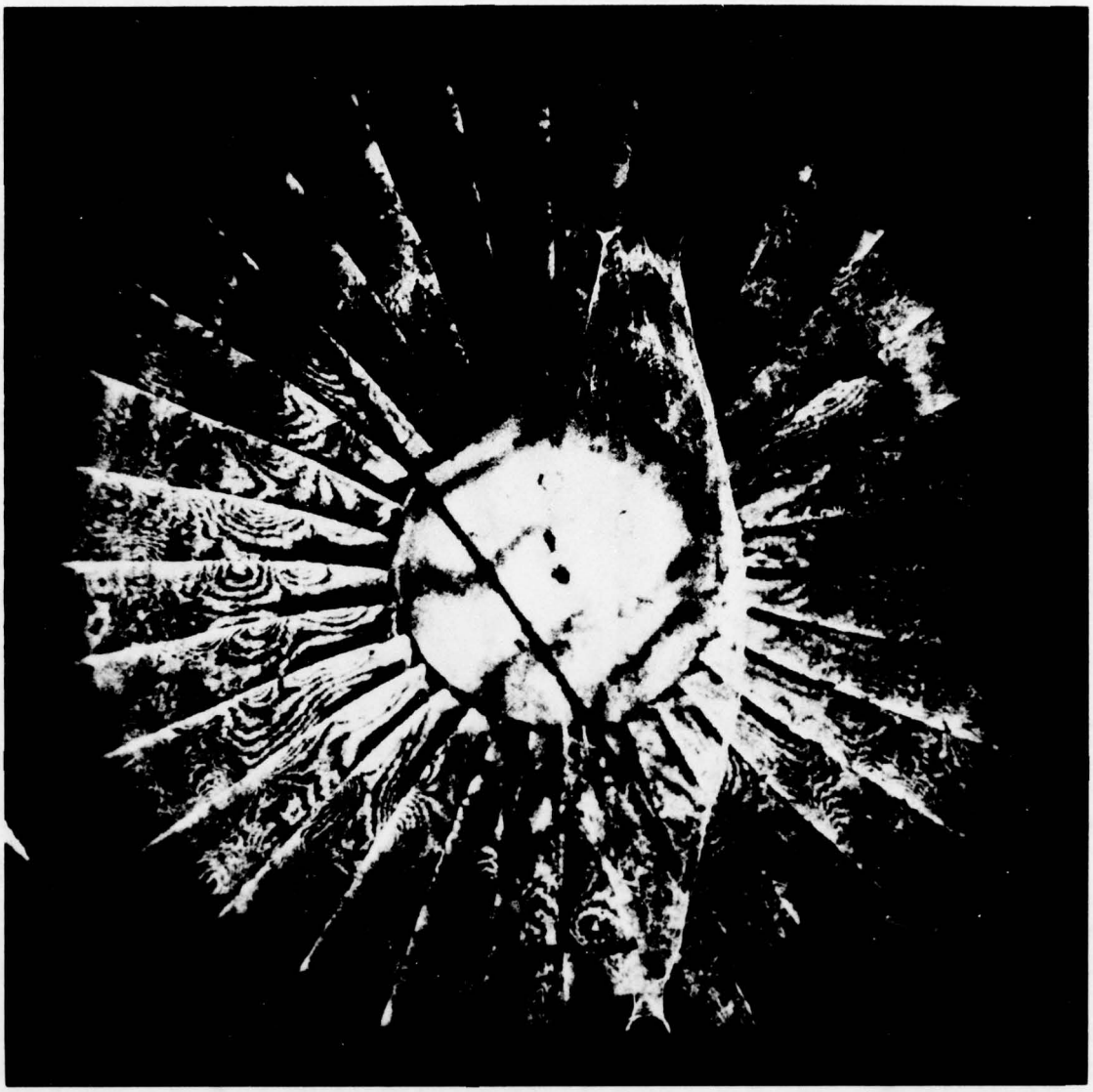

Fig. 43 TS22 Fan Flutter at ∿ 7500 RPM

Fig. 44 Flutter - Magnified View From Fig. 43

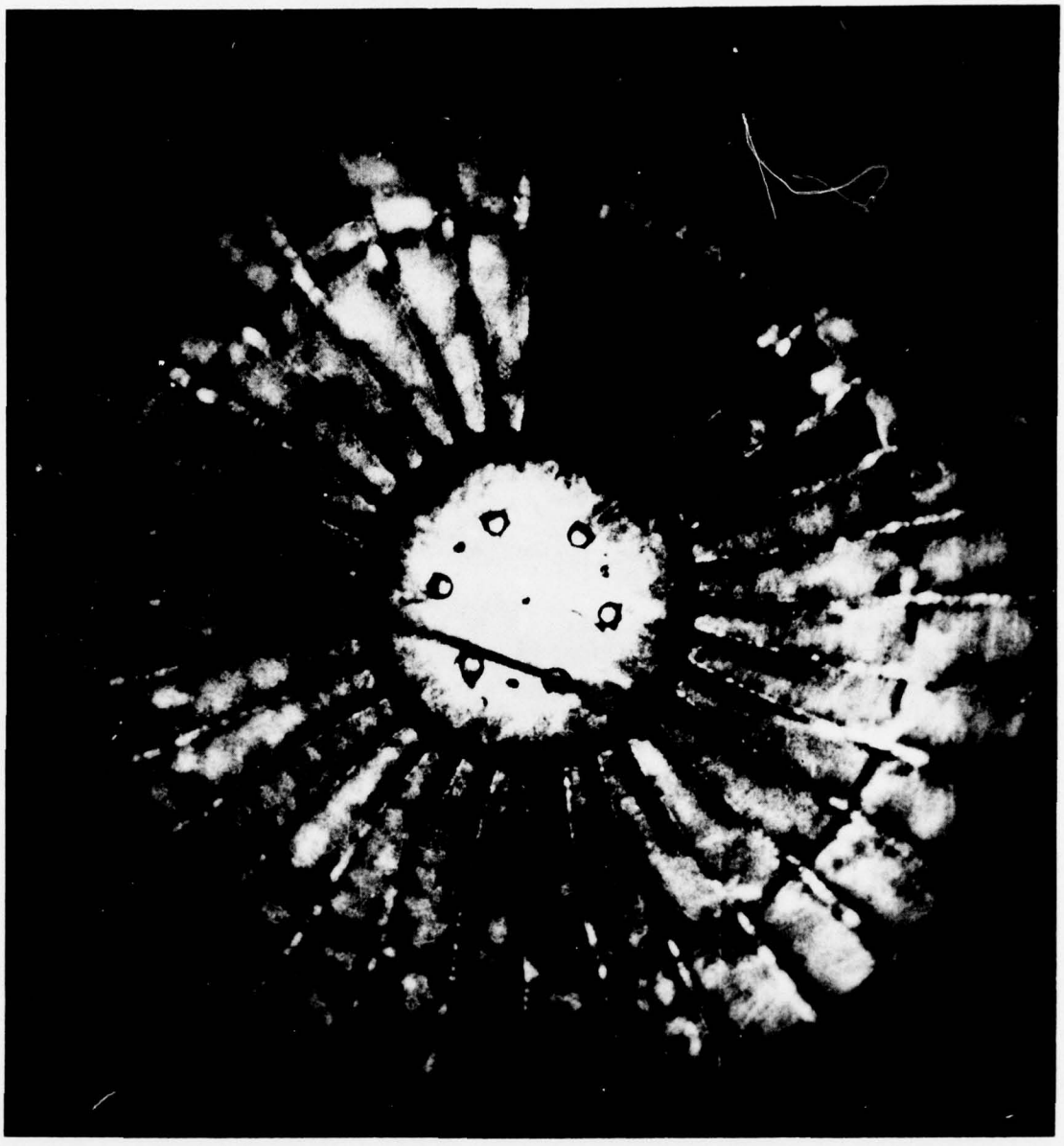

Fig. 45 Speckle Photograph; TS22 Fan - 7673 RPM

the image with a microscope to find the proper focal plane, then moving the film transport until the image of the film was in focus.

The sequence of speckle photographs taken at the various operating conditions showed halo fringes only on the region of the hub. This is due, most likely, to the fact that series of specklegrams were of very light exposure, owing to the lack of a reference leg (which builds up film exposure) and deterioration in the retro-reflective coating on the fan blades. In a previous sequence, recorded only at idle speed, a higher photographic density was obtained, and the bleached specklegrams showed clear halo fringes at the blade tips. Some typical results are presented in Fig. 46, showing the halo fringes from three successive blade tips from one of these specklegrams. (Halo fringes on the hub are the result of misalignment of the system and it was determined, after the speckle testing, that there was a small misalignment of the prisms in the derotator system. This was corrected before the holograms, discussed in the previous section, were recorded).

Theoretically, the halo fringes found on the hub could be subtracted from those found on the blade tips to yield the resultant motion of the blade tips. In practice, this is not practical for these specklegrams because the fringes from the hub show evidence of multiple pulse output of the laser, whereas those from the tips do not. This was also corrected prior to the holographic testing, but it was not possible to record additional specklegrams. The results obtained could be used, however, to obtain relative displacements between one blade tip and another. From calculations made of the expected motions of the fan blades, it was determined that these halo fringes would represent bending and torsional rotations of the blades rather than actual displacements.

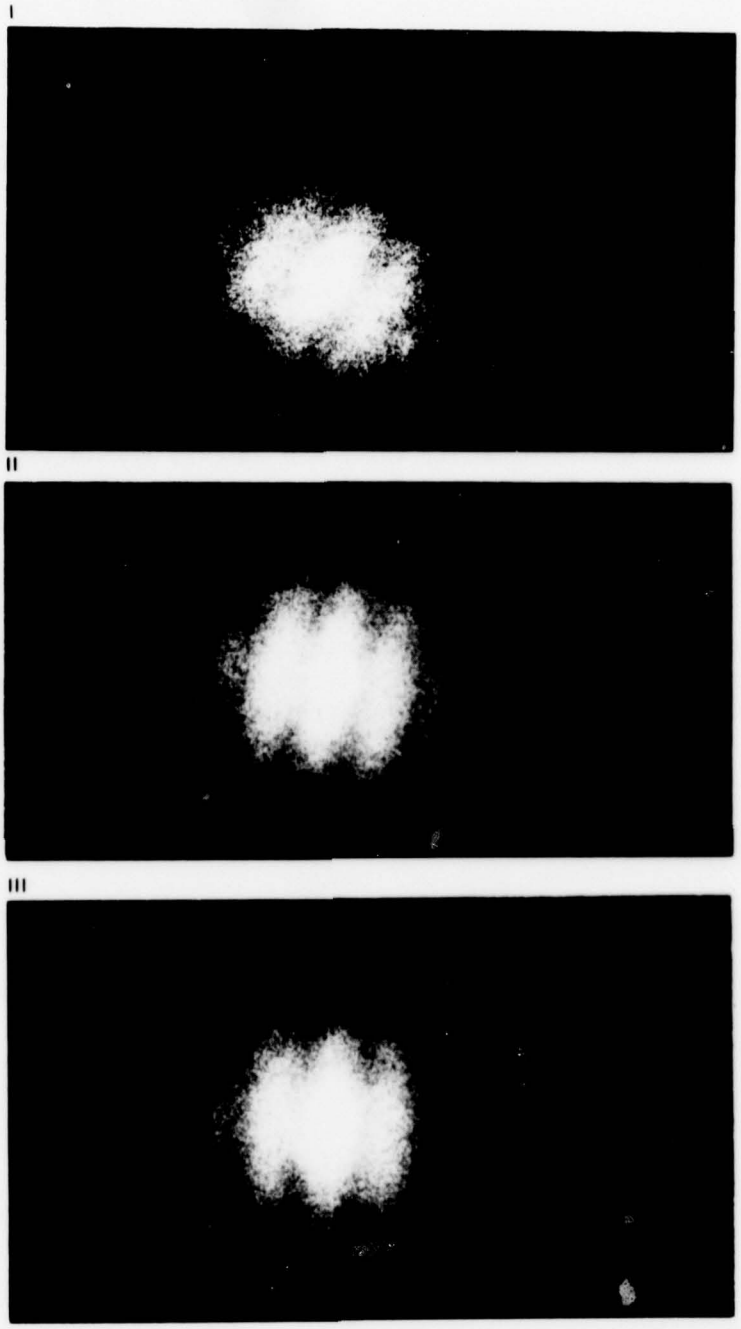

Fig. 46 Blade Tip Halo Fringes Obtained by Optically Processing a Speckle-gram Recorded of the TS22 Fan at Idle Speed

SECTION IX

CONCLUSIONS & RECOMMENDATIONS

In conclusion, it can be stated that the image derotation design principle, developed under this contract, can be hardware implemented in a manner suitable for performing dynamic analysis, via optical methods, on rotating structures in a test stand environment. This was demonstrated with the recording of both interferometric holograms and speckle photographs of a TS22 fan stage operating at speeds up to 8000 rpm. The enormous potential improvement in test stand data acquisition procedures which is offered by such a system includes, in particular, the availability of full field coverage over the entire visible surface of a structure, as opposed to discrete point data currently obtained, for example, by strain gages. Just as important is the sophisticated and proven electronic operational and control circuitry developed under the contract to run the image derotator system. Its versatility was well demonstrated with the ease of adaptation to the test stand series of tests, in which the object code wheel was replaced by the existing test stand instrumentation output, with proper signal conditioning, to provide the required number of pulses (16) to the derotator control logic. Based on these demonstrated accomplishments, further work is recommended to exploit the potential of this newly developed tool for the acquisition of dynamic structural data on rotating components. Current problems of interest in this area would include measurement of the vibration characteristics and strain in rotating bladed disks, as well as studies of flutter mechanisms and the effects of rotation on the vibrational mode shapes recorded at a zero speed condition.

APPENDIX

ELECTRONIC CIRCUITRY DETAILS*

Controls, Indicators, Connectors and Fuses

Front Panel

The controls, meters, and indicators available to the operator on the front panel are described below, with reference made to Fig. 29 of the main text. Also applicable is Drawing ESG535-5-21A.

POWER (CB1) - a 5 Ampere lighted switching circuit breaker which controls the 115VAC line power. The circuit breaker is push on - push off operated.

BEARING AIR LOW (PL3) - a pilot light which is illuminated when the air bearing pressure is below 50 PSIG. The pressure switch is located on the optics platform near the air bearing input. If PL3 is on, or if the cable to the switch is disconnected, the MOTOR ON switch is inoperative and dynamic breaking is applied to the torque motor which drives the derotator. This pilot light is not operative if the cable to the derotation motor is disconnected.

MOTOR (S1-PL1) - an alternate action, indicating push button switch which controls the AC line power to the DC power supply (PS1) for the brushless motor drive circuit. The control breaker (CB1) must be in the ON position, adequate air pressure must be applied to the air bearing, and the cable to the derotator motor must be connected before this control will be operative.

MANUAL-TRACK (S4) - a two position toggle switch. In the MANUAL position the torque motor rotation rate is controlled by the setting of the MOTOR RPM control. In the TRACK position the torque motor rotation rate is synchronized to half the object rotation rate. The PHASE LOCK control should be in the INHIBIT position when MANUAL control of the motor is utilized.

MOTOR RPM (R3) - a ten-turn control potentiometer which sets the rotation rate of the torque motor when the MANUAL-TRACK switch is in the MANUAL position. The range of control is 2KRPM to 5KRPM.

MOTOR X 1000 RPM (M1) - an analog panel meter calibrated to read out the rotation rate of the servo motor. The range of the meter is 0 - 5KRPM.

OBJECT X 1000 RPM (M2) - an analog panel meter calibrated to read out the rotation rate of the object. The range of the meter is 0 - 10KRPM.

---

* As noted earlier, a complete set of circuit drawings is available under separate cover; mention of specific Fig. Nos. refers to the main text of this report.

CALIBRATE (R1) - a ten-turn control potentiometer which fine tunes the rotation rate of the servo motor. With the PHASE CONTROL in the INHIBIT position, the CALIBRATE control is used to adjust the motor rotation rate to half the object rotation rate. This may be done by observing the motor RPM HIGH - LOW lights and the blink rate of the LEAD-LAG lights, or by observing the object through the derotator optics.

PHASE CONTROL - INHIBIT - ENABLE - LOCK (S3) - a three-position toggle switch with an on-on-momentary action. The LOCK position is momentary. In the INHIBIT position, the phase control loop is disconnected. This allows the rotation rate of the motor to be adjusted to be equal to half that of the object. The LOCK position forces the phase lock loop to close, and can be useful if the object rotation rate is oscillating, but within the phase lock loop capture range (RPM HIGH or RPM LOW indicators not illuminated). This is a back-up function, since the phase control loop automatically locks when the PHASE CONTROL switch is in the ENABLE position.

PHASE LOCKED (PL2) - a pilot light which indicates that the phase lock loop is actuated.

PHASE (R2) - a ten turn control potentiometer which is used to vary the phase relationship between the object and the derotator. This effects a rotation of the image over a range of approximately ± 150°. This control is functional when both the phase control loop is locked and the CALIBRATE control is properly adjusted.

RPM-LOW (PL7) - a pilot light which indicates when the rotation rate of the derotator is less than 95 percent of half the rotation rate of the object.

PRM-HIGH (PL6) - a pilot light which indicates when the rotation rate of the derotator is greater than 105 percent of half the rotation rate of the object.

LEAD (PL4) - a pilot light which indicates that the phase angle of the derotator is leading the phase angle of the object by more than 15°.

LAG (PL5) - a pilot light which indicates that the phase angle of the derotator is lagging the phase angle of the object by more than 15°.

Rear Apron

A photograph showing a view of the control chassis rear apron is presented in Fig. 1A and indicates the position of the connectors, fuses, and switch described below. Also applicable is Drawing ESG535-5-21A.

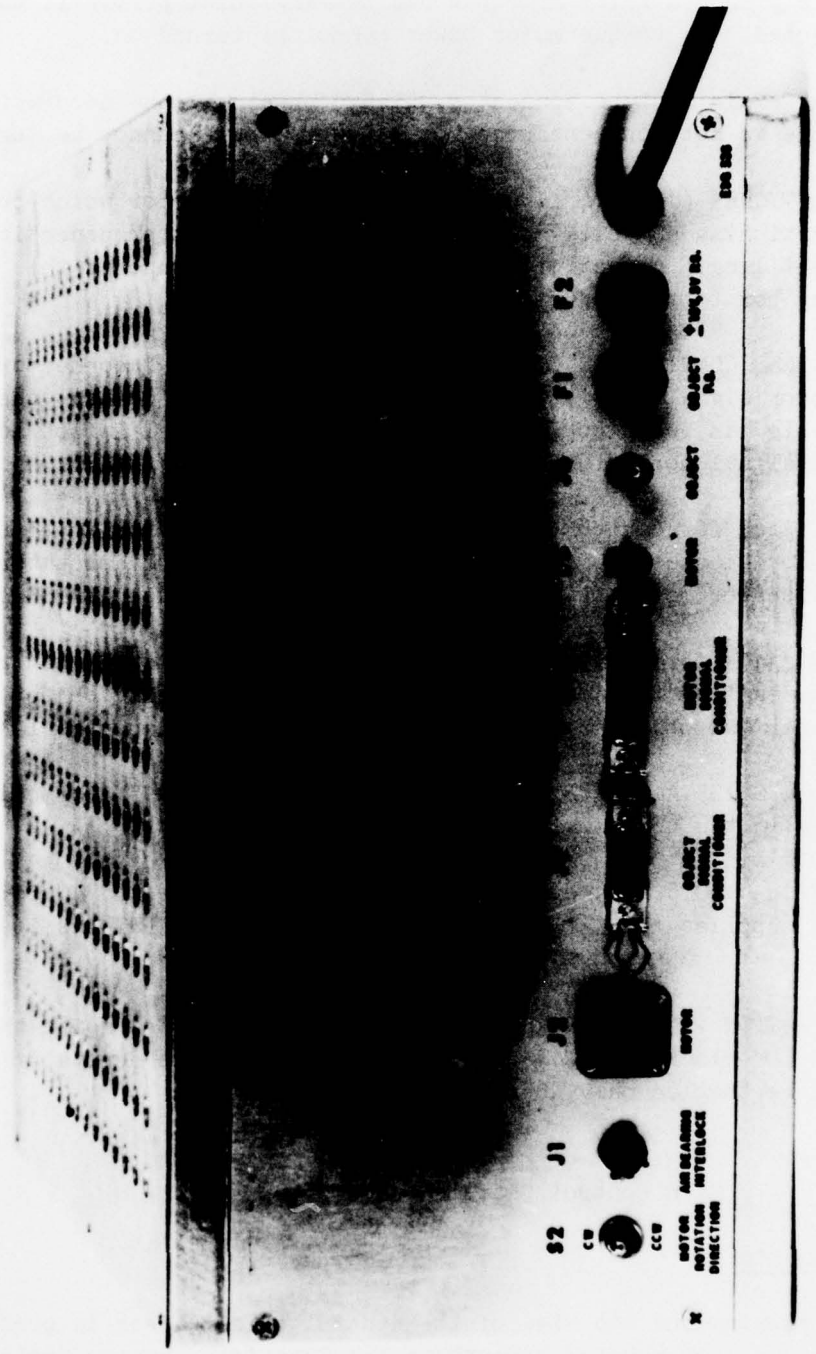

Fig. 1A Control Chassis Rear Apron

AIR BEARING INTERLOCK (J1) - a 5 pin female type 126 Amphenol connector which connects to the air pressure relay near the air bearing inlet port. If the cable is not connected, the torque motor power cannot be turned on.

MOTOR (J2) - 5 pin female MS type connector which connects to the derotator motor. If the cable is not connected the motor power supply cannot be turned on.

OBJECT SIGNAL CONDITIONER (J3) - a 15 pin female type D connector which connects to the signal conditioning and pick-up electronics box; the interconnection cable can be up to 40 feet long. An additional 4 foot long cable connects this signal conditioning box to the object pick-up head.

MOTOR (ERECTOR) SIGNAL CONDITIONER (J4) - a 25 pin female type D connector which connects to the motor signal conditioning and pick-up electronics box; the interconnection cable can be up to 150 feet long. An additional 1 foot long cable connects the signal conditioning box to the motor pick-up head.

MOTOR (J5) - a BNC jack for counter monitoring of the torque motor revolution rate. This signal originates from the code wheel mounted on the derotator shaft and outputs one pulse per motor revolution. The output impedance is 10K ohm.

OBJECT (J6) - a BNC jack for counter monitoring of the object revolution rate. This signal originates from the code wheel mounted on the rotating object and outputs one pulse per two object revolutions. The output impedance is 10K ohm.

OBJECT P.S. (F1) - a 0.125 Ampere, type 3AB line fuse for the 115VAC required by the power supply in the object signal conditioning box.

± 15V, 5V, P.S. (F2) - a 0.5 Ampere, type 3AB line fuse for the 115VAC required by the logic power supplies (PS2, PS3, and PS4). Power Supply PS1 has its own internal fuse.

MOTOR ROTATION DIRECTION - CW - CCW (S2) - a toggle switch for changing the rotation direction (CW-clockwise; CCW-counter clockwise) of the derotator motor. This switch should be toggled only when the motor is off.

Main Control Chassis Description

Deck Mounted Components

A photograph showing the top view of the control chassis deck is presented in Fig. 2A. The major deck mounted components are identified on the photograph. Also applicable is Control Chassis Interconnection Drawing ESG535-5-21A and Parts List ESG535-3-27 (under separate cover). Referring to the interconnection

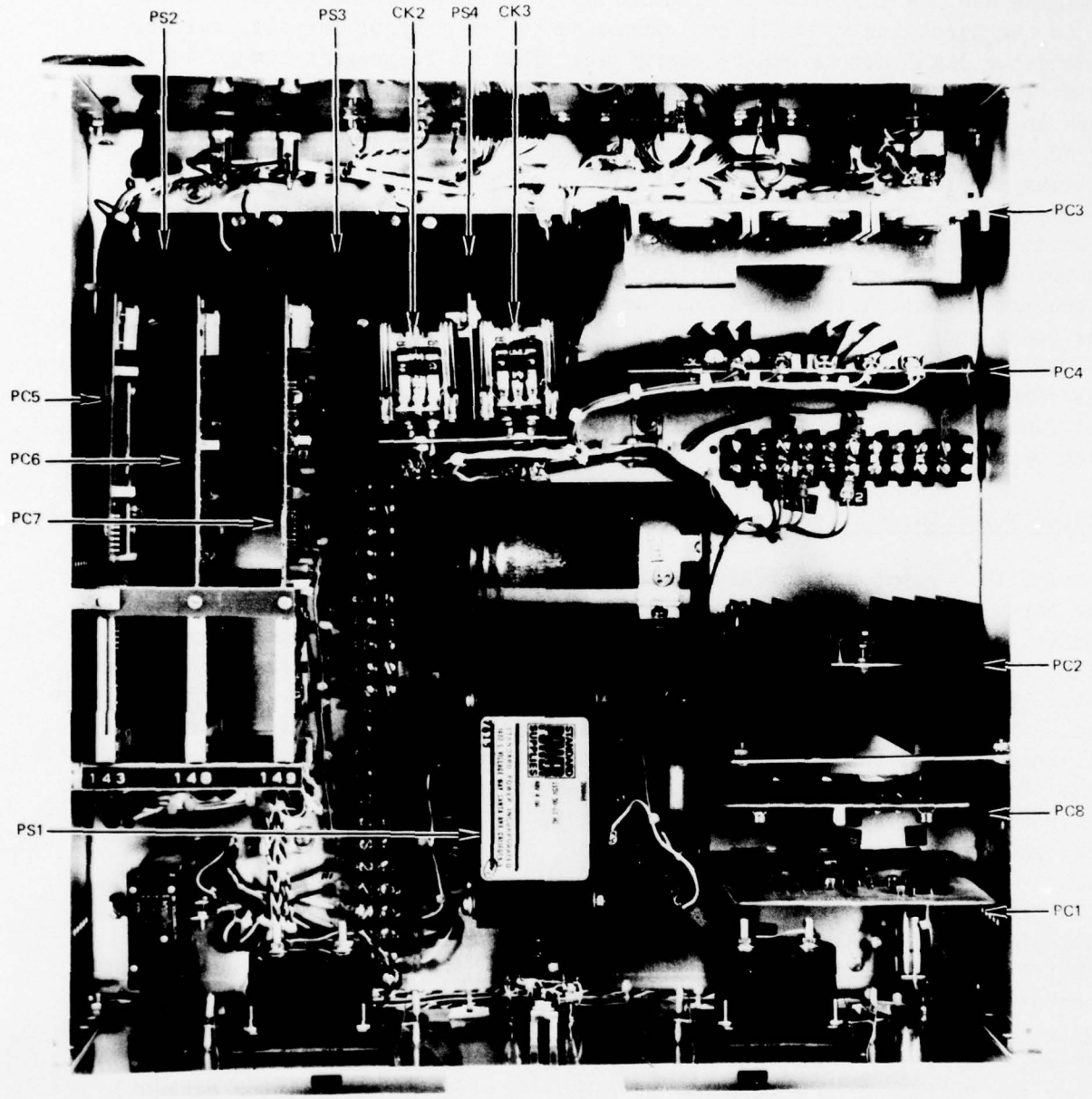

Fig. 2A Control Chassis Deck Layout

AD-A050 758 UNITED TECHNOLOGIES RESEARCH CENTER EAST HARTFORD CONN F/G 20/6
OPTICAL SYSTEM FOR DYNAMIC ANALYSIS OF ROTATING STRUCTURES.(U)
OCT 77 K A STETSON, J N ELKINS F33615-75-C-2013

UNCLASSIFIED UTRC/R77-992054 AFAPL-TR-77-51 NL

2 OF 2
AD
A060758

END
DATE
FILMED
4-78
DDC

drawing it can be seen that relay K1 works in conjunction with the air bearing pressure monitoring relay. If the air pressure is below the set value, and the BEARING AIR LOW indicator is illuminated, K1 cannot be energized. If the cable to the derotator motor is not connected to the control chassis, neither the indicator light nor K1 can be energized. This is to prevent damage to the motor driver circuit which could occur if left open circuited. Since contacts CK1 are in series with the MOTOR ON switch S1 and the motor power supply control relay K2, no power may be applied to the motor driver circuit unless the above conditions are satisfied. Note that K3 is in parallel with K2 and when K3 is not energized a 3 ohm resistor is connected across each of the 3 motor windings to provide dynamic braking to the motor. This dynamic braking occurs whenever the motor is turned off, or if the bearing air pressure drops below minimum. When the motor control is turned on, the dynamic braking is removed, the motor driver power supply (PS1) is energized, and the MOTOR ON indicator is illuminated. The line fuse for PS1 is located within the power supply module. Power to the remaining low voltage power supplies (PS2, PS3, and PS4) is applied thru a line fuse (F2) when the POWER ON circuit breaker is closed. The function of each printed circuit is described in the following sections.

Derotator Motor Current Source

Refer to Derotator Motor Driver Interconnection Drawing ESG535-5-24. This driver circuitry is located on three different printed circuit cards and is presented in this composite form as an aide to understanding the circuitry and as an aide in trouble shooting. The output of this driver connects to the brushless DC motor 3ϕ switch and provides an output current proportional to the input voltage signal. The 0 to $\pm$ 10 volt input signal is transformed to a 0 to 3.3 amperes output which drives the torque motor, which in turn drives the image derotating optics. To protect the DC motor from inadvertent demagnetization of the permanent magnet rotor during starting or fast reversal, the circuit also includes a hard current limiter.

The input voltage signal is attenuated by a factor of 3 and inverted by operational amplifier A1 and associated components. The A2 stage has a unity gain but inverts the signal and clips any negative going signal component; thus the output of A2 is an attenuated signal in phase with positive input signals. The Q1 stage converts the voltage signal at the output of A2 to a current amplifier. The voltage drop across D1 offsets the base-emitter drop of Q1 and thus the voltage drop across R9 and R10 (a measure of the emitter current) is approximately equal to the output voltage of A2. Since Q1 is a high gain transistor, the collector current is nearly equal to the emitter current. The emitter current is proportional to the output of A2; therefore the collector current of Q1 is proportional to the output voltage of A2. Using reasoning similar to that above it can be seen that almost all of the Q1 collector current flows thru R12 and the Q2/Q6 current gain is approximately equal to the ratio of R12 to R2.

The hard current limiting is provided by the Q1/Q2 stage. D2 and D3 are constant current diodes which provide the current to zener diode D1. If the current through R1 and R2 is low enough such that the voltage across these resistors is 0.5 volt less than the D1 zener voltage, Q1 and Q2 will be saturated and 0.5 volts or less will be dropped across Q2 collector to emitter. If the current demand causes the voltage across R1 and R2 to approach the D1 zener voltage, Q1 will begin to turn off Q2 and the voltage across Q2 will begin to rise and limit the current to this level. As mentioned previously this protects the motor from inadvertent demagnetization.

Motor Current Limiter

Applicable documentation:

Derotator Motor Driver Interconnection Schematic	ESG535-5-24
Current Limited Schematic	ESG535-1-30
Current Limiter Parts	ESG535-3-30
Current Limiter PC Layout	ESG535-8-30

The motor current limiter circuit board assembly is identified as PC4 on the control chassis interconnection diagram. This assembly provides drive current to the output stages. The current path is from the B+ terminal (PIN 2), through the parallel combination of R1 and R2, through Q2 and out the +OUT terminal (Pin 6). Q1 maintains Q2 in a saturated condition if the load current is such that the drop across R1 and R2 is less than the D1 zener voltage. As the D1 zener voltage is approached, base drive current for Q1 is diverted into D1 and, consequently, the base drive of Q2 decreases, it comes out of saturation, and a sharp current limit occurs at this output current level. The current limit point may be altered by changing D1 to a different zener value or by changing R1 and/or R2. Note: this current limit must be less than the maximum allowable stator current for the servo motor (3.47 amperes).

Current Control Element - PC3

Applicable documentation:

Derotator Motor Driver Interconnection Schematic	ESG535-5-24
Bridge Control Element	ESG535-1-28
Bridge Control Elements Part List	ESG535-3-28
Heat Sink Assembly Board Layout	ESG535-8-28

The current control element assembly consists of printed circuit mounted components and heat sink mounted components. The plug-in assembly is identified as PC3 on the control chassis interconnection diagram. Q2 is the main series

pass device and is driven by Q6. Q4 acts to compensate for the base to emitter voltage drop of Q6. Refer to the Derotator Motor Current Source section for a complete description of the operation of the devices on this assembly.

Driver Amplifier and 3ø Switch

Applicable documentation:	Driver Amplifier and 3ø Switch	ESG535-1-29
	Driver Amp and 3ø Switch Parts List	ESG535-3-29
	Driver Amp and 3ø Switch Layout	ESG535-8-29

A description of the A1, A2, and Q1 stages was presented in the Derotator Motor Current Source section of this appendix. The calibraton procedure for the I GAIN potentiometer is described in the Board 361-Driver Amplifier and 3ø Switch section under "Calibration Procedures" of this appendix.

Integrated circuit stages, A3, A4, and A5 are connected as differential inputs to single ended output line receivers. These line receivers are designed for industrial logic application requiring high immunity to electrical noise. Using stage A3A as an example, when pin 6 is positive with respect to pin 2 then output pin 1 is high. When pin 2 is positive with respect to pin 6, then output pin 1 is approximately at circuit common potential. When A3A pin 1 is high, Q2 is turned on which turns on Q5 and connects the øA output to circuit common. If neither A3A pin 1 nor A3B pin 1 is high, the øA output is open circuited, Diodes D7, D8, and D9 clamp the negative spikes from the motor stator and prevent the output transistors from being reverse biased. The motor drive switching logic is such that the Q3 stage and Q5 stage are never on simultaneously.

Line Receiver

Applicable documentation:	Digital Line Receiver Schematic	ESG535-1-31
	Digital Line Receiver Parts List	ESG535-3-31
	Digital Line Receiver Layout	ESG535-8-31

This printed circuit board contains six channels of differential input to high or low level single ended output line receivers. These are high noise immunity receivers designed for industrial logic applications. The IC1, IC2, and IC3 stages each are dual receivers. The IC4 and IC5 stages are triple high level to TTL level translators. One section of IC1 and one section of IC4 will be used to illustrate circuit operation. When board input pin A is positive with respect to board input pin B, IC1 pin 7 will also be high. When board input pin B is positive with respect to board input pin A, IC1 pin 7 will be low. This high level signal is brought out to board pin C (not used in the Derotator) and also applied to the level translator input pin 1 of IC4. This high level logic signal is translated to TTL level and brought out to pin D. The level translator is noninverting. Voltage regulators VR-1 and VR-2 are not used. An input to output jumper has been installed in their place.

Two Channel Frequency-to-Voltage Converter

Applicable documentation:	2-Channel F/V Schematic ESG	ESG535-1-6B
	2-Channel F/V Parts	ESG535-3-6B
	2-Channel F/V Layout	ESG535-8-6F&6R

The frequency-to-voltage plug-in printed circuit card is identified as PC5 on the control chassis interconnection diagram. The circuits on this card convert the incremental signals from the motor driven optics and the rotating object to DC analog voltages proportional to the rotational rate of the motor and object, respectively. These analog voltages are used to drive the rotational rate meters, provide a signal proportional to the rotational rate difference, and provide signals to the motor rotational rate control loop.

Integrated circuit IC1 is a dual one-shot multivibrator connected such that one of the one-shots is triggered on the positive going excursion of the motor incremental signal and the other is triggered by the negative going excursion. These two signals are combined by a section of OR gate IC10; thus the output of IC10 is triggered by each edge of the motor rotational rate (incremental) signal. The output of IC3 is brought out to board pin L through a section of OR gate IC10. This is a good place to monitor the motor rotation rate by use of a counter. The output of IC3 is also level conditioned by IC8 transistors and associated components and filtered by a low pass filter made up of IC4B, R19, and C9. The filtered signal is amplified by the IC5B stage and brought out to board pin R as the inverted signal proportional to the motor rotational rate. The output of IC5B is also applied to the IC6B follower stage and brought out to board pin X. The signal at pin X is used to drive the MOTOR RPM meter on the front panel.

The object rotation rate signal is processed in a similar manner through the "B" channel up to the output of IC6A. The full output of IC6A is applied across the derotation calibration potentiometer DE (R41). The signal level at the R41 slider is inverted by the IC7A stage and brought out to board pin T as the signal proportional to the object rotation rate. This signal is also summed with the inverted motor rotation rate signal from IC6B by the IC7B stage. This IC7B output is brought out to board pin V as the signal proportional to the rotational rate difference between motor and object.

Refer to the Board 143-Two Channel F/V section of the calibration procedures applying to this printed current card.

Amplifier, Threshold, and Logic Board

Applicable documentation:

Amplifier, Threshold, and Logic Schematic	ESG535-1-33A
Amplifier, Threshold, and Logic Parts	ESG535-3-33
Amplifier, Threshold, and Logic Layout	ESG535-8-33

The amplifier, threshold, and logic board is identified as PC6 on the control chassis interconnection diagram. The track, manual, minimum revolution rate, motor rotation rate high, motor rotation rate low, phase lock loop control circuits, and status readout logic is located on this circuit card.

The front panel manual MOTOR RPM signal is low pass filtered by IC1 and associated components and summed with the MIN RPS control level. This signal is applied to summing amplifier IC3 through an IC8 analog switch when the front panel MODE switch is in the MANUAL position. When the MODE switch is in the TRACK position, the output of the object F to V converter is applied to the IC3 summing amplifier through an IC8 analog switch. If a phase lock signal is present at pin 11 of IC7, the phase control signal at board pin L will also be applied to the IC3 summing amplifier through an IC8 analog switch section. When the front panel motor control switch is in the ON position, the output of summing amplifier IC3 is applied to follower stage IC4. The output of IC4 provides the input to the motor driver amplifier circuit.

The motor RMP HIGH-LOW dual threshold detector is IC5, IC6 and associated components. The dead band of this detector is set by the +LIM and -LIM potentiometer. If the motor rotation rate exceeds the object by an amount in excess of the dead band, the output of IC5 goes high. This signal is applied to the readout driver on PC7 and generates an inhibit-to-phase lock signal through the upper two OR gates of IC7 to board pin P. If the rate is below the motor by an amount in excess of the deadband, the output of IC6 goes high. This signal is applied to the readout driver on PC7 and generates an inhibit to phase lock signal in the same way as the output of IC5.

Refer to the Board 148-Amplifier, Threshold, and Logic section of the calibration procedures applying to this printed circuit card.

Phase Detector

Applicable documentation:

Phase Detector Schematic	ESG535-1-34
Phase Detector Parts	ESG535-3-34
Phase Detector PC Layout	ESG535-8-34

The phase detector board is identified as PC7 on the control chassis interconnection diagram. IC1 and IC4 and associated components comprise a flip-flop multivibrator with stable output levels of +5 volts and -5 volts. The 0° index pulse from the motor sets the output to +5 volts at the FF1 test point. The 180° index pulse from the motor sets the output to -5 volts at the FF1 test point. IC2, IC3, IC4 and associated components comprise a bistable multivibrator. Successive index pulses from the object cause the output at FF2 to switch from one stable state to the other. The output states are +5 volts and -5 volts at the FF2 test point. The output signals from the flip-flop and the bistable are applied to the IC5 multiplier input and the multiplier output is filtered by the low pass filter IC6 and associated components. The output of IC6 is an analog signal which is proportional to the cosine of rotational phase angle between the object and the motor driven optics.

The phase offset control voltage from the front panel PHASE control is filtered by the IC7 low pass filter stage and summed with the phase difference signal by summing amplifier IC8 and associated components. The output of IC8 is the phase control signal which is applied through IC10 to the phase correction summing amplifier on PC6. The phase offset voltage is inverted by the IC9 inverting amplifier stage and applied to the bias input of a dual threshold detector consisting of IC11, IC12, and associated components. The input to the dual threshold detector is the phase signal. If the phase angle of the rotating optics leads the phase angle of the object by more than the detector dead band, the output of IC11 is high and the LEAD indicator is illuminated. If the phase angle of the rotating optics lags the phase angle of the object by more than the detector deadband, the output of IC12 is high and the LAG indicator is illuminated. IC15 and associated components comprise a flip-flop multivibrator. It is set to a high output state by either holding the phase control switch in the LOCK position (SET input) or by the LEAD or LAG signal being generated, provided the INHIBIT IN signal is not present. The flip-flop is reset by the INHIBIT IN signal which occurs if the RPM HIGH or RPM LOW signal is generated or if the INHIBIT-ENABLE-LOCK front panel switch is in the INHIBIT position. The IC14 stage and the two IC16 transistors provide a regulated-5Vdc to operate the flip-flop and the bistable multivibrator.

Refer to the Board 149-Phase Detector section of the calibration procedures applying to this printed circuit card.

Torque Direction Controller

Applicable documentation:	Torque Direction Controller Schematic	ESG535-1-35
	Torque Direction Controller Parts List	ESG535-3-35
	Torque Direction Controller Layout	ESG535-8-35

This printed circuit is identified as PC8 on the control chassis interconnection schematic. The circuitry provides the rotation direction signal through a remote electronics line receiver to the motor rotation logic circuitry. If the motor control loop command signal is such as to require the motor to slow down, this circuit generates a rotation direction reversing signal and hence changes the direction of rotational torque being applied to the optics. Provision is also made through this circuitry for selection of the direction of rotation of the optics; the operator selects the rotation direction by a rear apron mounted toggle switch.

The IC1 and IC2 stages are functionally connected as an absolute value circuit. Regardless of the polarity of the input signal at board pin A, the output will be proportional to the input, and positive. This absolute value signal is brought out to board pin D and is used as the input signal to the motor driver circuitry. To illustrate how the absolute value circuit works consider a positive polarity signal at TP1. The output of IC1 is negative going and clamped by D1 and blocked by D2. D3 will be reversed biased, D4 will be forward biased, IC2 acts as a voltage follower, and the output (TP2) signal is equal to the input signal and positive. For a negative signal at TP1, the output of IC2 is negative going, clamped by D3, and blocked by D4. The output of IC1 will be positive going, D1 will be reversed biased, D2 will be forward biased, and the output (TP2) signal is equal to the input signal but positive.

The input signal (board pin A) is also applied to the parallel connected IC3A and IC3B comparator stage. The trip level of the comparator is set by R7 and R9 and approximately 2 percent of deadband is provided by R5 and R4. Parallel connected comparators IC3C and IC3D are configured to function as a logic level inverter. Depending on the position of the MOTOR ROTATION DIRECTION switch (S2), either the IC3A/IC3B output or the IC3C/IC3D output will be connected to the IC4A line driver input. The output of IC4A commands the rotation direction of the motor. Assume the rotation control switch is in the position as drawn on ESG535-1-35. If the input is positive the IC3A/IC3B output will be high, the IC6A input will be high, IC4A pin 1 will be positive with respect to pin 7, and the torque direction command will be for CW rotation. If the motor control loop needs to slow the motor down, the input signal will be negative, the IC3A/IC3B output will be low, the IC6A input will be low, IC4A pin 7 will be positive with respect to pin 1, and the torque direction command will be for CCW rotation (to slow the motor down dynamically in this case). IC4B is a spare line driver section brought out to card edge pins (not used).

Remote Electronics

Motor Signal Conditioner Box

Applicable documentation: Motor Signal Conditioner and Control Logic Interconnect ESG535-5-22A
Interconnection Block Diagram ESG535-4-22
Motor Code Wheel Layout ESG535-6-23A

A long cable is usually required between the control chassis and the derotator motor driven optics. To keep the number of interconnecting wires to a minimum, and to signal condition the signals for long cable transmission, a considerable amount of electronics must be located close to the derotation motor. A 25 wire cable connects the motor signal conditioning electronics to the control chassis and a 15 wire cable connects the motor signal conditioning electronics to the motor code wheel pickup head. The motor signal conditioning box houses the following three printed circuit cards: a transmission signal conditioning card of line drivers and line receivers, a card with two pickup head receivers and the motor rotation logic, and a card with two pickup driver/receiver circuits and a divider for generating the rotation index pulses.

Object Signal Conditioner Box

Applicable documentation: Object Signal Conditioner Box Interconnection ESG535-5-23
Interconnection Block Diagram ESG535-4-22
Object Code Wheel Layout ESG535-6-24

The function of the object signal conditioner box is similar to the motor signal conditioner box. A 15 wire cable connects the object signal conditioner electronics to the control chassis and an eight wire cable connects the object signal conditioner electronics to the object code wheel. The object signal conditioning box houses a miniature regulated power supply, a power conditioning and distribution card, and a card with two pickup driver/receiver circuits.

Pickup Head Driver and Detector:

Applicable documentation: Pickup Head Drive and Detector Schematic ESG535-1-21A
Pickup Head and Detector Conditioner Parts List ESG535-3-21
Pickup Head Drive and Detector Conditioner Layout ESG535-8-21

A Pickup Head Drive and Detector circuit card is located in both the motor and the object signal conditioner boxes. The divide by 16 counter is located only on the card used in the motor signal conditioner box. These cards control the power to the light-emitting diodes (LED), and detect the chopped signal from the photo transistors in the pickup heads. The power to the LED's is controlled so as to obtain a symmetrical square wave from the incremental track on the code wheel. Parallel connected comparators IC1A and IC1B detect the signal from the pickup head photo transistor. The output of the comparators is brought out to board pin 2 as the incremental signal output. The output of the comparators is also filtered

by R5 and C10 and applied to the IC2 differential amplifier stage. The slider of the symmetry pot (R18) is set to be equal to the average valve of the incremental signal when it is a symmetrical square wave. If the high level of the incremental signal tends to become narrower than the low level, the filtered signal applied to IC2 becomes less positive, the output of IC2 gets more positive, the current thru the incremental light emitting diode is increased, the signal out of the photo transistor will increase, and the high level of the incremental signal width will be increased. The above illustrates how this circuit regulates the symmetry of the incremental signal. The level trim pot (R17) sets the level of current thru the light emitting diode at symmetry.

The index marker LED receives a constant current thru a 1.2K ohm resistor and the index phototransistor output is detected by the parallel connected IC1C and IC1D comparators. No calibration is required for the index channel. For the complete calibration procedure for this board refer to the Board 145-Pickup Head Driver and Detector section of Calibration Procedures.

Line Driver/Receiver

Applicable documentation: Motor Line Driver/Receiver ESG535-1-22
Motor Line Driver/Receiver Parts List ESG535-3-22
Motor Line Driver/Receiver Layout ESG535-8-22

The Line Driver/Receiver card is used only in the motor signal conditioning box. The card has three each triple level translators (IC6, IC8, IC9), five each dual line driver/receivers (IC1-IC5), and a dual one-shot multivibrator (IC7). The level translators translate the input TTL level signal to the high level signals required by the line drivers. The differential line drivers are designed for this type of logic application where a high immunity to electrical noise is required.

To illustrate the functioning of the translator/driver circuits assume the ϕA Hi input (board pin C) to be high. The output at IC6 pin 3 will be high and pin 7 of IC1 will be negative with respect to pin 1. If board pin C is low, the output at IC6 pin 3 will be low and pin 7 of IC1 will be positive with respect to pin 1. The differential line receiver section of IC5 receives the motor rotation direction control signal. When board pin A is positive with respect to board pin B, IC5 output pin 15 will be high. When pin A is negative with respect to pin B, IC5 output pin 15 will be low. The input to one-shot multivibrator IC7 is a full square wave signal for each full revolution of the motor. The upper section of the one-shot is triggered by the positive going edge of the input signal and outputs the 0° index pulse. The lower section of the one-shot is triggered by the negative going edge of the input signal and outputs the 180° index pulse.

Motor Rotation Logic

Applicable documentation: Motor Rotation Logic Schematic ESG535-1-23
Motor Rotation Logic Parts List ESG535-3-23
Motor Rotation Logic Layout ESG535-8-23

The motor rotation logic card is used in the motor signal conditioning box. The upper two parallel connected comparators are used to detect the signal from the ØB photo transistor. The lower two parallel connected comparators are used to detect the signal from the ØC photo transistor. The nine gates of the Motor Driver Simplified Schematic (Fig. 3A) are located on the printed circuit card. For example, gate 1 of Fig. 3A is the uppermost IC5 exclusive OR gate on ESG535-1-23. The operation of this circuit is completely described by the truth table included in Fig. 3A and the accompanying explanation in the Brushless DC Motor and Drive Electronics Section of this appendix.

Pickup Head Drive and Detector Power Supply

Applicable documentation: Pickup Head Drive and Detector Power Supply Schematic ESG535-1-25
Pickup Head Drive and Detector Power Supply Parts List ESG535-3-25
Pickup Head Drive and Detector Power Supply Layout ESG535-8-25

The Pickup Head Drive and Detector Power Supply card is used in the object signal conditioning box and contains a 5 VDC regulator (A1) and a TTL signal level controlled switch (Q1, Q2 and associated components) in series with the regulator output. When a HIGH signal is present at the SET IN 1 input, Q2 is turned on which turns on Q1 and connects the regulated 5 volt to the SWITCHED +5 volt OUT 1 output. This card also serves as a general power distribution point for the low voltage DC power. No calibration adjustments are located on this card.

Brushless DC Motor and Drive Electronics

Motor Description

The conventional dc motor uses brushes and a commutator to properly distribute current through the windings as the motor rotates. In a continuous rotation brushless motor, this mechanical switching is replaced with electronic switching. The brushless dc motor is not simply an AC motor powered by an inverter; it has position feedback so that the input waveforms are kept in proper timing with the rotor position. They have some of the same basic motor operation characteristics as the

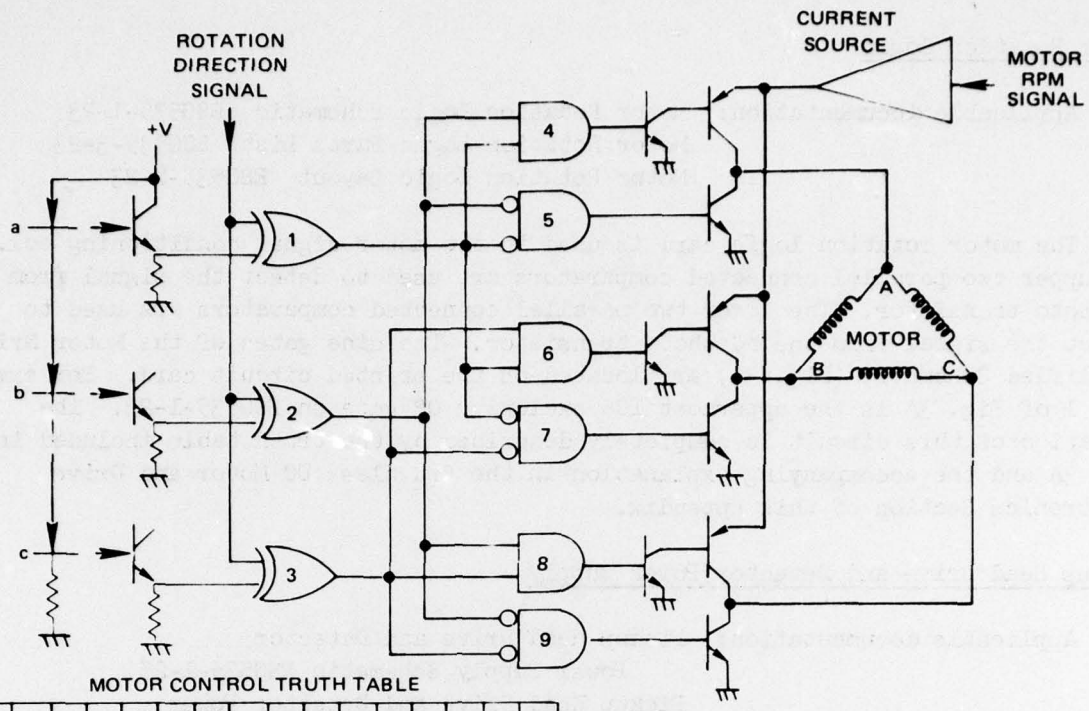

MOTOR CONTROL TRUTH TABLE

					A7	A9	B9									
					B6	A8	B8									
				A3	B5	A5	B7									
	B1	B2	B3	A2	B4	A4	A6									
DES	a	b	c	A1	Q1	Q2	Q3	Q4	Q5	Q6	Q7	Q8	Q9	A	B	C
0	1	0	0	0	1	0	0	0	0	0	1	1	0	X	0	1
12	1	1	0	0	1	1	0	1	0	0	1	0	0	1	0	X
24	1	1	1	0	1	1	1	1	0	0	0	0	1	1	X	0
36	0	1	1	0	0	1	1	0	0	1	0	0	1	X	1	0
48	0	0	1	0	0	0	1	0	1	1	0	0	0	0	1	X
60	0	0	0	0	0	0	0	0	1	0	0	1	0	0	X	1
72	1	0	0	0	1	0	0	0	0	0	1	1	0	X	0	1
0	1	0	0	1	0	1	1	0	0	1	0	0	1	X	1	0
12	1	1	0	1	0	0	1	0	1	1	0	0	0	0	1	X
24	1	1	1	1	0	0	0	0	1	0	0	1	0	0	X	1
36	0	1	1	1	1	0	0	0	0	0	1	1	0	X	0	1
48	0	0	1	1	1	1	0	1	0	0	1	0	0	1	0	X
60	0	0	0	1	1	1	1	1	0	0	0	0	1	1	X	0
72	1	0	0	1	0	1	1	0	0	1	0	0	1	X	1	0

CW ROTATION

CCW ROTATION

LOGIC KEY

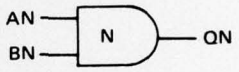

Fig. 3A Motor Driver Simplified Schematic

dc servo motor, but with the following advantages: much higher operating speeds with full torque at these speeds; the stator is the wound member and may be mounted on a substantial heat sink; the EMI normally associated with the arcing of a brush-commutator interface is eliminated; and they have a very long life because there are no brushes to burn and wear out.

Some means of sensing the position of the rotor in reference to the stator is necessary so that the input currents are applied properly. With the derotator drive motor this is accomplished by the use of a coded light chopper wheel which rotates between photo transistors and light emitting diodes. The code wheel has the proper sequence of windows arranged in three separate tracks to provide the three phase switching signals needed to rotate the motor. The windows in this wheel are positioned with respect to the back emf waveforms of the motor. The code wheel provides the positional information required to excite the stator windings in a sequence that keeps the stator approximately 90 electrical degrees ahead of the rotor field.

Drive Electronics Description

A simplified schematic, and a switching logic truth table, for the brushless dc motor drive electronics is shown in Fig. 3A. As previously described, a code wheel is positioned between light emitting diodes and photo transistors. Each 12° of motor rotation changes the binary word generated at the inputs to the exclusive OR gates. As an example of the use of the truth table, consider the 0° position with a clockwise (CW) rotation direction signal. Only the "a" photo-transistor is illuminated; the outputs of gates 1 (Q1), 7 (Q7), and 8 (Q8) are high; the other gate outputs (Q2, Q3, Q4, Q5, Q6, and Q9) are low; neither transistor connected to the A motor winding is on; the lower transistor connected to the B winding is on and B will be switched to circuit common; and the upper transistor connected to the C winding is on and C will be switched to the positive current source. The main current flow in the motor is from C to B. After 12° of motor rotation, the abc binary word changes from 100 to 110, the upper transistor connected to the A winding is on, the lower transistor connected to the B winding is on, and neither transistor connected to the C winding is on. The main current flow in the motor is from A to B.

The simplified circuit schematic of the motor driver, and the associated truth table is included as an aide to trouble shooting the motor driver circuit. The abc binary word being generated for a given position of the code wheel can be determined by inspection with the motor stopped. The truth table gives the on/off condition of each gate and transistor in the circuit. Refer to the proper printed circuit card schematic for more details concerning each circuit.

Board 143 - Two Channel F/V

1. Front panel controls

   a) Set CALIBRATE and PHASE pots to 500.
   b) Set TRACK-MANUAL switch to MANUAL.
   c) Set INHIBIT-ENABLE-LOCK switch to INHIBIT.
   d) Turn POWER and MOTOR on.
   e) Set MOTOR RPM pot to 000.

2. Input one shots

   a) Rotate object at some convenient speed.
   b) Check for 30 μsec ±20% pulse at the OSA (TP3) test point.
   c) Check for 15 μsec ±20% pulse at the OSA (TP4) test point.

3. Precision one shots

   a) Adjust the ACAL (R35) trimpot for a 0.3 msec pulse at the TPA (TP8) test point.
   b) Adjust the BCAL trimpot for a 0.15 msec pulse at the TPB (TP7) test point.

4. MOTOR rotation rate and readout

   a) Connect scope probe to test point FF1 on board 149.
   b) Adjust front panel MOTOR RPM pot for a 20 msec pulse-to-pulse interval. This corresponds to 3000 RPM (1 rev/.02 sec x 60 sec/min = 3000 RPM).
   c) Adjust the AFV (R37) trimpot for a reading of 3000 RPM on the MOTOR meter.
   d) Iterate between the MOTOR RPM control and the AFV trimpot to obtain a correct MOTOR RPM reading and pulse-to-pulse interval; i.e., iterate between steps 4b and 4c.

5. OBJECT tracking and readout

   a) Connect scope probe to test point FF2 on board 149.
   b) Adjust the RPM of the object for a 20 msec pulse-to-pulse interval. This corresponds to 6000 RPM (2 rev/.02 sec x 60 sec/min = 6000 RPM).
   c) Switch the MANUAL-TRACK front panel switch to TRACK.
   d) Adjust the BFV (R36) trimpot for a reading of 6000 RPM on the OBJECT meter.
   e) Adjust the DE (R41) trimpot for derotation of the object - maintain object at 6000 RPM during this adjustment.

Board 145 - Pick-Up Head Driver and Detector

1. Initial Conditions

   a) Set LEVEL TRIM (R17) and SYM (R18) trimpots to approximately mid-position.
   b) Load to be driven must be connected across pins 2 and 3.
   c) Pick-up head and code wheel in mechanical alignment and rotating.

2. LEVEL TRIM and SYM calibration

   a) Measure the average voltage level at the INC (TP4) test point $(V_{max} + V_{min})/2$.
   b) Adjust the SYM trimpot slider voltage to be equal to the results of Step 2a.
   c) Adjust the LEVEL TRIM trimpot to obtain 3.3 Vdc at the I test point.
   d) Fine adjust the SYM trimpot for a symmetrical square wave at the INC test point.
   e) Iterate between steps 2c and 2d in order to satisfy both conditions.
   f) Check for a TTL level pulse at the INDEX test point.

Board 148 - Amplifier, Threshold, and Logic

Note: Calibrate Board 143 before proceeding with this procedure.

1. Front panel controls

   a) Set the TRACK-MANUAL switch to MANUAL.
   b) Set the MOTOR RPM control to 000.
   c) Set the INHIBIT-ENABLE-LOCK switch to INHIBIT.
   d) Turn POWER and MOTOR on.

2. HIGH, LOW, and MIN RPS calibration

   a) Adjust the MIN RPS (R42) trimpot for a MOTOR RPM of 1500.
   b) Adjust the +LIM (R43) trimpot for 0.50 V at the +LIM test point.
   c) Adjust the -LIM (R44) trimpot for 0.50 V at the -LIM test point.

Board 149 - Phase Detector

Note: Calibrate Boards 143 and 148 before proceeding with this procedure.

1. Front panel controls

   a) Set INHIBIT-ENABLE-LOCK switch to INHIBIT.
   b) Set TRACK-MANUAL switch to TRACK.
   c) Set PHASE control to 500.
   d) CALIBRATE as required to derotate the image in the INHIBIT and TRACK mode with an object rotation rate of 6000 RPM.

e) MOTOR RPM - not used.
f) Turn POWER and MOTOR on.

2. PHASE, LEAD, and LAG calibration

a) Set the BIAS (R101), LEAD (R104), and LAG (R103) trimpots full CCW and insert the card.
b) Fine adjust the front panel PHASE control to obtain 0V at the BIAS test point.
c) Adjust the LEAD trimpot to obtain +0.64 V at the LEAD test point. This represents 15° of LEAD (sin 15° x 2.5 = .64).
d) Adjust the LAG trimpot to obtain -0.64 V at the LAG test point. This represents 15° of LAG.
e) Switch the front panel INHIBIT-ENABLE-LOCK switch to ENABLE and check for proper automatic image lock-on.
f) Adjust front panel CALIBRATE control as in Step 1d. Switch back to ENABLE and adjust the front panel PHASE control for a 000 reading. Adjust the BIAS trimpot cw until the image begins to roll, then back off 1.5 turns. If the image rotates at 999 on the PHASE control, back off an additional 0.5 turn on the BIAS trimpot.
g) Phase lock an image and adjust the front panel PHASE control to 900. Adjust the -BIAS (R102) trimpot such that the voltages at the -BIAS and LP test points are equal.

Board 361 - Driver Amplifier and 3 ϕ Switch

1. Preliminary Steps

a) Remove board 148
b) Connect the + side of an ammeter to the X5 terminal of board 126. Connect the - side to the X4 terminal of board 126. Set the ammeter on a convenient range for measuring 3 to 4 amperes.
c) Connect the + side of a 10 Volt source to TP4 of board 361. Connect the - side to TP31.

2. Current gain

a) Turn POWER and MOTOR on.
b) Turn the 10 Volt source on.
c) Adjust the I Gain (R10) pot for a reading of 3.3 A on the ammeter.

REFERENCES

1. Stetson, K. A. and J. N. Elkins: Optical System for Dynamic Analysis of Rotating Structures.
   a. First Interim Technical Report, Phase I - Design Study. UTRC Report R75-992054-100, June 1975.
   b. Second Interim Technical Report, Phase II - Hardware Development. UTRC Report R76-992054-200, January 1976.
   c. Third Interim Technical Report, Phase III - System Application. UTRC Report R76-992054-300, July 1976.
   d. Fourth Interim Technical Report, Phase IV - Analytical Study. UTRC Report R76-992054-400, September 1976.

2. Waddell, P., et al.: Pockel Cell Stroboscopic Holography for the Vibration Analysis of Objects. International Symposium on the Applications of Holography (Paper 6-6), Besancon, France, July 6-11, 1970.

3. Tsuruta, T.: Holographic Interferometry for Rotating Objects. International Symposium on the Applications of Holography, (Paper 17-9), Besancon, France, July 6-11, 1970.

4. Tsuruta, T., et al.: Holographic Interferometry for Rotating Subjects. Applied Physics Letters, p. 85, January 1970.

5. Sikora, J. P., et al.: Holographic Vibration Study of a Rotating Propeller Blade. Experimental Mechanics, p. 230, June 1974.

6. Sikora, J. P., et al.: Holographic Analysis of Rotating Objects. Conference on the Engineering Uses of Coherent Optics, Glasgow, Scotland, April 8-11, 1975.

7. Waddell, P.: A Stepper Motor Controlled Image Derotator System to Non-Stroboscopically Visualize Stress, Vibration and Epicycle Motion in Real Time on High Speed Rotating Components. 4th Annual Symposium on Incremental Motion Control Systems and Devices, University of Illinois at Urbana-Champaign, April 1-3, 1975.

8. Waddell, P., et al.: A Non-Stroboscopic System for Examining High Speed Rotating Objects. Strain, p. 73, April 1973.

9. Waddell, P., et al.: The Non-Stroboscopic Visualization of Vibration Patterns by Real Time -- Time Average Hologram Interferometry, Electro-Optics International 1972, Brighton, England, February 28 - March 1, 1972.

REFERENCES (Cont'd)

10. Waddell, P.: How to Observe Strain in High Speed Rotating Objects. OEM Design, p. 81, May 1973.

11. Waddell, P.: Strain Pattern Examination. Engineering Materials and Design, p. 3, March 1973.

12. Waddell, P.: Stopping Rotary Motion with a Prism. Machine Design, p. 151, May 1973.

13. Waddell, P., et al.: The Real Time Non-Stroboscopic Examination of Centrifugal Stress on Rotating Photoelastic Discs Utilizing an Optical Image Derotation Technique. Conference on Optical Methods in Scientific and Industrial Measurements, Tokyo, Japan, August 1974.

14. Swift, D. W.: Image Rotation Devices - A Comparative Survey. Optics and Laser Technology, p. 175, April 1974.

15. Stetson, K. A.: A Review of Speckle Photography and Interferometry. Opt. Eng., Vol. 14, No. 5, pp. 482-489 (1975).

16. Chiang, F. P. and R. M. Jung: Bending and Vibration of Plates by Laser-Speckle Interferometry. J. Opt. Soc. Am., Vol. 65, No. 10, p. 1196A (1975).

*U.S.Government Printing Office: 1977 — 757-080/281